Renewable and Sustainable Energy Reviews 36 (2014) 149–179

Contents lists available at ScienceDirect

Renewable and Sustainable Energy Reviews

journal homepage: www.elsevier.com/locate/rser

Properties and development of Ni/YSZ as an anode material in solid oxide fuel cell: A review

B. Shri Prakash*, S. Senthil Kumar, S.T. Aruna

Surface Engineering Division, Council of Scientific and Industrial Research-National Aerospace Laboratories, Bangalore 560017, India

ARTICLE INFO

Article history:
Received 21 June 2013
Received in revised form
16 December 2013
Accepted 12 April 2014
Available online 14 May 2014

Keywords:
Solid oxide fuel cell
Anode
Ni/YSZ
Polarization

ABSTRACT

In recent times, synthesis, development and fabrication of anode component of solid oxide fuel cell (SOFC) have gained a significant importance, especially after the advent of anode supported SOFC. The function of the anode electrode involves the facilitation of fuel gas diffusion, oxidation of the fuel, transport of electrons and transport of by-product of the electrochemical reaction. Although impressive progress has been made in the development of alternative anode materials with mixed conducting properties and few of the other composite cermets, Ni/YSZ continues to be the most sought after anode for high temperature SOFC applications. Despite of its poor carburization and sulfidation capabilities during the operation of SOFC directly on hydrocarbons, Ni/YSZ continues to be the most opted anode electrode material due to its high catalytic activity for hydrogen oxidation, methane reforming, high electronic and ionic conductivity and stability.

Present review focuses on the various aspects pertaining to Ni/YSZ as an anode in SOFC. Various factors that influence the ohmic, activation and the concentration polarization contribution of anode while using Ni/YSZ are discussed. Importance of optimizing the composition, microstructure and porosity to minimize the above mentioned polarizations are discussed extensively. Various synthesis methods that are used in the preparation of optimized NiO/YSZ composite powder and the methods that are adopted to fabricate anode component are provided in detail in the article. Information on Ni/YSZ anode failure and strategies to improve the long term stability are also discussed exhaustively. Parameters that influence the carburization and sulfidation of Ni/YSZ while using hydrocarbons as fuel are elaborated in this article and means to minimize the same are also discussed.

Contents

* Corresponding author.

http://dx.doi.org/10.1016/j.rser.2014.04.043
1364-0321/

1. Introduction

Fuel cells are electrochemical devices used for the conversion of chemical energy into electrical energy, essentially like batteries, but with external fuel supplies. Solid oxide fuel cells (SOFC) are class of fuel cells in which all the components are solids and their operating temperature varies between 500 and 1000 °C. Due to all solid-state construction, high operating temperatures and non-polluting by-products of the reaction, SOFC offers many advantages over conventional power generating systems, even in comparison to other fuel cells, in terms of its efficiency, reliability, size flexibility, fuel flexibility, and environmental friendliness. They offer high chemical to electrical conversion efficiencies (~50%) due to the absence of the Carnot limitation, and further energy gains (up to ~70%) can be achieved when produced heat is used in combined heat and power (CHP), or gas turbine applications. Targeted applications of SOFC's include the stationary power generation, CHP, etc.

In its simplest form, a single cell of SOFC consists of two porous electrodes (anode and cathode) and a dense solid electrolyte membrane separating the two (Fig. 1). Mostly, electrolytes are oxygen ion (O^{2-}) conductors. The operating principle of a SOFC involves the oxidation of hydrogen (H_2) at the anode (on using H_2 as fuel), reduction of molecular oxygen (O_2) at the cathode and the diffusion of the produced O^{2-} through an electrolyte into the anode where it reacts with H_2 ions (H^+) to produce water. At the same time, electrons flow from the anode to the cathode through an external circuit to generate power. In this way, the conversion from chemical energy into electrical energy is realized. Power generation would continue as long as fuel and oxidants are supplied. Reactions occurring at anode, cathode and overall reaction on using H_2 as fuel, are summarised in Eqs. (1)–(3).

Anode reaction: $2H_2 \rightarrow 4H^+ + 4e^-$ (1)

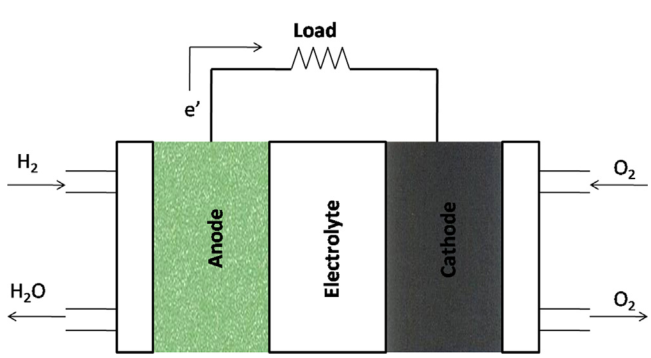


Fig. 1. Schematic of single solid oxide fuel cell.

Cathode reaction: $O_2 + 4e^- \rightarrow 2O^{2-}$ (2)

Overall cell reaction: $2H_2 + O_2 \rightarrow 2H_2O$ (3)

When CO and hydrocarbons (such as methane) are used as fuels, following overall reactions occurs:

$$CO + O^{2-} = CO_2 + 2e^- \quad (4)$$

$$CH_4 + 4O^{2-} = CO_2 + 2H_2O + 8e^- \quad (5)$$

In a SOFC stack, single cells are connected in electrical series via a component called the interconnect.

Theoretically, SOFC's look very attractive due to their operational versatility, efficiency and other advantages. But in reality they are plagued with many challenges. The actual performance and long term stability of existing SOFC systems are not yet satisfactory, and they are far from being economically competitive. While the high operating temperature leads to improved performance, on the downside, it not only throws severe restrictions on materials choice but can also lead to increased materials degradation and finally to system failure. Due to multi-components and the multi-interfaces that are involved in SOFC stack, physio-chemical phenomenon occurring at each location of cell is very complex and prior knowledge of each phenomenon is very essential to optimize the performance and to achieve high efficiency. Detailed investigations on the reaction mechanism and kinetics at each electrode, electrolyte, electrode/electrolyte interface, determination of degradation mechanism, production of

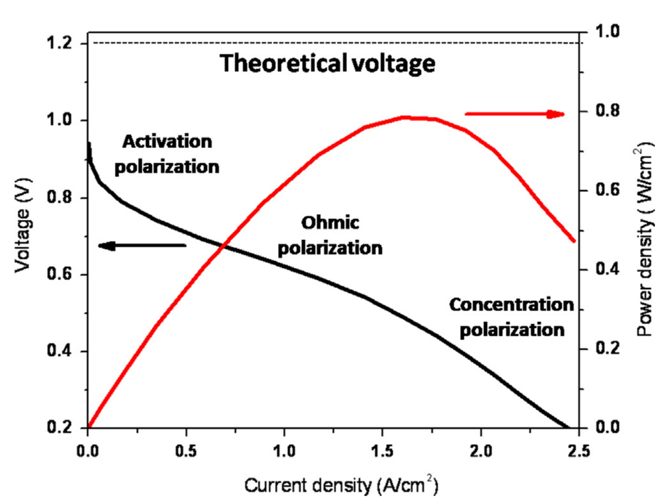


Fig. 2. A typical polarisation curve of a fuel cell.

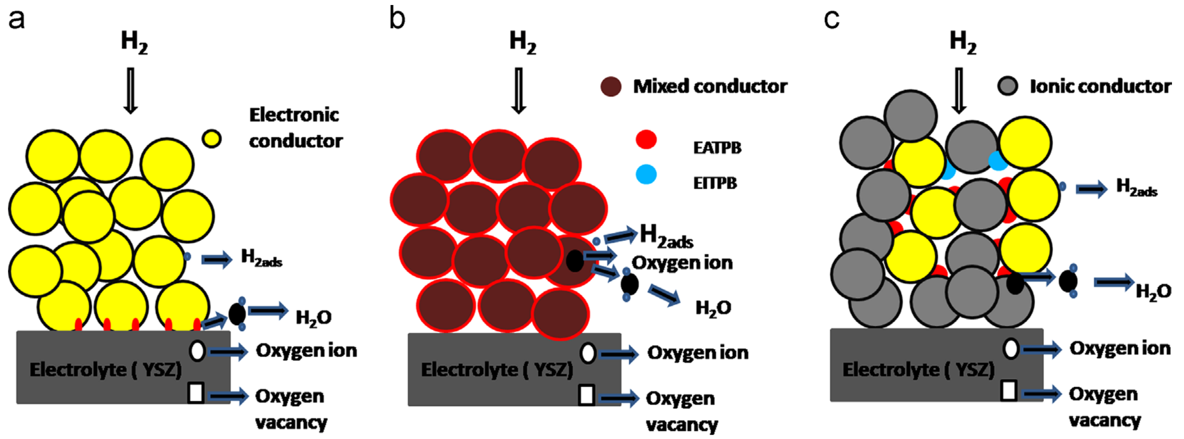


Fig. 3. TPB regions for (a) pure electronic conductor anode, (b) mixed electronic ionic conductor anode and (c) electronic–ionic composite anodes.

cheap and efficient electrodes, improving the long term stability, etc., are the need of the hour.

Electrochemical systems, including SOFC, are governed by few fundamental physicochemical processes. These include charge-transfer reactions (electrochemistry), chemical reactions (both bulk reactions and heterogeneous reactions), and transport (charge transport of electronic and ionic charge carriers, mass transport through diffusion and convection). As calculated from the Nernst equation, ideal voltage (E°) from a single cell of SOFC under open circuit conditions is close to 1.1 V dc. When an electrode is polarized, due to the electrochemical reactions occurring at the electrode surface, current flows through external circuit. The amount of current is controlled by the kinetics of the reactions and the diffusion of reactants both towards and away from the electrodes. Useful voltage output (V) under load conditions, that is, when a current passes through the cell, is given by

$$V = E^o - IR - \eta_c - \eta_a \quad (6)$$

where IR is the ohmic resistance, η_c is the cathodic polarization and η_a is the anodic polarization.

Kinetic restriction imposed by various components of SOFC's result in decreased voltage and performance of the cell. Fig. 2 shows a typical SOFC polarization curve, which consists of three main regions of interest.

In the low current density region, reduction in voltage is caused mainly by the electrochemical reaction rate limitations and is commonly referred to as activation polarization. The exchange current density is a parameter that determines this drop in voltage. In intermediate current densities, cell is predominantly affected by the ohmic losses in the cell, caused by both ionic and electronic resistances that linearly affect the voltage drop with increased current density. If the current density is increased to high enough levels, voltage will fall off rapidly. This occurs because of a phenomenon called concentration polarization. When the current density is high enough, gases are utilized in the cell at a faster rate than fuel or oxidant can reach the cell surface, leading to the concentration polarization. In order to pursue cell development work, it is desirable to separate the cell losses into elements associated to the individual cell components.

The resistance of a cell is the sum of a number of contributions

$$R_{measured} = R_{elec} + R_{cath} + R_{ano} + R_{conc} \quad (7)$$

where R_{elec} is the resistance of the electrolyte, R_{cath} is the ohmic and electrochemical losses at the cathode, R_{ano} is the ohmic and electrochemical losses at the anode and R_{conc} represents the diffusion and gas conversion losses at the anode and cathode.

Factors influencing the polarization include material properties, microstructure, temperature, atmosphere, current density, etc. It is essential to minimize these polarization losses for efficient conversion of chemical energy into electrical energy. Identification of source of polarization is very critical, but is challenging. Present review focuses on the various aspects pertaining only to the anode component of SOFC.

Table 1
Physical properties of Ni.

Melting point	**1453 °C**
TEC	**$\sim 13.3 \times 10^{-6}$ cm cm^{-1} K^{-1}**
Electronic conductivity @ 25 °C	**$\sim 138 \times 10^4$ S cm^{-1}**
Electronic conductivity @1000 °C	**$\sim 2 \times 10^4$ S cm^{-1}**

1.1. An overview of the anode component

The function of the anode (fuel electrode) is to facilitate the oxidation of the fuel and transport of electrons from the reaction site to the current collector. In addition, it must allow diffusion of fuel gas to reaction site and reaction products away from it. Aspects pertaining to structural, electrical and electrochemical properties have to be taken into consideration while choosing the material for anode.

High temperature and strong reducing atmosphere that anode needs to operate in, imposes stringent restrictions on the anode material selection and poses special challenges related to its chemical stability and materials degradation. To minimize the polarization losses of the oxidation reaction, anode materials should meet the following basic requirements:

- High electro-catalytic activity towards oxidation of fuel gases.
- Preferably a mixed conductor with predominant electronic conductivity to permit the passage of electrons.
- Thermal expansion coefficient (TEC) and chemical compatibility with the adjoining components.
- High wettability with respect to the electrolyte substrate.
- Should possess continuous porous structure to allow rapid transport of fuel and reaction by-products.
- Fuel flexible, ease of fabrication, and low cost.
- Excellent carburization and sulfidation resistance on using hydrocarbons as a fuel.

Electrochemical reaction in anodes are believed to occur only at the regions called three phase boundary (TPB); which is defined as the collection of sites where oxygen ion conductor, the electron-conducting phase, and the gas phase, all meet together. The H_2, which needs to be oxidized in to H^+, diffuses through the open pores of the anode and is oxidized somewhere within this matrix

and reacts with O^{2-} to produce water. Location of the TPB, where the electrochemical reaction takes place between O^{2-} and H^+ to produce water, depends on the material in use. If the anode exhibits solely electronic conduction, the effective electrochemical reaction zone (ERZ) of anode is mainly limited to the double-phase boundary between the electrolyte and anode (Fig. 3a). In contrast, the use of anodes which are mixed ionic and electronic conductors (MIEC) in the reducing atmosphere, drastically enlarges the ERZ over the entire anode–gas interfacial area; and hence delocalized to provide a volumetric reaction region in three dimensions (Fig. 3b).

In composite anode materials, consisting of mixture of electronic and ionic conductors (Fig. 3c), electrochemical reactions are confined to the sites where oxygen ion conductor, the electron-conducting phase, and the gas phase all meet together. To achieve a significant drop in the activation polarization and improvement in the electrical efficiency, in addition to maximizing TPB's, it is necessary to ensure that TPB's are connected three dimensionally to electronic, ionic and gas chains. Only these TPB's will be electrochemically active (EATPB). Reaction would not occur if there is a breakdown in connectivity in any one of the three phases. TPB's become electrochemically inactive under the following circumstances: (a) ions from the electrolyte do not reach the reaction site, (b) fuel gas molecules do not reach the site and (c) electrons cannot be removed from the site. TPB concept has important implications in the optimization of the anodes.

During the early stages of SOFC development, single phase materials like graphite, platinum group, and transition metals (related to Fig. 3a) were investigated as anode materials [1]. Graphite corroded electrochemically. Platinum spalled off in service, presumably due to water vapor evolution at the metal–oxide interface. Several metals such as Fe, Co, Ni [2], Pt [3] and Ru [4] have also been studied as anode materials. Among the transition metals, iron corrodes with the formation of an iron oxide when the partial pressures of oxidation products in the anode compartment of an operating cell exceed a critical value. Cobalt is somewhat more stable, but expensive. Among Ni, Co, Fe, Pt, Mn and Ru, Ni exhibits the highest electrochemical activity for H_2 oxidation reaction [5] and hence is a natural choice for anode. Apart from higher electrochemical activity, it is cheaper when compared Co and noble metals like Pt, Ru. Hence Ni is more economical to use as anode material. The physical properties of Ni are summarized in Table 1.

However, on using Ni alone as the anode material, the pores might get closed due to relatively low melting temperature and higher sinterability of Ni. In addition, TEC of Ni is much higher than that of YSZ electrolyte (TEC of YSZ $\sim 0.5 \times 10^{-6}\,K^{-1}$), a common electrolyte material used in high temperature SOFC. Application of pure Ni as anodes would lead to the performance degradation of fuel cell on repeated use. As a consequence, all-metal anodes have not found acceptance.

Recently, mono-phasic oxides with MIEC characteristics (related to Fig. 3b) have been emerging as strong candidates as anode materials of SOFC; especially for the oxidation of hydrocarbons. The structural types that have been considered include perovskite, pyrochlore, and spinel, with perovskite structure being prominent among them. Conductivities approaching $100\,S\,cm^{-1}$ have been achieved with $SrTiO_3$ in a reducing atmosphere on doping Sr with lanthanum/yttrium and niobium on the titanium site. Titanates have also been shown to have good dimensional and chemical stability upon redox cycling. Electrocatalytic activity has been improved by dopants such as Mn and Ga on the Ti site ($La_4Sr_8Ti_{11}Mn_{0.5}Ga_{0.5}O_{37.5}$) [6,7]. Similar results have been obtained with $La_{0.4}Sr_{0.6}Ti_{1-x}Mn_xO_{3-x}$. The B-site of strontium-doped lanthanum chromite has been doped with various transition metals (Mn, Fe, Co, Ni andCu) to introduce oxygen vacancies. The perovskite system $(La_{1-x}Sr_x)Cr_{0.5}Mn_{0.5}O_{3-x}$ has shown good results for oxidation of wet H_2 and CH_4 at 900 °C. In recent times, appropriately doped double perovskites e.g., $Sr_{2-x}La_xMg_{1-x}Mn_xMoO_{6-x}$, have also been found to be promising [8–11].

Third category of anode is a composite material consisting of a mixture of electronic and ionic conductors (generally cermets), in which role of electronic and ionic conductions are performed independently by two different materials. Among the various cermets that have been tested as anodes, Ni/8 mol% yttria stabilized zirconia (YSZ) cermet fulfils most of the requirements of anode and abundant amount of literature is available on its electrical, electrochemical and mechanical properties. However, the disadvantages of this material are: its poor redox stability, low tolerance to sulfur, carbon deposition on using hydrocarbon fuels and the tendency of nickel coarsening after prolonged operation. Cu–CeO_2–YSZ is an alternative cermet anode used to minimize the carbon deposition in which Cu acts as an electronic conductor and CeO_2 acts as an electro catalyst [8–11]. Often, metal alloys such as Cu–Ni, Cu–Co are used along with YSZ to overcome the issues associated with pure Ni/Co pertaining to carbon deposition, electrocatalytic activity, etc. A number of other bi and tri metallic alloy systems in combination with

Table 2
Vol% of different components of Ni/YSZ anode for different starting compositions of NiO and YSZ.

Solid content								**Including porosity**		
Wt%		Vol%		Wt%		Vol%		Vol%		
NiO	**YSZ**	**NiO**	**YSZ**	**Ni**	**YSZ**	**Ni**	**YSZ**	**YSZ**	**Ni**	**Pore**
10	90	8.95	91.05	8.03	91.97	5.47	94.52	91.05	5.262	3.688
20	80	18.11	81.89	16.42	83.58	11.51	88.49	81.89	10.65	7.46
30	70	27.49	72.51	25.19	74.81	18.24	81.76	72.51	16.16	11.33
40	60	37.10	62.9	34.38	65.62	25.76	74.24	62.9	21.8	15.3
50	**50**	**46.94**	**53.06**	**44.00**	**56**	**34.23**	**65.77**	**53.06**	**27.6**	**19.34**
60	**40**	**57.02**	**42.98**	**54.10**	**45.9**	**43.84**	**56.16**	**42.98**	**33.53**	**23.49**
70	30	67.36	32.64	64.71	35.29	54.84	45.16	32.64	39.60	27.76
80	20	77.96	22.04	75.86	24.14	67.55	32.45	22.04	45.84	32.12
90	10	88.84	11.06	87.61	12.39	82.41	17.59	11.06	52.23	36.61

Component	**Mol.-wt.**	**Density (g cm^{-3})**	**Molar volume (cm^3)**
Ni	58.69	8.907	6.589
NiO	74.69	6.67	11.198
8YSZ	131.42	5.90	22.27

ceria have also been investigated. Examples include Ru/YSZ, Cu–CeO_2–ScSZ and Ir/$Ce_{0.9}Gd_{0.1}O_{2-x}$.

Although impressive progress has been made in the development of alternative anode materials, significant problems persist, particularly due to their low catalytic activity and electronic conductivity. Some of the MIEC-materials and few of the composite cermets indeed appear appealing for the anode applications and suitable for the operation of SOFCs directly on hydrocarbons. However, the difficulty to date has been finding a material that has the catalytic activity for H_2 oxidation and methane reforming comparable to Ni and electronic conductivity close to Ni, while having good mixed conductivity. MIEC-materials are not sufficiently stable under operating conditions. The composition and microstructure of these new anodes need further optimization in order to improve their electrochemical characteristics. Hence, despite of its poor carburization and sulfidation capabilities; even today, Ni/YSZ continues to be the most sought after anodes for high temperature SOFC applications. YSZ being cheaper O^{2-} ion conductor, Ni/YSZ is appealing even economically also. The concept, microstructure and the composition of Ni/YSZ composite envisaged by Spacil [12] 43 years ago is very relevant even today. However, substantial improvements in its performance has been achieved though many modifications over the years.

1.2. Ni/YSZ cermet as anode

Modified porous Ni/YSZ cermets fulfill most of the requirements of an ideal anode. To be precise, following characteristics of Ni/YSZ make them especially attractive:

- Ni is as an excellent electrocatalyst for the electrochemical oxidation of H_2 with high electronic conductivity ($\sim 2\times10^4$ S cm^{-1} at 1000 °C).
- The YSZ constitutes a framework for the dispersion of Ni. It also acts as an inhibitor for the coarsening of Ni during the operation [13]. YSZ offers a significant part of ionic contribution to the overall conductivity, thus effectively broadening the TPB's.
- Chemically stable in reducing atmospheres at high temperatures.
- Its TEC is close to that of YSZ-electrolyte when compared to pure Ni and TEC of Ni/YSZ anode can be matched with other SOFC components by varying the composition [14].
- Intrinsic charge transfer resistance that is associated with the electrocatalytic activity at Ni/YSZ boundary is low.
- Ni and YSZ are essentially immiscible with each other and non-reactive over a very wide temperature range.

Ni/YSZ cermet was introduced to overcome the issues associated with pure Ni with regard to TEC and coarsening effects [12]. Since then there have been tremendous progresses and achievements in SOFC technologies, materials aspect, design and fabrication and in the fundamental understanding of the mechanism and kinetics of electrode reactions in SOFC.

As described earlier with regard to electronic–ionic composite cermet anode, electrochemical reaction in Ni/YSZ occurs at a point where Ni, YSZ and pore coexist and the points which are connected to the chains of Ni, YSZ and pores (EATPB). Maximisation of EATPB is essential to enhance the electrochemical performance of Ni/YSZ anodes and fine tuning of the microstructure is necessary to maximize the EATPB density. Electrical and mechanical properties of anodes should also be considered while fine tuning the microstructure to maximize EATPB.

Based on the conventional ceramic powder mixing process, general processing route for the preparation of Ni/YSZ cermet anodes involves the following steps: (1) homogeneous mixing of appropriately sized NiO and YSZ in an appropriate composition, (2) firing of anodes at high temperature and (3) reduction of NiO/YSZ into Ni/YSZ during the operation of SOFC or external reduction in the N_2+H_2 atmosphere at fuel cell operating temperature (600–1000 °C). Reduction of NiO into Ni is associated with the generation of pores as volume reduction of about ~41% occurs during the conversion of NiO into Ni.

Amount of porosity created during the reduction depends on the composition of the cermet. It increases with increase in the amount of NiO. Vol% of different components of anodes (NiO, Ni, YSZ and porosity), calculated based on the molar volumes of YSZ, Ni and NiO, for different starting composition are summarized in Table 2.

It has been found that there is negligible change in the bulk dimensions when NiO/YSZ composites are reduced to the initial Ni/YSZ anode cermet, when vol% of YSZ is $\geq$ vol% of NiO. The decrease in solid volume due to the reduction of NiO into Ni mostly appears as an increase in the volume fraction of porosity. Electrical, electrochemical and mechanical properties of Ni/YSZ anodes are strongly influenced by the composition, microstructure and porosity in the composites.

Present review intends to provide an overall perspective on the compositional, microstructural, electrical, electrochemical and thermo-mechanical aspects of Ni/YSZ composite. It would also summarize the influence of various parameters on the properties of the Ni/YSZ anode, methods employed for the synthesis of anode material and the fabrication of anode components. Drawbacks of the composite and the advancements that have taken place in composite characterization are also discussed in this article.

1.3. Geometries and configuration of SOFC

SOFC geometries can be broadly grouped into two categories, namely, planar and tubular (Fig. 4). In the planar geometry, the electrodes, the electrolyte and the current collectors are present as flat planar components, and are arranged in the sandwich fashion. In this geometry, air and fuel flowing through channels are built into the cathode and anode. In the tubular design, components are assembled in the form of a hollow tube, with the cell constructed in layers around a tubular cathode/anode; air/fuel flows through the inside of the tube and fuel/air flows around the exterior.

In each geometry, SOFC can be fabricated into three configurations, namely, anode supported, cathode supported and electrolyte supported, named based on the major component that provides the mechanical stability to the entire cell. For instance, in the anode supported SOFC, thick (~0.5–1.5 mm) porous anode provides the mechanical support to the entire system. Essential porosity levels, microstructural features and conductivity requirements of anode component vary for each category. Fig. 5 shows the different configurations of planar SOFC.

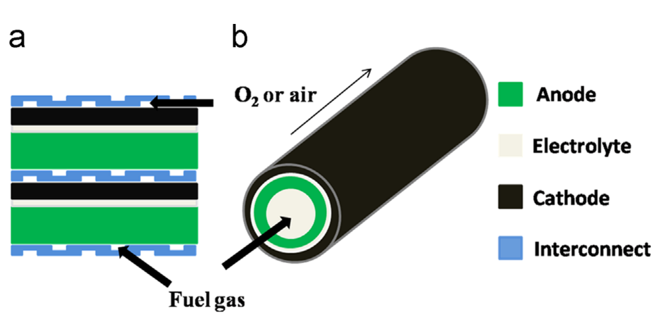


Fig. 4. Solid oxide fuel cell with (a) planar and (b) tubular geometry in anode supported configuration.

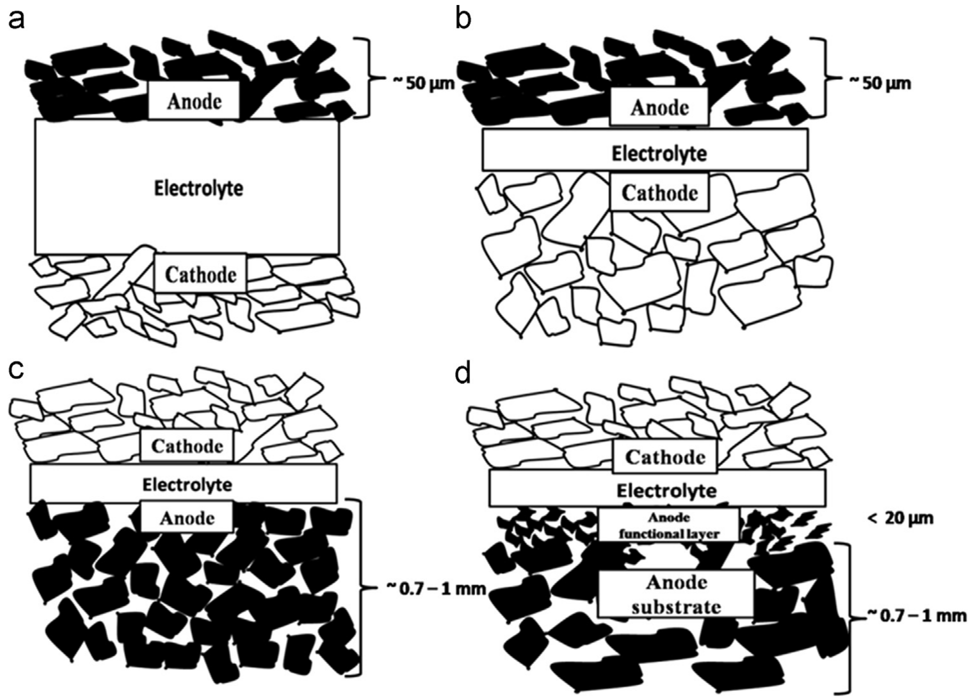


Fig. 5. Planar solid oxide fuel cell with different configurations: (a) electrolyte supported, (b) cathode supported, (c) anode supported monolithic structure and (d) anode supported bi-layered structure.

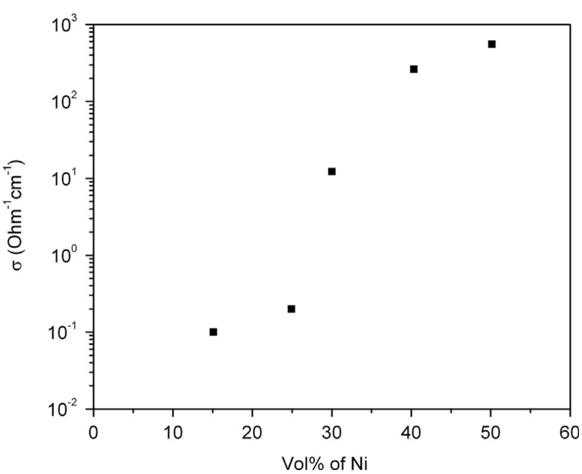


Fig. 6. Conductivity of Ni/YSZ cermets vs. the vol% of Ni of total solids at 1000 °C [15].

2. Polarization in Ni/YSZ anode

Anode component contributes to the overall polarization of SOFC through its share of ohmic, activation and concentration polarization. Various factors influencing these polarizations on using Ni/YSZ as anode are described in this section.

2.1. Ohmic polarization – Electrical conductivity

An important factor which needs to be optimized in the formulation of an anode cermet is the electrical conductivity (σ_e), as low σ_e results in ohmic polarization. A typical range of σ_e expected for an anode operating at 1000 °C is 100–400 S cm^{-1}. While maximizing σ_e, aspects pertaining to the activation polarization (maximisation of TPB) and concentration polarization (porosity optimization) should also be given due consideration, as all the three factors are interlinked and cannot be optimized independently. Though σ_e of Ni is high ($\sigma_e \sim 140 \times 10^4$ S cm^{-1} at 25 °C), overall conductivity of Ni/YSZ cermet is low as electronically insulating YSZ ($\sigma_e \sim 6 \times 10^{-3}$ S cm^{-1} at 25 °C) interrupts the Ni–Ni contact [15]. Electrical properties of Ni/YSZ cermet anodes are reported to be critically dependent on the composition, microstructure, distribution of Ni and YSZ phases and porosity. Factors influencing these parameters are composition of NiO and YSZ phases, NiO and YSZ powder characteristics, fabrication process, sintering temperature, reduction temperature, etc.

Conductivity of the Ni/YSZ-like cermet composites is generally explained based on the effective percolation theory and percolation threshold. For simple biphasic cermet system consisting of equi-sized spherical particles, percolation theory predicts S-shaped curve for the properties, such as σ_e, as a function of conductive phase (metallic phase in cermets) and a percolation threshold of 30 vol%. Below percolation threshold, σ_e of the composite is very low due to the isolation of metal particles and above 30 vol% metal, σ_e is about three-orders of magnitude higher, corresponding to a change in the mechanism of conduction from ionic to electronic through the percolating metallic phase. In accordance with the theory, S-shaped curve and percolation threshold of ~30 vol% was observed even in Ni/YSZ anodes (Fig. 6) on measuring σ_e as a function of Ni content and σ_e jumped from 0.1 to 10^3 S cm^{-1} [15].

Nature of transition, percolation threshold, and conductivity values of Ni/YSZ are revealed to be influenced by distribution of Ni and YSZ. For instance, owing to the microstructural features with good dispersion of the Ni component, smooth transition instead of S-shape threshold was observed in Ni/YSZ cermet prepared using powders prepared by self-propagating high temperature synthesis (SHS). High temperature experienced for a short period of time during the SHS process results in the unique microstructure with homogeneous dispersion of small sized Ni and YSZ particles. Solution based synthesis methods, in which homogeneous mixing of Ni and YSZ precursor is possible, generally result in cermet with higher conductivity values, that too at lower percolation value. For instance, the cermets prepared by buffer solution [16], electroless coating [17] were found to be electronically conducting even with

20 vol% Ni which is substantially lower than that of normally reported values (∼30 vol%). Percolation threshold was even lower (∼15 vol%) while using Ni-coated graphite and decrease was attributed to large effective Ni content created by the thin Ni layers in the cermet [18–20]. Low σ_e and high percolation threshold values are the features that are generally observed in the samples prepared by solid-state method [17].

Microstructural features and connectivity of Ni phase, which influences the electrical conductivity and percolation threshold of Ni/YSZ cermets, are reported to be strongly dependent on the particle size and distribution of both Ni and YSZ phases, which in turn are related to the YSZ/NiO size ratio (d_{YSZ}/d_{NiO}) in the starting powder [21–23]. General observation on the size dependency is that the cermets with smaller Ni particles (higher d_{YSZ}/d_{Ni} ratio) result in smaller percolation threshold and higher conductivity. Electrical conductivity variation from 300 to 4000 S cm^{-1} at 800 °C has been observed by using NiO powder with decreasing size. Enhanced conductivity on increasing the d_{YSZ}/d_{NiO} ratio can be attributed to the easy interconnection of finer NiO surrounding bigger YSZ particles. To increase d_{YSZ}/d_{NiO} ratio, efforts such as pre-calcination of YSZ have been made and improved conductivity has been achieved [24,25].

Connectivity of Ni and YSZ phases can also be expected to be affected by the heat treatment and sintering temperatures of the anodes through the variation in the connectivity of NiO and YSZ phases. Improvement in the electrical conductivity from 4 to 800 S cm^{-1} at 1000 °C has been observed while increasing the sintering temperature from 1300 to 1500 °C. Increase in sintering temperature also resulted in lower percolation threshold, which might be due to the decreased porosity, narrowed pore size distribution and increased connectivity between Ni [26]. Increase in reduction temperature also resulted in enhanced conductivity, which can be speculated to be due to the formation of a continuous Ni network at higher temperature due to a redistribution of the freshly formed metal while it is still surface active [27].

Increased electronic conductivity can be achieved by increasing the vol% of Ni beyond percolation threshold. However, Ni vol% cannot be increased as desired, as effect of increased Ni vol% on other polarizations need to be given parallel importance, which is usually adverse. Aim should be to find out an optimum composition of Ni/YSZ at which all the three polarizations are synergistically low. Though electronic resistance decreases continuously with increase in the vol% Ni, activation polarization generally exhibits a minimum at some intermediate value and increases on further increase in the Ni content. Hence optimum amount of Ni should be considered to minimize both ohmic and activation polarization, for which finding out percolation threshold is very essential.

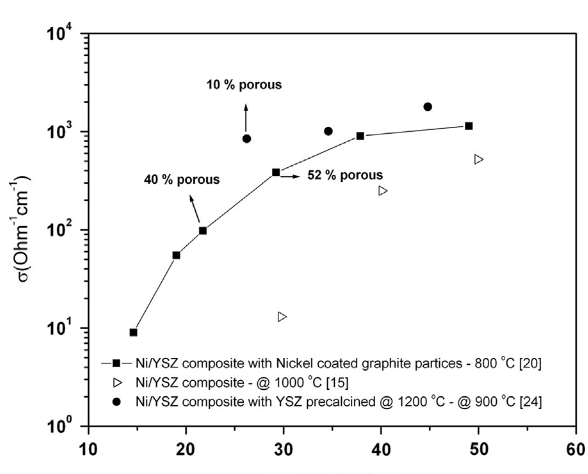


Fig. 7. Electrical conduction of Ni/YSZ composites with different amount of porosity as a function of the Ni content [20].

Though general informations about percolation threshold can be obtained by electrical conductivity measurements, more reliable information about the percolation threshold and electrical conductivity and their correlation can be gathered from advanced microstructural characterization techniques such as focussed ion beam scanning electron microscope (FIB–SEM) [28–30]. Precise information about percolation threshold can be used to choose an optimum composition of maximum performance.

In the anode supported SOFC, conductivity requirements, porosity levels and microstructural features of anodes in functional layers of bi-layered configuration, conduction layers of bi-layered configuration and anodes in the homogeneous monolayered structures are vastly different from each other. In the conduction layer, Ni vol% might go even up to 70% to achieve high electrical conductivity, but in functional layer it would be appropriate to restrict Ni content to a minimum required level. Achieving low percolation threshold in the anode functional layer is of great significance, as higher YSZ in the cermet would provide a better TEC match with the YSZ electrolyte. This would result in better operational reliability of the cell. Low percolation should also increase conductivity above the threshold volume, leading to lower electrical losses in the anode material.

Porosity, third component in the cermet, is another factor which influences the overall conductivity. Porosity is generated due to the reduction of NiO into Ni, poor sintering of the cermet or addition of extra pore formers. Irrespective of the source of the origin, porosity level has a strong effect on the electrical conductivity through its impact on the Ni-to-Ni connectivity. Therefore the electrical conductivity of porous Ni/YSZ cermet coatings is expected to be considerably smaller than that of the Ni/YSZ cermet material. Increased porosity in the cermet composite influences the electrical conduction of the composite in two ways: (1) it increases the percolation threshold at which conduction occurs and (2) once above the percolation threshold, increased porosity decreases the conductivity of the composite at a particular sample nickel solids loading.

It is reported that for a given vol% of porosity, the decrease in the conductivity values also depend on the size of the pores and the prediction is that pores with size significantly larger than the size of Ni and YSZ have a minimal impact on the conductivity [18–20]. On the other hand, fine scaled porosity is more likely to interrupt the continuity of the Ni phase and thus impacting on the conductivity to a larger extent. Attaining a high conductivity in a Ni/YSZ cermet with higher level of porosity is of great significance. In this regard, high conductivity (∼10^4 S cm^{-1}) achieved with 40% porosity and 30 vol% of Ni by adding Ni coated graphite particles to the starting composition instead of separately adding graphite and Ni particles is significant (Fig. 7) [20].

In conclusion, conductivity of Ni/YSZ anode is influenced by various factors such as composition, microstructure, size ratio of Ni and YSZ, sintering temperature, reduction temperature, porosity, etc., and its maximization is essential to minimize the ohmic polarization. During the process, attention should also be paid to minimize the other polarizations. Achieving lower percolation is of great significance as cermet with lower value of Ni result in better adhesion with the YSZ electrolyte layer due to the comparable TEC and shrinkage characteristics.

2.2. Activation polarization – Triple phase boundary

Activation polarization of an anode is related to its ability for electrochemical oxidation of a fuel and it contributes to the polarization even in the low current ranges (Fig. 2). Factors that

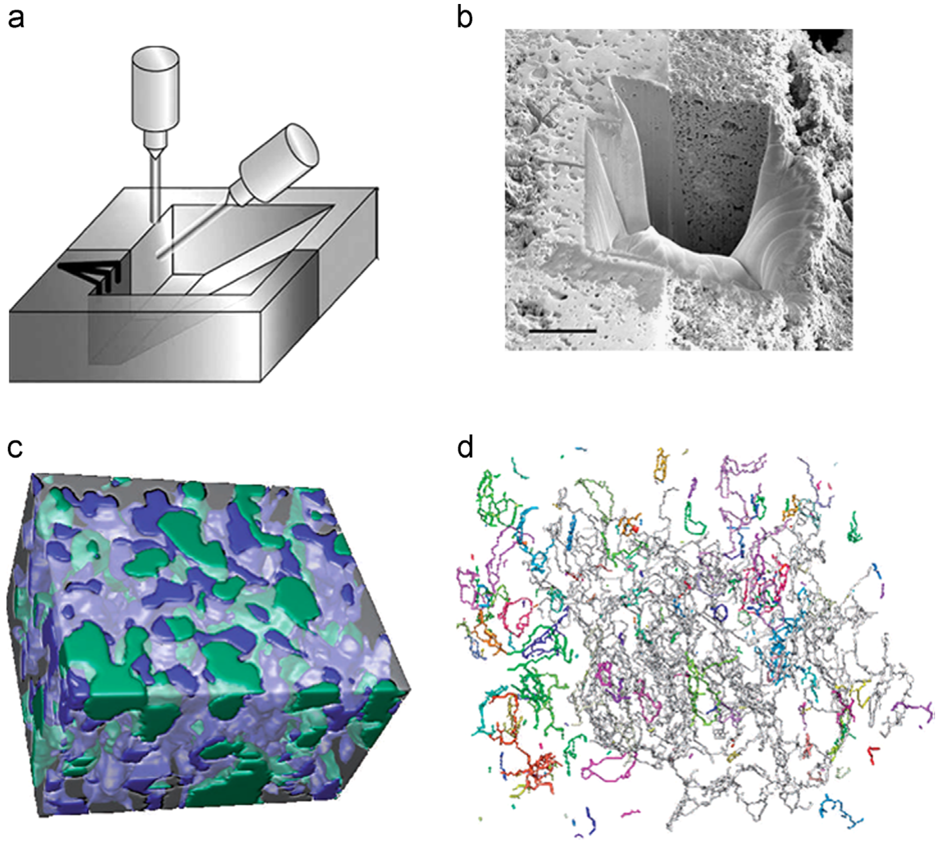


Fig. 8. (a) Schematic diagram showing the FIB–SEM geometry, (b) low-magnification SEM image of a FIB-etched region at the anode/electrolyte interface of a SOFC, (c) 3D anode reconstruction (Ni (green), YSZ (translucent/grey), and pore (blue) phases) and (d) 3D map of the three-phase boundaries in the anode (grey – connected TPB) [34].

Table 3
Percolated TPB density obtained by different models and FIB–SEM reconstructed experimental electrodes.

Source	Particle diameter (μm)	Volume fractions			Percolated TPB (μm^{-2})	Comments
		Ni	YSZ	Pore		
[57]	1	0.395	0.395	0.21	3.40	Model with mono sized particles
	0.5	0.395	0.395	0.21	13.81	
	1	0.38	0.31	0.31	2.72	
[35]	2	0.4	0.4	0.3	0.4	Model with mono sized particles
[40]	1	0.4	0.3	0.3	2.9	Model with mono sized particles
[41]	0.5	0.395	0.395	0.21	10.4	FIB–SEM
[34]	Not reported	0.259	0.546	0.195	2.70	FIB–SEM
[47]	Not reported	0.25	0.25	0.5	1.539	FIB–SEM
[58,59]	Not reported	0.45	0.35	0.2	9.34	FIB–SEM
		0.63	0.274	0.094	4.25	
[34]	Not reported				3.7–4.9	FIB–SEM

influence the electrochemical activity of an anode include TPB, connectivity, catalytic surface area and tortuosity. Investigations on nickel patterned anodes have provided enough evidences to prove that length of the TPB (generally mentioned in the units of $\mu m/\mu m^3$ (μm^{-2})) can be directly linked with the electrode's performance [31–33]. The numbers of percolated TPBs are believed to be the direct indicator of the electrochemical performance of an electrode, although it is not the only factor that determines an electrode's performance. Factors that might influence the electrochemical performance of anode are mostly known, but it is difficult to control them during the fabrication. Nonetheless, these parameters are dependent on the "controllable" factors such as electrode composition, particle sizes, and their distribution. For the optimization of Ni/YSZ anode and the minimization of activation polarization, a thorough understanding of the relationships between "controllable" and "uncontrollable" factors is essential. Controllable parameters have to be adjusted in such a way that resulting anode possesses large TPB density and low tortuosity factor. Many model systems and experimental methods have been put into use to quantify and correlate "controllable" and "uncontrollable" factors. Both in modeling and experiments, it is essential to distinguish between active (EATPB) and inactive components of TPB's.

Electrode microstructure models may be constructed in 1D, 2D or 3D with 3D being the best to mimic the actual microstructural features [35–38]. 3D synthetic microstructures are generated by randomly distributing the spherical particles corresponding to YSZ, Ni and pores into either a fixed bed or cubic lattice. Monte Carlo techniques are used for the same [35,39–42]. For particle packing through a numerical sintering process, which mimics the densification process in real electrodes, discrete element method (DEM) can be employed [43]. Some researchers have used a

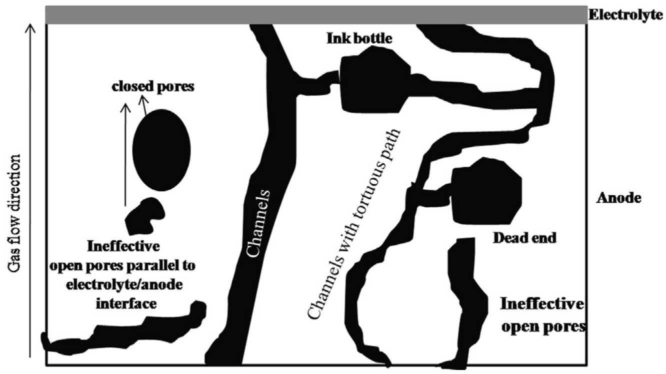


Fig. 9. Scheme of pore shapes.

correlated resistor network model to represent the electrodes by discretizing the particle packing into a resistance network, through which the resistance and the effective conductivity of the electrodes have been calculated [43,44]. In the experimental front, though 2D stereological methods involving SEM studies have been partially successful [45]; advent of FIB–SEM has substantially increased the valuable microstructural information that can be extracted [34,46–51]. In FIB–SEM method, FIB is first used to ion mill a trench in the SOFC in the region of interest such as anode–electrolyte interface. Subsequently, thin sections are removed from an exposed surface by the FIB, followed by SEM imaging of the surface, and the process is repeated to yield a series of consecutive SEM images. A 3D reconstruction of the anode is obtained by stacking the 2D SEM images in 3D space [34]. Thus FIB–SEM produces 3D digital recreations of real microstructures with resolution as low as ~10 nm and volumes > 100 μm^3 (Fig. 8).

These digital recreations can be used to quantify and distinguish between TPB and EATPB. Subsequently, density of EATPB of anode can be correlated with its electrochemical performance. EATPB numbers are generally much lower than the total TPB numbers and correspond only 60–80 %, with their number decreasing further for coarser grained Ni/YSZ anode [49]. Table 3 compares the percolated TPB density obtained from different model electrodes and from FIB–SEM reconstructed experimental electrodes.

Number of TPB's, EATPB's and the difference between them depends on the composition, size and shape of the particles. Composition at which maximization TPB and EATPB values occur depends on size and the size ratio between different components. From microstructural modeling, it was observed that for equi-sized particles of Ni and YSZ, variation of TPB with volume fraction of Ni gives a curve with a maximum at equal volume of Ni and YSZ. An asymmetric curve would be obtained for unequal sized particles with optimum volume shifting to higher volume fraction for bigger sized Ni particles [40,52,53]. Furthermore, microstructural modeling also predicts a significant decrease of the EATPB length for compositions below the percolation threshold [54,55]. However, experimental quantifications observed highest TPB density at a Ni solids volume fraction of ~0.34 (corresponding to 50 wt% NiO), where difference between TPB and EATPB was also low. At the composition corresponding to the maximum TPB density, anode polarization resistance was minimum. At higher vol% of Ni, though difference between TPB and EATPB remained lower, their actual number decreased [56]. Maximum EATPB observed at lower volume fraction of Ni might be due to the smaller size of the Ni.

A substantial difference between experimental and model results might arise due to the difficulties that are involved in the experimental FIB–SEM and simplified assumption that are considered in the model. In modeling different components of anodes are considered as spheres. However, the microstructures of real composite anodes are strongly disordered and the particles tend to have complex shapes due to the processes such as agglomeration and coarsening. Nonetheless, based on the literature (both experimental and modeling), following conclusions can be drawn on the TPB's:

(i) Both experimental and modelling studies suggest that there is an optimum compositional value at which TPB is maximum and there is a decrease on either side.
(ii) Reported TPB values are in the same order of magnitude (~5–10 μm^{-2}), both in experimental and modelling studies.
(iii) For a given particle size, TPB density decreases with increase in the porosity.
(iv) Both modeling and experiments suggests that TPBL can be effectively increased by decreasing the particle sizes. It is reported in the literature that TPB density decays with particle diameter (D) as a function of $1/D^{1/2}$ [60].

2.3. Concentration polarization – Porosity

For efficient functioning of Ni/YSZ as an anode, an optimum amount of porosity, its appropriate distribution and connectivity are very essential to facilitate easy transportation of fuel gas towards the reaction site and the reaction product diffusing out of the electrode [61]. In addition to the vol% of porosity, factors such as nature of the pores (closed pores or open pores), size of the pores, pores size distribution, pore tortuosity, etc., play a dominant role in impacting the polarization characteristics of Ni/YSZ anode. TPB's which are not connected to gas chains through open pores are electrochemically inactive. In addition, when reduced vol% of pores is present or size of the existing pores is small, diffusion becomes increasingly difficult, especially with increase in the operating current density. It results in a concentration polarization and reduced efficiency. Closed pores are not only ineffective in supplying the gas, but also detrimental, as they might occupy the regions which otherwise would have been occupied by EATPB's. Different types of pores that can be present in Ni/YSZ anode substrate are schematically depicted in Fig. 9. Evaluation of pores for its quantity and quality/nature can be done by the combination of characterization methods such as, density measurements, optical microscopy, SEM studies, FIB–SEM studies, mercury porosimetry, permeability tests, etc. [62].

Depending on the amount of NiO present, some amount of pores (either closed or open) are generated during the formation of Ni/YSZ as reduction of NiO into Ni is associated with 40% reduction in the volume (Table 2). For efficient functioning, state-of-the art homogeneous Ni/YSZ anodes are expected to possess ~30–35 vol% porosity and a Ni content of ~30–35 vol% (as a fraction of the total solids, i.e., Ni and YSZ). However, only 17–20 vol% of porosity would be generated during the reduction of NiO corresponding to 30–35 vol% Ni. Moreover, it is unlikely that entire vol% porosity is retained after the completion of the reduction process due to pore coalescence and/or vanishing processes. It would be ideal if all the pores that are generated during the reduction are open, as these pores are created in the neighborhood of Ni and would facilitate effective conversion of TPB into EATPB. However, depending on the initial NiO size, only small sized pores (~1.0–2.0 μm) are formed during the reduction and are not sufficient for the diffusion of large amount of fuel and product, especially when the cells are operated at high current densities. Increased vol% of porosity achieved by increasing amount of NiO is not advisable as it leads to the reduction in the number of TPB's. Increased porosity achieved by reducing the sintering temperature is also not acceptable, as it leads to Ni

coarsening on reduction, and in turn reduced TPB and reduced mechanical properties.

Porosity and pore size requirements of Ni/YSZ anodes would vary depending on whether it serves simply as an electrode or it serves a dual role of providing the mechanical support and the electrode. In cathode and electrolyte supported SOFC, porosity requirements of anode are not very stringent, as anode thickness in these configuration is lower (~20–50 μm). In addition, due to the reduced firing temperature of the anodes (~1300 °C) in such configurations, Ni/YSZ would possess inherent additional pores even prior to the reduction. Most state-of-the art anodes in such configuration are homogeneous in structure, in which existence of a large amount of very fine components (Ni, YSZ and pores) can increase the reaction area tremendously. Small sized pores that are generated during the reduction of NiO corresponding to 30–35 vol % of Ni along with the pores that are inherently present, would probably be sufficient if all the pores are connected, especially when SOFC is operating at lower current density. Increased amount of porosity or very large sized pores in such cases will reduce the total amount of TPB available for reaction. If diffusion of gas within the fine pores is relatively slow and limits the overall reaction rate, especially at higher current rates, optimum amount of small sized pore formers (2–3 μm) can be added.

In recent years, after the advent of anode-supported design, where the anodes are required to be relatively thicker than in the other two configurations, porosity engineering has attained a greater significance. For an anode-supported SOFC, thickness of anode needs to be higher (~0.5–1.5 mm) to perform the role of both mechanical support and an electrode. In addition, unreduced anode substrate in such configuration is likely to contain lesser amount of inherent pores and minimum (or no) open pores due to high firing temperature (~1400–1450 °C). In such thick anodes, diffusion of gases through the pores produced due to the reduction of NiO into Ni would be extremely difficult even if all the pores are connected and cells are operated at lower current density.

In the anode-supported design, anodes with bi-layered configuration have attracted more attention due to the higher efficiency. Microstructural engineering aspects encompassing porosity, pore size, particle size, etc., are different while pursuing mono-layered and bi-layered anode supported configurations. The main requirements of the anode part which serves only as a mechanical support (called anode support layer) in bi-layered anode structure are mechanical strength, gas permeability (higher porosity), and electronic conductance (higher volume fraction of Ni). Thus aspects of porosity engineering vary vastly depending on the configuration of the cell.

Depending on the configuration (mono or bi-layered), many methods/approaches have been employed to introduce additional porosity in the anode. e.g., varying the composition of Ni [63], pre-calcining the starting YSZ powder in the NiO/YSZ anode [24,25], adjusting the sintering temperature [64] and using organic pore-formers [65,66]. During porosity engineering to enhance the gas permeability, it has to be kept in mind that it is not always higher porosity that is important, but right distribution of appropriately sized pores and proper connectivity between those pores is more important than apparent total porosity itself. Also, porosity engineering must be carried out by keeping both TPB and gas diffusion in mind and optimization demands greater attention to minimize both concentration and activation polarization.

In gradient type of anodes, increased porosity has been achieved by way of increasing amount of NiO [63]. Layers close to the electrolyte had smaller NiO content (say 40 wt% of NiO) and layers farther away from the interface had the highest NiO content (say 70 wt% of NiO). Porosity gradient, with increasing amount of porosity from the anode/electrolyte interface was thus achieved. However, the strategy of increasing the NiO content to increase the porosity cannot be employed for homogeneous anodes, in which pre-calcining of YSZ (around 1000 °C) is an alternative option [25]. As coarsened YSZ particles lead to the reduction in the TPB sites, improved electrochemical performance cannot be guaranteed in such anodes. Porous microstructure achieved by reducing the sintering temperature is also not acceptable as reduced contiguity among the constituent phases degrades electrical, electrochemical and mechanical integrity of anodes. Pores created due to the incomplete sintering might also provide room for the coalescence of Ni during the reduction, leading to excessive grain growth and major microstructural modifications on long term use in SOFC. Poor connectivity of YSZ component due to the reduced sintering temperature would compromise on the mechanical integrity of anode. Low temperature sintered anode might also lead to amplified anode over potential due to the bad anode/electrolyte contact. Hence, generation of porosity through the above mentioned methods are less recommended.

Alternatively, by altering the components and the composition of constituent's of fabrication process, additional porosity can be generated. For instance, by increasing the amount of gelling agent (such as urea-formaldehyde), increased amount of open pores can be achieved in the anode substrates fabricated by gel casting [67]. Relatively coarse pore channels with high gas permeability have been achieved in anode substrate by using coat mixed NiO/YSZ powders, instead of mechanically mixed powders [67]. Coat mix powders are the flowable powders obtained by agglomeration process by using higher amount of binder solution.

On the other hand, usage of a pore former is an alternative option, through which continuity of both phases (Ni and YSZ) could be achieved along with the retention of required level of

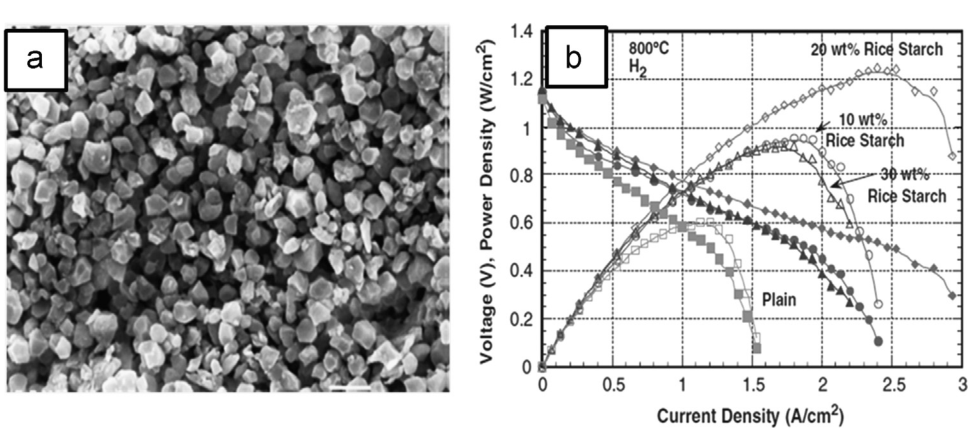


Fig. 10. (a) Micrograph of rice starch particles used as pore formers and (b) performance of single cells tested with different anodes that had rice starch as a pore former [66].

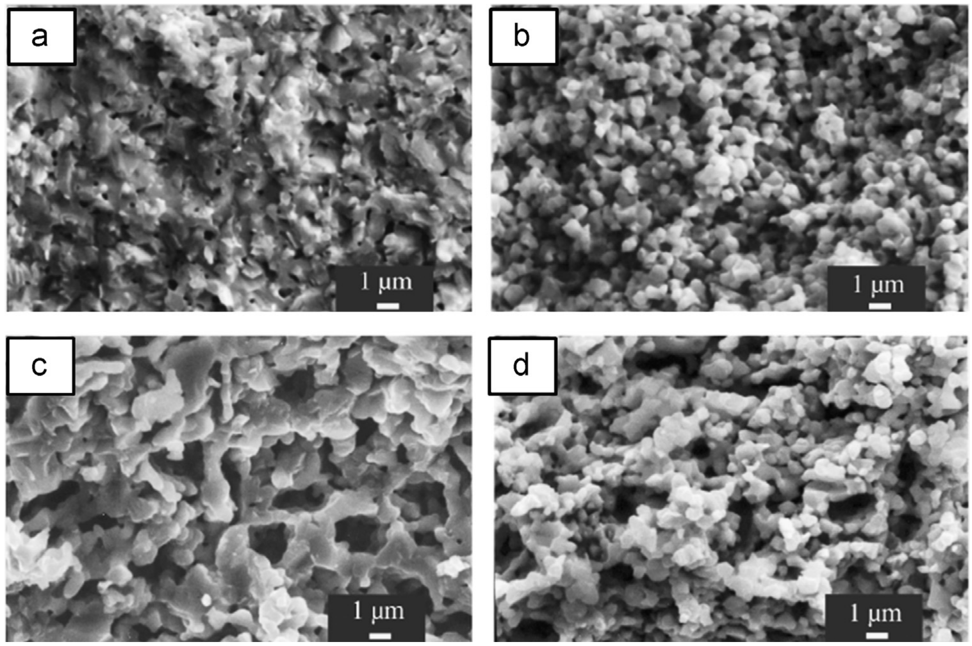


Fig. 11. Anode microstructures before and after reduction in hydrogen at 800 °C: (a) & (b) plain anode microstructure without any pore former and (c) & (d) 20 wt% rice starch pore former [66].

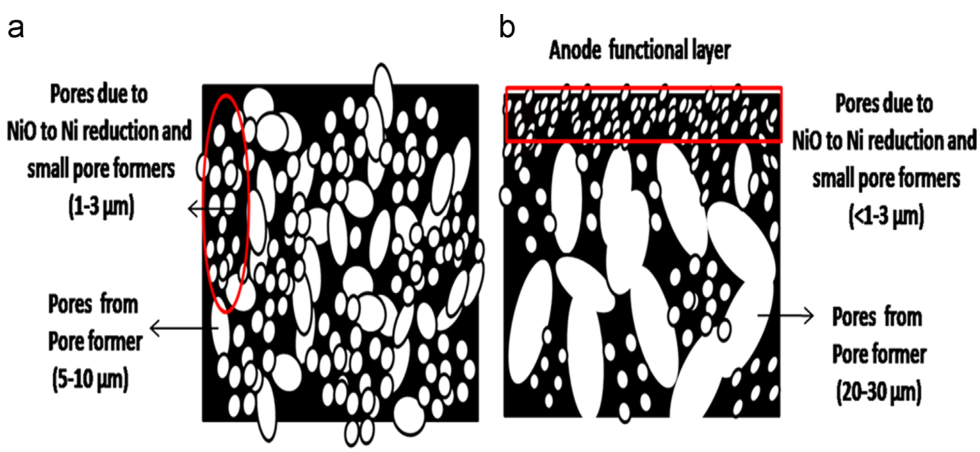


Fig. 12. Porosity distribution in (a) homogeneous mono-layered anode and (b) bi-layered anode.

porosity and pore size distribution. As a result, usage of pore formers has emerged as an effective way to tailor the porosity and minimize the polarization. These pore formers are often organic materials, which decompose to gases during heat treatment processes. These organic particulates are chosen such that they pyrolyze during the binder removal step, leaving stable voids that are not removed during the subsequent sintering process. Graphitic carbon [68], short carbon fibers, polymer spheres [69,70], flour [71], rice and starch [66,71], etc., are the pore formers that are generally being used in SOFC anodes. Criteria for selection of the pore former include particle size, decomposition with minimal residue at reasonably low temperatures, and compatibility with other materials in the anode. The effect of additional porosity produced by the pore former on the TPB areas is usually paid more attention. Other factors which deserve due consideration are: (1) electrical conductivity, (2) CTE that matches the other cell components, (3) a high degree of porosity to supply fuel and remove reaction products and (4) sufficient mechanical strength to support the cell. In addition, if the anode has to be co-sintered with the other cell components like electrolyte, influence of pore formers on the shrinkage and sintering characteristics of the anode, should also be taken into account. Small sized pore formers (<3 μm) such as activated carbon significantly influence the shrinkage (and consequentially sintering kinetics) and conductivity of anode when compared to the bigger sized pore formers such as flour, starch ($\sim$20 μm) [72]. Bigger pore formers adjust the porosity and resultantly increase gas diffusion more effectively.

Owing to the improved gas diffusion, reduction in the polarization resistance from 0.15 to 0.08 Ω cm^2 at 850 °C have been reported for mono-layered anode substrates added with 40 vol% corn starch as pore former. As increased gas diffusion, achieved through increased pore former amount, is not the sole criterion for enhanced performance; optimization of pore former amount is very essential. This optimum can be attributed to the consequence of trade off between increasing gas diffusion to the active TPB region of the anode and the loss of performance because of the replacement of active TPB regions of the anode with porosity. At lower %, pores generated due to the pore formers can be expected to form isolated islands and pores due to the reduction of NiO forming a link between those pores.

In such case, porosity generated due to the pore former would serve only as local gas reservoir and permeability of such anode

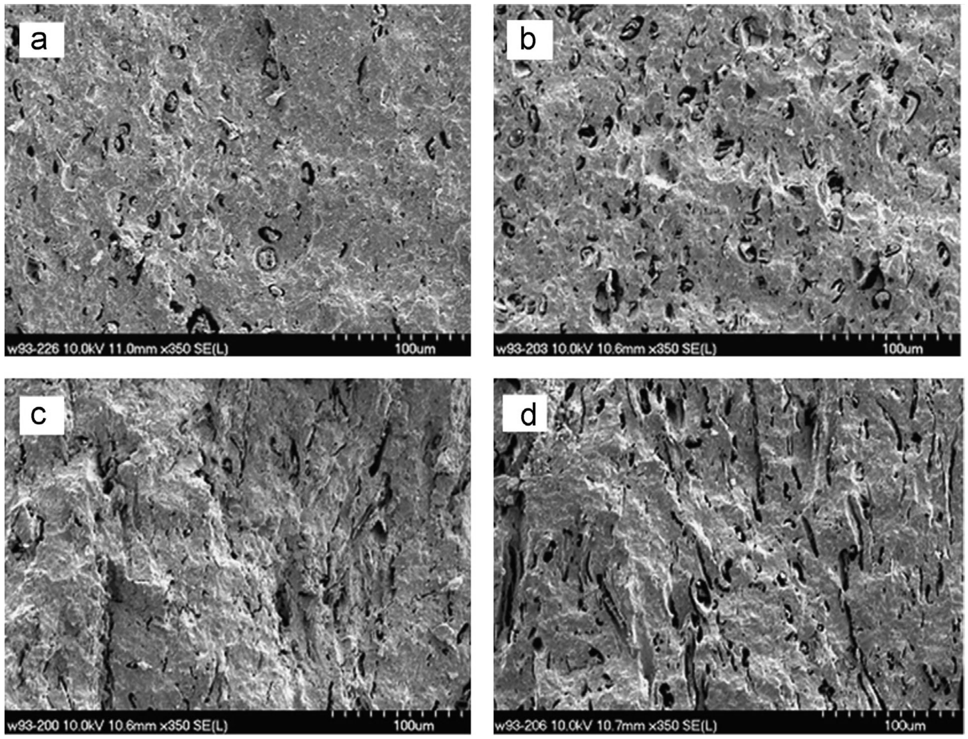


Fig. 13. Cross-sectional SEM images the anode substrates before reduction using (a) flour and (b) fibers as pore former [74].

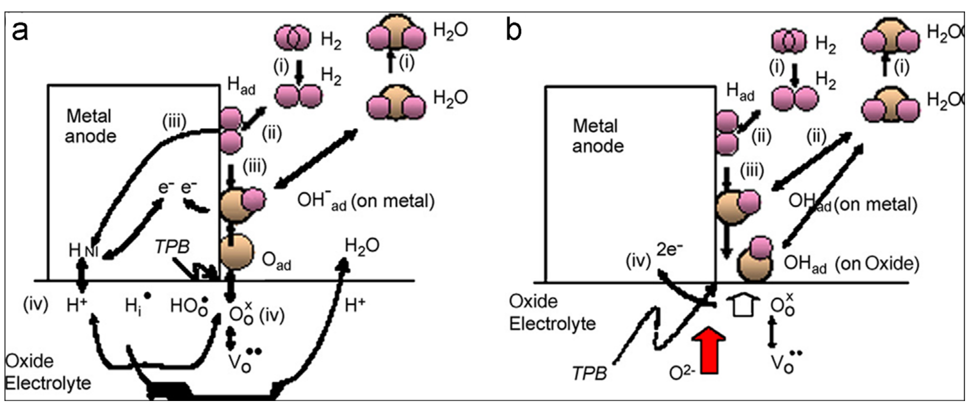


Fig. 14. Schematic diagram of possible reaction process for H_2 oxidation around the H_2 H_2O/anode/electrolyte interfaces [86]: (a) depicting the role of interstitial hydrogen and hydroxyl formation at the Ni/YSZ interfaces [79,84] and (b) showing two electrode process on the surface of Ni particles and a charge transfer process on zirconia electrolyte surface [2,77].

would not be superior to the pore former-free anodes. Hence, pores generated due to the pore formers have to result in continuous channels among themselves for them to be effective in providing the pathways for gas diffusion, especially at high power conditions. Highest performance observed in the case of anode added with 20 wt% of pore former (starch-particle size 4–5 μm) when compared to 10 and 30 wt% pore former added samples, might have stemmed due to the above reason [66] (Figs. 10 and 11). Similar observations have been made in the case of anodes added with flour as a pore former [71]. Optimum wt% of pore former corresponding to maximum power density would be different for different pore formers due to the differences in their density and corresponding difference in the vol% they occupy. In mono-layered homogeneous anodes, pore formers in the size range of 5–10 μm and wt% corresponding to ~30 vol% (where isolated pores are expected to become percolated pores) are generally added. In a bi-layered anode structure, bigger sized pore formers (20–30 μm) in higher quantity (to achieve porosity of 50–60%) are incorporated in to the anode substrate (Fig. 12b) [71].

If porosity level in the functional layer is required to be enhanced, smaller sized pore formers like activated carbon are added. Usage of nickel coated graphite particles to the tape casting slurry instead of separate graphite has resulted in a large amount of fine scaled porosity in the functional layer [19]. These samples consisted of finer scaled microstructure of Ni, YSZ and pores. On the contrary, graphite pore formers added separately resulted in larger sized pores to be appropriate to be used in a conduction layer.

Instead of single pore former, composite pore-former containing two or more pore formers in the different size range can be used to enhance the pore network and alter the shrinkage kinetics [71,73]. While bigger pore formers like PMMA, flour, etc., adjust the porosity effectively through the generation of stable and larger sized pores (> 5 μm), smaller pore formers like activated carbon

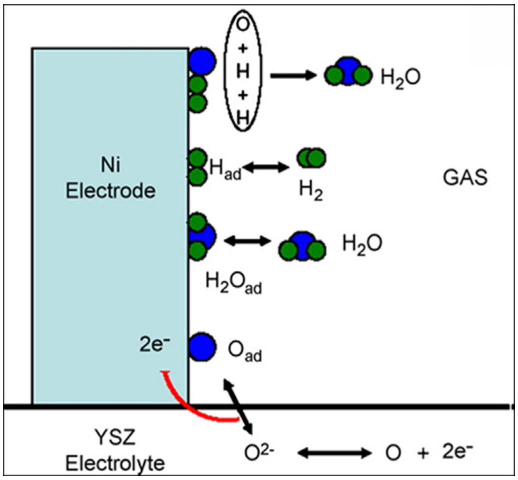


Fig. 15. Schematic diagram of the competitive adsorption mechanism on Ni/YSZ anode [87].

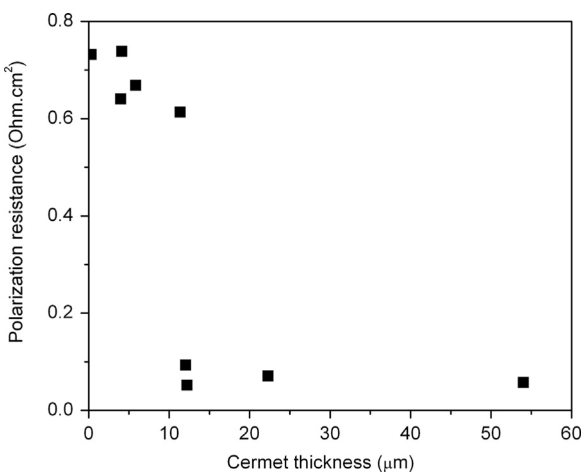


Fig. 16. Effect of anode thickness on the overall resistance of an anode [81].

tailor the shrinkage. In addition to adjusting the shrinkage, smaller pores (~1 μm) produced by small sized pore formers promote the increase in the TPB length. Amount of bigger pore formers has to be adjusted to a level where isolated pores begin to percolate to form a pore network channel.

Apart from overall open porosity, factors such as tortuosity of the pores and orientation of the pores should also be given due attention as tortuous path hinders the easy diffusion of the gas and pores that are oriented in the direction parallel to the anode/electrolyte interfaces are highly ineffective [75]. When compared to spherical shaped pore formers, anisotropic pore formers such as the graphite have greater tendency to get aligned in the direction parallel to the anode surface during the fabrication processes such as uni-axial pressing and tape casting, resulting in pores parallel to the anode/electrolyte interface, which is unwarranted [76]. By producing cylindrical gas channels aligned perpendicular to the anode/electrolyte interface on using pore formers such as paper fiber and employing appropriate fabrication technique, gas diffusion can be enhanced significantly (Fig. 13) [67,74].

3. Kinetics, reaction mechanism and models for Ni/YSZ anode

For the synthesis and development of an optimized Ni/YSZ anode material and the electrode, understanding the reaction mechanism and kinetics that occurs at the anode and elucidating structure–property–performance relationships is essential. Understanding requires extensive experimental investigation as well as the modeling.

Overall reaction occurring at the anode may be given as

$$O^{2-}\ (\text{electrolyte}) + H_2\ (\text{fuel gas}) \rightarrow H_2O\ (\text{product}) + 2e'(\text{anode})$$

Above reaction might occur through following steps:

1) Adsorption of H_2 on the surface of YSZ or Ni of anode.

$$H_2\ (\text{fuel gas}) \rightarrow H_{2ads}\ (\text{YSZ or Ni})$$

2) Surface diffusion of adsorbed H_2 to TPB

$$H_{2ads}\ (\text{YSZ or Ni}) \rightarrow H_{2ads}\ (\text{TPB})$$

3) Anodic electrochemical reaction

$$O_o^x(\text{electrolyte}) + H_{2ads}\ (\text{TPB}) \rightarrow H_2O\ (\text{product}) + 2e'\ (\text{anode}) + V_o^{\cdot\cdot}\ (\text{electrolyte})$$

On successful identification of the rate limiting step, electrode could be specifically designed to reduce or even to avoid the limitation.

In the last decade, numerous mechanistic theories have been proposed debating the different rate determining steps. That particular step might include, adsorption [31,77], surface diffusion [77–80], reactivity's and charge transfer [77–84], hydrogen desorption rates [23,78,81,85], catalytic effects of water [31], the role of the YSZ support [81], and others.

Any of the following steps, which might be involved in the Ni/YSZ anodic reaction, could be rate determining: (i) electronic conduction of Ni and ionic conduction of YSZ, (ii) surface adsorption (either on Ni or YSZ), (iii) surface diffusion of species (H_{ad}, O_{ad}, OH_{ad}^-) on anode surface or diffusion of H in the anode metal to the reaction sites, (iv) electrochemical and chemical reaction steps at the TPB, and (v) concentration polarization in the anode structure. The rate determining reaction process must be clarified to minimize anodic over potential and improve the performances of SOFCs.

There is a general consensus among different models with regard to the adsorption and to the desorption behavior of hydrogen as well as to the formation of hydroxyl. However, these models opine differently with regard to the following points: (i) location of chemical and the electrochemical reactions (either merely on the Ni surface or equally on the Ni and on the YSZ surface, respectively), (ii) reactions related to the interstitial oxygen in the YSZ, (iii) the adsorption and the desorption behavior of water, (iv) charge transfer step and (v) means of removal of oxygen from the YSZ. Oxygen becomes either adsorbed onto the YSZ surface, or it forms a hydroxyl interstitial, or a negatively charged hydroxyl on the Ni surface, or water is immediately formed without any intermediate step.

Possible role of interstitial hydrogen and hydroxyl formation at the Ni/YSZ interfaces, as suggested in the literature, are schematically shown in Fig. 14a. Some other groups found that hydrogen oxidation in Ni anodes is controlled by two electrode process on the surface of Ni particles and a charge transfer process on zirconia electrolyte surface (Fig. 14b). In the presence of H_2O, the adsorption of H_2O occurred preferably on the Ni surface, which forms OH–Ni as a reaction species. These schematic representations clearly suggest that reaction steps assumed to take place at the interface of metal anode, electrolyte, and gas phase indicating the important role of TPB in the kinetics of the hydrogen oxidation reaction.

Table 4
Summary of the active anode thickness reported in the literature and operating conditions adopted for the experiment.

Source	Particle size (μm)	Operating conditions temp. (°C)	Active thickness (μm), conclusions	Methods
[89]		1000, wet hydrogen	< 20	Experimental
[63]	NiO – 0.53 YSZ – 1.42	800	40–50	Experimental
[90]		700	20	Experimental
[71]	NiO – 0.6 YSZ – 0.2	800	20	Experimental
[91]	0.2 0.4 1.0		50 100 160	1D modelling
[92]	1.0		30–40	3D random resistor network
[93]			10–15	Numerical simulation from 3D microstructure reconstructed by FIB-SEM
[94]		800 600	10–15	Modelled using 3D structure reconstruction.
[57]			5–15 , depends on the over potential, temperature and the particle size	3D Monte Carlo packing of spherical particles

Langmuir reaction model proposed based on the studies related to the dependence of dc polarization and interfacial conductivity of Ni/YSZ cermet anode on the partial pressure of hydrogen is shown in Fig. 15. Model assumes the competitive adsorption equilibrium of H_2, H_2O, and O on Ni surfaces at the TPB and considers the rate-determining step to be Langmuir-type reactions of H_{ad} with O_{ad}.

Models pertaining to concentration polarization in anode propose that the polarization at high current density is dictated by two localized phenomena, namely, competitive adsorption and slow surface diffusion. Results suggest that future SOFC anode design improvements should focus on optimization of the reactive area, adsorption, and surface diffusion at the anode/electrolyte interface.

In summary, experimental observations and models cumulatively suggest that it is essential to have many such locations where H_2 molecules can be adsorbed and get incorporated into YSZ. Hence, the aim of microstructural engineering should be to maximize the number of active TPB's and the same can be achieved by increasing the thickness of the anode.

However, observations have shown that a pronounced decrease in the resistance occurs beyond a certain thickness of cermet anode and resistance remains unaltered on further increase in the thickness (Fig. 16) which suggests that active thickness of the cermet is very less and any thickness of cermet beyond this limit acts only as a current collector and does not participate in the electrochemical reaction [88]. The above constraint may be due to the low ionic conduction in electrolyte and the O^{2-} ions reaching the anode get readily reduced at the anode–electrolyte interface or within the short distance in anode without necessarily travelling deep inside the anode. It is essential to determine the active layer thickness for designing anodes with optimum characteristics. The values of effective electrode thickness reported in the literature have significant variation. Table 4 summarizes the active thickness of anode that is reported in the literature along with the operating temperature of the fuel cell, method adopted to measure the active thickness, etc.

All the experimental results suggest that active layer thickness is within 40 μm. Slight difference in the results for different electrodes can be attributed to the difference in the microstructure, composition and the temperature at which experiments are performed. Among the models, studies presented using 3D models match better with experimental observation when compared to 1D and 2D models. Increasing the anode thickness beyond a certain limit to enhance the TPB is futile as electrochemical reactions are confined to only few microns from the electrolyte–anode interface. An alternative strategy to enhance the TPB could be to use fine structured cermet. However, it would result in increase of concentration polarization due to the reduction in the pore size, especially in anode supported configuration, where thickness of anode lies in the range of ~1–2 mm. In an attempt to minimize both the concentration and activation polarizations, a two-layered anode structure and gradient anode have been envisaged, especially for the anode-supported cells.

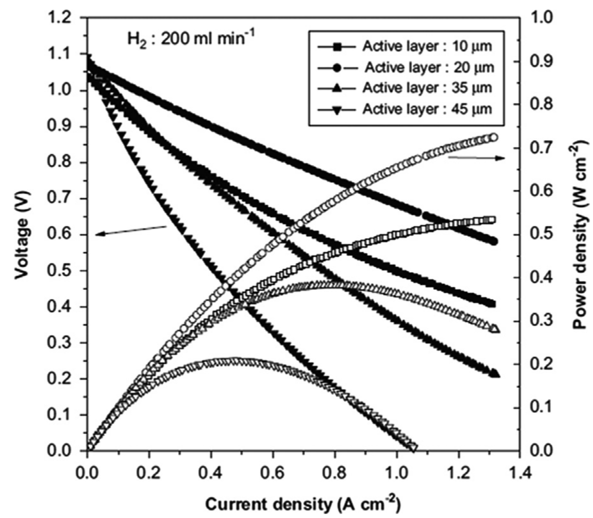


Fig. 17. Power characteristics of anode supported fuel cell as a function of active layer thickness in bi-layered anodes [90].

4. Bi-layer and gradient anodes

In recent times, it has increasingly been recognized that in the anode supported configuration, though thicker anodes are generally used (~1 mm); most of the electrochemical activity is confined to a thin layer near the electrolyte, generally termed as the anode functional layer (AFL) (< 50 μm). It means that a large portion of the anode is not participating in the electrochemical activity. To maximize the electrochemical activity, it is essential to achieve a fine microstructure in AFL with homogeneous distribution of Ni, YSZ and pores, i.e., maximization of TPB density. However, electrochemically idle part of the anode with similar microstructure will contribute to the concentration polarization.

Based on the above observation, to minimize concentration and activation polarizations, a dual-layered anode structure for the anode-supported SOFC has been proposed [95]. A dual-layered anode structure would consist of fine microstructured AFL fabricated onto the coarse anode substrate prior to the fabrication of an electrolyte layer [96]. The coarse anode substrate facilitates the rapid diffusion of fuel gas to the active reaction area and the removal of resultant bi-product out from the anode to mitigate the concentration polarization of an anode. The fine AFL maximizes the TPB length and minimizes the activation polarization of an anode.

In bi-layered structures, factors such as fabrication method, thickness, composition, level of porosity, etc., of each layer has to be optimized independently. Anode supported SOFC with

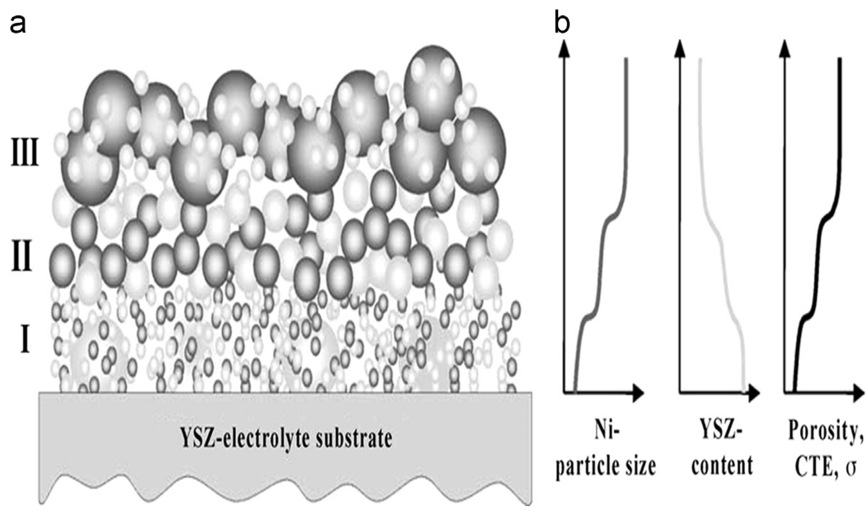


Fig. 18. (a) Illustration of a multilayer anode with gradients in composition and microstructure and (b) variation of physical properties of anode from electrolyte/anode interface to anode surface [101].

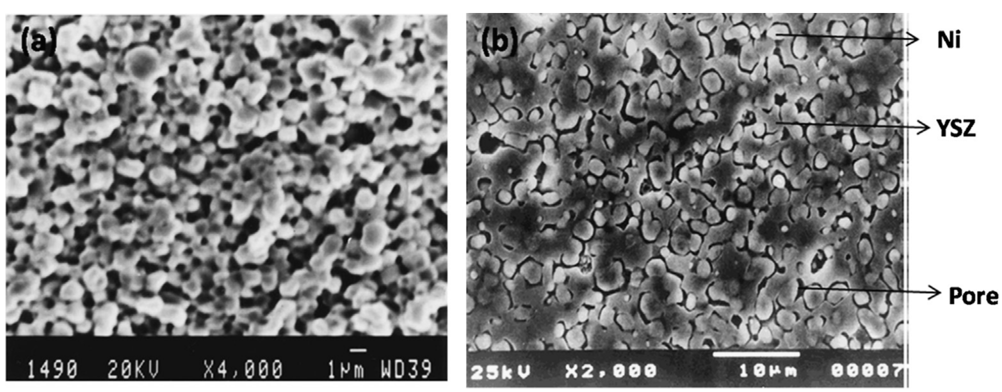


Fig. 19. SEM image of Ni/YSZ cermet prepared by solution combustion method by using: (a) carbohydrazide as fuel [116] and (b) glycine as fuel [117].

bi-layered anode can be easily fabricated by tape casting and co-firing [90]. Two independent methods can also be employed to fabricate substrate and functional layer separately. While simple methods like pressing can be used to fabricate substrates, functional layers can be prepared by wet powder spraying [97], dip coating, slurry spin coating [71], electroless technique [98,99], etc.

Due to counter active effects of TPB and permeability, maximum power can be expected to be achieved for the optimized thickness of active layer [63,71]. Functional layer thickness in the range of ~5–40 μm has been reported to be ideal for good performance. Further increase in the AFL thickness resulted in a decreased performance (Fig. 17). Apart from having fine microstructure and optimized thickness, it is advisable to restrict the amount of Ni in the functional layer to minimum required level to have better TEC and shrinkage compatibility between anode and the electrolyte and resultantly better adhesion. High power density (2 W/cm^2) achieved in the cells with AFL fabricated by electroless technique has been attributed to the better adhesion between anode and electrolyte due to the lower concentration of Ni in the functional layer [98].

In an effort to improve the overall performance of the cell further, graded anodes were envisaged, especially in anode supported configuration. In graded anode structure, factors such as Ni content, Ni particle size, level of porosity, pore size changes gradually from electrolyte/anode interface to anode surface and effectively gradient in the parameters such as conductivity, TPB, gas diffusion and TEC are achieved [100]. A model anode which preferentially fulfills the local requirements is schematically depicted in Fig. 18.

Like bi-layered anodes, gradient anodes can also be fabricated by hot pressing lamination of tapes containing varying amount of Ni, pore formers, etc. [93]. Fabrication techniques such as electrophoretic deposition [102], dry uni-axial pressing [103] have also been employed to fabricate a continuously graded anode layer. Though it is ideal to have gradation in all the parameters mentioned above to achieve good performance, reports of improved power density in the cells with gradation in one or two parameters can also be seen in the literature [103,104]. By varying the amount and size of the pore former and adjusting the particle size distribution in the NiO/YSZ ceramic, samples with gradually changing porosity have been fabricated. It was observed that gradient in pore size was more effective in improving anode performance than the actual porosity [104]. Porosity, conductivity and TEC parameters have also been varied by gradually varying the amount of Ni and particle size. Anode with optimum composition led to the good adherence of anode and electrolyte and consequentially resulted in low polarization resistance.

5. Synthesis of NiO/YSZ

In order to achieve high performance, long-term durability, and thermal/redox cycling stability, the process adopted for NiO/YSZ powder preparation should yield a homogeneous mixture of NiO

and YSZ with appropriate composition and size ratio. A major consideration in the synthesis of composite anode powders is the effect of the process on the powder morphology and phase distribution. In recent times, the selection of an appropriate method for the synthesis of anode powder has gained significant importance, especially after the advent of anode supported cell design [105]. The powder characteristics like agglomerate size, surface area, crystallite size, distribution of NiO and YSZ, etc., which ultimately affect the sintering characteristics and anode microstructure, are influenced by the methods adopted for the synthesis of the powder. Apart from the conventional mixing of NiO and YSZ powders, homogeneous NiO/YSZ cermets have been directly synthesized by many methods. In this section, important synthesis methods that have been used for the preparation of NiO/YSZ anodes are discussed.

5.1. Mechanical processing

Owing to the convenience and the ease of commercialization, NiO/YSZ anode materials are usually prepared by mechanical mixing of NiO and YSZ powders [106]. If necessary, both NiO and YSZ are subjected to an additional processing step, such as coarsening, prior to the mixing. Either planetary or attrition milling can be used for the synthesis of the composite [107]. High shear and compression force exerted during the milling results in the intimate mixing of fragmented particles. Due to the associated high energy, attrition milled powder would consist of smaller particles with sharper size distribution when compared to the ball milled powder and thus results in enhanced electrochemical activity with smaller polarization resistance and long-term stability [108]. Mechano-fusing of the NiO and YSZ sometime results in a powder consisting of fine NiO powder partially covered YSZ fine particles. Such a configuration successfully prevents the growth of NiO powder during the sintering process [109].

Despite of many favorable advantages, the main drawback of mechanical mixing, however, has been the non-uniform distribution of the Ni phase in cermets, leading to poor performance. On the contrary, different wet chemical processes, which allow for the precursor mixing in molecular level, often result in the homogeneous mixing in the crystallite level and hence lead to the superior performance.

5.2. Combustion synthesis

Combustion synthesis is a versatile and simple method employed for the synthesis of ultrafine ceramic powders with a small average particle size and high porosity. It takes advantage of the large exothermicity ($1500 < T < 3500$ °C) of reactions propagating in a self-sustained manner at a relatively high speed (0.1–10 cm s^{-1}). Combustion method possesses some unique characteristics particularly useful for the synthesis of composite materials [110–115]. In regard to NiO/YSZ cermet mixture, high surface area powders with intimately mixed NiO and YSZ could be prepared by combustion reaction.

The powder characteristics like crystallite size, surface area, extent and nature (hard or soft) of agglomeration of the powder

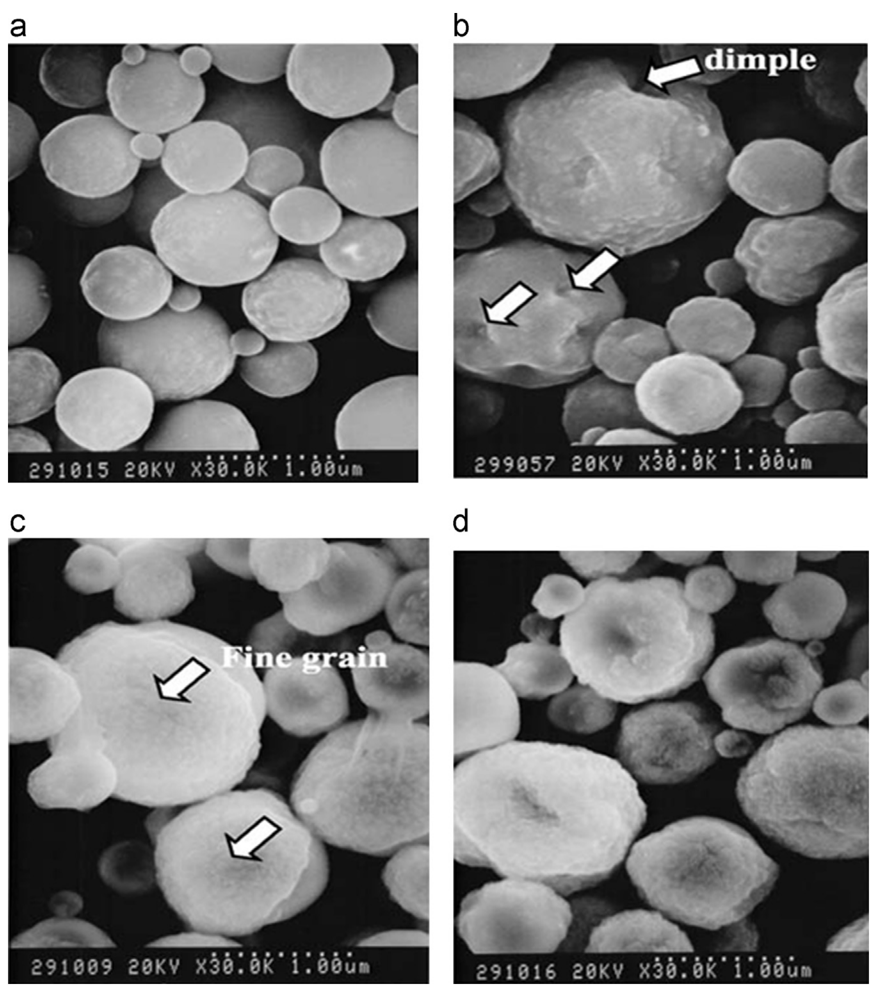


Fig. 20. SEM images of NiO/YSZ composite particles fabricated at (a) 200 °C, (b) 300 °C, (c) 400 °C and (d) 1000 °C in the spray pyrolysis process [126].

produced by combustion synthesis are primarily governed by the enthalpy or flame temperature generated during combustion, rate of combustion and gases evolved during the reaction, which in turn is dependent on the nature of the fuel and oxidizer to fuel (O/F) ratio. Hence in combustion synthesis, the fuel and O/F ratio need to be carefully chosen to achieve powders with desired characteristics. For instance, on using carbohydrazide as the fuel in solution combustion synthesis, powders with high surface area (27–32 m^2/g) with small agglomerates ($\sim$0.25–0.8 μm) consisting of smaller crystallites ($\sim$5–15 nm) were obtained [116]. Resultant Ni/YSZ cermet had a fine distribution of Ni, YSZ and pores (Fig. 19a). Absence of any Ni growth during the reduction could be attributed to the homogeneous distribution of NiO and YSZ. On the other hand, while using glycine as a fuel, powders with decreased surface area (15–18 m^2/g) were obtained [117]. Resulting Ni/YSZ consisted of 3–5 μm Ni metal particles encapsulated by a pore space and YSZ skeleton. For the same fuel, crystallinity of the powder improves and surface area decreases with increase in the amount of the fuel used [118]. Powders with agglomerated particles and smaller surface area are produced when high temperature is attained during short combustion time. Fine powders with large surface area are produced when the combustion reaction is sluggish and less vigorous [119].

Citrate/nitrate gel combustion is an appropriate alternate method to the solution combustion to prepare sub-micron sized NiO/YSZ powder [120,121]. In the gel combustion, initial citrate/nitrate molar ratio critically influences the prepared powder characteristics. Dense NiO/YSZ has been achieved at temperatures as low as 1200 °C using soft agglomerated gel combustion synthesized powder. Small crystallites were retained even after sintering and reduction (Ni size $\sim$0.2 μm) and high contiguity was achieved (Fig. 19b). Usage of such powders in the fabrication of AFL component would result in the large number of TPB's and the cells with superior performance. Agglomerated powders with coarse features produced during the combustion may be ideal for the fabrication of anode substrate.

5.3. Precipitation

Precipitation is a promising and facile chemical route that is often used to prepare oxide powders with less agglomeration. In precipitation process, it is essential to find out the exact pH value at which precipitation occurs [122]. The resulting precipitate is filtered, washed and fired at higher temperature if necessary. In the precipitation synthesis, pH of the medium influences the powder characteristics to a great extent. While highly basic solutions have been reported to result in fine powders ideal for functional layer and solutions with lower pH resulted in coarse powders suitable for anode substrate [16]. The gel-precipitation method is an attractive alternative for the preparation of Ni/YSZ cermet. In the gel-precipitation method, powder characteristics are affected by precipitating agents used during the process [123]. For instance, on using NH_3–NaOH as the precipitating agent, powders with narrow particle size distribution and with homogeneous dispersion of NiO within YSZ were achieved. This translates into an enhanced TPB. The synthesis with NaOH as the precipitating agent yielded powder with uneven dispersion of NiO. Though electrical conductivity of Ni/YSZ (NaOH) sample was higher, TPB in these samples can be expected to be lower.

5.4. Spray pyrolysis

Spray pyrolysis is an effective synthesis method that leads to fine and homogenous anode composite powders [124]. Spray pyrolysis apparatus consists of an atomizing chamber with an ultrasonic vibrator for producing droplets of the starting materials from the solutions of corresponding metal salts [125]. Droplets are conducted to a reactor, with air as the carrier gas. During the spray pyrolysis, the solution is atomized into a series of reactors where the aerosol droplets undergo evaporation and solute condensation within the droplet. The drying and thermolysis of the precipitate particle at higher temperatures forms a microporous particle. Finally, sintering of the microporous particle forms a dense particle. Spray pyrolysis generally leads to spherical, non-agglomerated, submicrometer particles. Formation of composite NiO/YSZ particles takes place through the evaporation, thermolysis and sintering stages [126]. At first, an atomized droplet containing Ni ion and dispersed YSZ sol goes through the evaporation stage at temperatures up to 200 °C. Subsequently, a filled particle with both $Ni(CH_3COO)_2$ and YSZ fine grains is formed by volume precipitation. Next, during the thermolysis stage and at temperatures up to 400 °C, YSZ grains are almost organized on the surface of the particle by the out gassing and oxidation of $Ni(CH_3COO)_2$, and a particle covered with YSZ grains forms. Finally, the dense composite particle, which has NiO grains covered uniformly with fine YSZ grains, is successfully formed by NiO grain growth during the sintering stage [109,126,127] (Fig. 20). Such a microstructure is expected to increase the TPB's length and successfully prevent the Ni grain growth, resulting in a stable long-term SOFC operation.

5.5. Pechini process

NiO/YSZ powders with particle sizes ranging from hundreds of nanometers to several micrometers can be synthesized by modified Pechini-type sol–gel method [128–130]. Chelating agents used in the process have strong influence on the thermal decomposition of gels and on the morphology of final products.

Homogeneously dispersed Ni in a YSZ ceramic matrix have been obtained by employing modified pechini method in which YSZ, $Ni(NO_3)_2\cdot 6H_2O$, ethylene glycol and citric acid were used as a starting materials [131]. YSZ powder was added to the polymeric gel containing Ni^{2+} cations leading to an organic resin in which the YSZ particles are embedded. By further heat treatment a composite of ultrafine nickel oxide dispersed in the YSZ matrix was attained. After sintering and reducing treatment of nanocrystalline NiO/YSZ composite, the microstructure of the Ni/YSZ cermet showed a uniform distribution of the porous metallic Ni particles of about 1–2 mm surrounded by a microporous space.

Pechini process has also been used to synthesize NiO-coated YSZ, NiO and YSZ co-conjugated mixture on YSZ powder [132]. The configuration of the powder on the surface is porous (porosity > 41%) consisting of primarily nano-sized (10–30 nm) NiO and YSZ co-conjugated or NiO ($\sim$30 nm) on YSZ particles ($\sim$300 nm) (Fig. 21). Cermets with such a configuration had necessary electrical conductivity, durability and improved performance. Core YSZ provided the necessary structural stability and conjugated NiO/YSZ resulted in improved performance.

5.6. Electroless technique

Electroless method of preparing cermet Ni/YSZ results in a core–shell structure with YSZ as core and fine Ni particulates as shell. Preparation of Ni/YSZ powder by electroless technique involves an initial sensitization process of the YSZ particulates followed by an in situ reduction of Ni^{2+} to Ni and its corresponding deposition onto sensitized YSZ. The amounts of Ni required for completely covering the YSZ surface will depend on the YSZ particle size. Owing to the unique microstructure, percolation threshold in the anode prepared by electroless technique are reported to be low [133–136](Fig. 22).

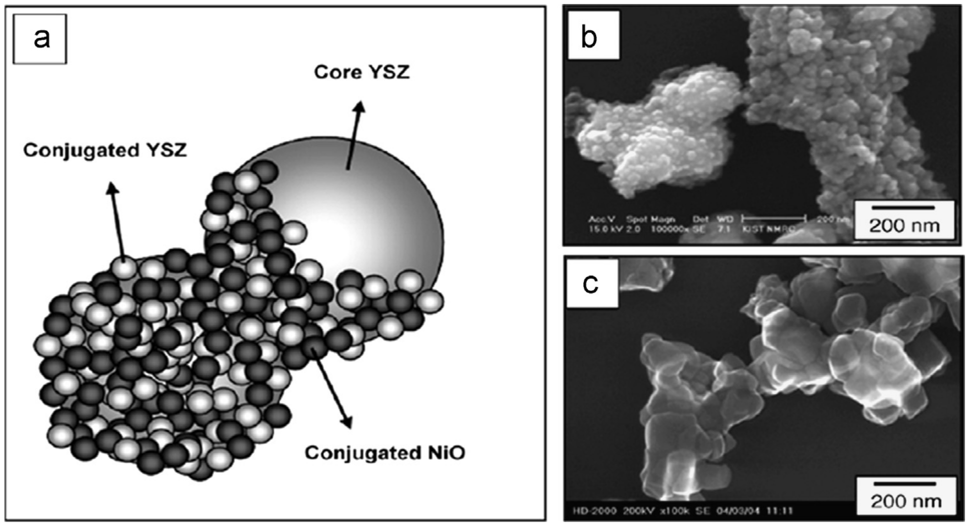


Fig. 21. (a) Schematic diagram of the dual composite powder, (b) SEM image of the dual composite powder which is composed of nano-sized NiO and YSZ co-conjugated on YSZ particle, and (c) SEM image of the commercial YSZ core material of the dual composite powder [132].

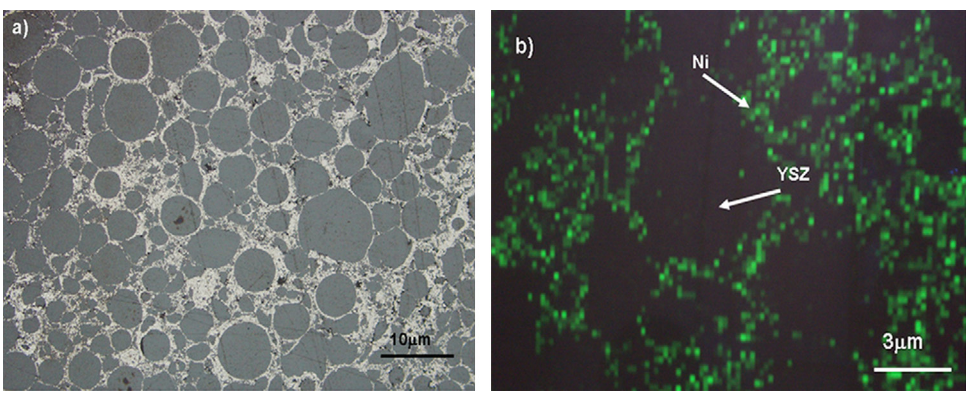


Fig. 22. (a) Optical micrograph of polished Ni–YSZ surface (33 vol% Ni) prepared by electroless technique and (b) corresponding Ni-mapping of the selected area [133].

Table 5
Commonly used components in the tape casting.

Solvent	Binder	Plasticizer	Dispersant
Methyl ethyl ketone (MEK), Ethanol, Butanone, Toluene, Water	**Polyethylene glycol (PEG), Poly vinyl alcohol (PVA), Polyvinyl butyral (PVB)**	**Dibutyl *o*-phthalate, Benzyl butyl, Phthalate**	**Triethanolamine, Glycerine trioleate, Glycerol trioleate, fish oil**

6. Fabrication of NiO/YSZ anode component

Fabrication process of the anode component varies depending on the geometry (planar or tubular) and the configuration (anode, cathode or electrolyte supported) of the cell. In the anode supported configuration, thicker anode substrates (in the ~mm range), which serves both as mechanical support and electrochemical active layer, need to be fabricated. Whereas, in the cathode and electrolyte supported configuration, maximum thickness of the anode component is ~200 μm. As mentioned in the previous section, microstructure requirement of anode in these configurations is also different. Accordingly, suitable fabrication method needs to be adopted [137].

6.1. Anode supported cell

6.1.1. Anode substrate

6.1.1.1. Planar SOFC. Various techniques have been explored and investigated in the fabrication of porous anode support substrates for the state-of-the-art anode-supported planar SOFC based on Ni/YSZ cermet. These techniques include die-pressing, tape-casting, gel casting, etc.

6.1.1.1.1. Die pressing. The dry pressing process is a simple and cost-effective method, and has been widely used to make parts thicker than 0.5 mm. Pressing methods might include cold, warm, hot, cold-isostatic (CIP) or hot-isostatic pressing (HIP). Compared to tape casting, the main disadvantage of pressing technique is the discontinuous and time consuming overall operation. This method is however still used when thick substrates need to be fabricated and in the fabrication of the button cells at laboratory level [63,138]. For the fabrication of the substrate by pressing, a pre-conditioned powder mixture known as "coat-mix powder" is used. On sintering and reducing the anode substrates prepared by coat mix powders, relatively coarse pore channels with high gas permeability are obtained. These coarse channels supply gas to the pores generated by the reduction of NiO into Ni.

6.1.1.1.2. Tape casting. Tape casting is a well established industrial process to make large and flat ceramic tapes, plates and laminated ceramic structures, and thus is suitable for the fabrication of porous anode substrate in anode-supported planar SOFC.

In the tape-casting process, NiO/YSZ slurry containing a dispersing agent, a polymer binder, required amount of pore formers and a plasticizer is used to prepare thin flexible green tapes using a doctor blade. Dried substrate, cut into required geometries, is pre-sintered to remove the binder and the pores formers and subsequently functional layer or other components of SOFC are applied. Alternatively, green anode tape can be applied with layers of the other components (for instance, electrolyte) and co-fired. Typically, 1–2 mm thick tape casted anode layer and 40–100 μm thick tape cast electrolyte layer are produced and these two tapes are laminated and after rolling or calendaring, the green laminates are cut to required size and sintered at 1400 °C [139,140]. For almost all anode-supported planar cells the substrate is now mostly manufactured by tape casting [141–143]. Different components that are generally used in the tape casting process are summarized in Table 5.

6.1.1.1.3. Gel casting. Gelcasting is a process used for the preparation of near-net-shape bodies from concentrated ceramic powder suspensions by setting them in a mould containing a pre-mixed monomer and cross-linking solution [144–146]. Gelcasting is a forming technique with many advantages such as low cost, good product homogeneity and high green strength [146]. With heating or addition of a catalyst, cross-linking polymerization occurs to form a three-dimensional network structure, and the slurry is solidified in-situ, to form ceramic objects of the desired shape. In this process, slurry with a high solid loading is obtained by dispersing the ceramic powders in a pre-mixed monomer and cross-linking solution. With heating or addition of a catalyst, cross-link polymerization occurs to form a three-dimensional network structure, and the slurry is solidified in-situ, to form ceramic objects of the desired shape. Recently, gel casting has gained attention as a new method in the fabrication of electrode-supported substrates for SOFCs [147]. Organic monomers such as acrylamide and urea–formaldehyde have been widely used for gel casting of aqueous ceramic powder suspensions. Polymers present in excess generally act as template for pore formation.

6.1.1.2. Tubular SOFC. Several methods, such as slip casting, iso-static pressing, gel casting, extrusion [148,149], are being used to fabricate tubular substrate in anode supported SOFC. Iso-static pressing offers a high and well-distributed product-forming pressure but the throughput rate is low and hence sometimes used to fabricate micro-tubular cells. Among all these processes, the extrusion technique is most suitable process for mass production and is widely used.

6.1.1.2.1. Extrusion. Extrusion is used in the ceramic industry whenever a continuous structure with an elongation in one direction is required. In extrusion, shaping occurs by forcing a cohesive plastic material through the orifice of a rigid die of the desired cross section. For extrusion, the powders are usually mixed with water-based plastics. During extrusion process, water-soluble binders such as methylcellulose, polyacrylamide, polyvinyl alcohol, etc., are added. Extrusion slips have extremely high viscosities in the range of 1000 Pa s. After extrusion, the tube is cut into the desired length by wire-cutting. For SOFC fabrication, anode substrate is usually de-bindered/prefired and subsequently coated with functional layers, electrolyte and sintered at high temperature (1400 °C) [150]. Up to meter long tubular substrates with a diameter of 10 cm have been fabricated by the extrusion process.

6.1.1.2.2. Slip casting. Though not as extensive as extrusion process, slip casting process has been used by many groups, at least at laboratory level, for the fabrication of tubular anode substrates, especially micro-tubular. To begin with, a plaster mould having a tube shaped cavity is fabricated. Anode suspension is then continuously poured into a porous plaster mould until the required anode layer thickness is reached. Anode tube is formed with the absorption of liquid in the suspension by the intimate contact mould. On drying, the green layer shrinks and separates from the plaster wall and can easily be removed from the plaster mould. Subsequent YSZ electrolyte membrane deposition can be done on the tube pre fired at higher temperature. However, the drawback of employing slip casting method for tubular substrate is that it might result in varied compaction along the length [151,152].

6.1.2. Anode functional layers in anode supported configuration and anode coating in the cathode/electrolyte supported configuration

Techniques involved in the fabrication of anode functional layers in the anode supported configuration and for anode coatings for cathode/electrolyte supported cells are generally the same, though microstructural and compositional requirements of these coatings are slightly different. Desired microstructures in each case are achieved by choosing the starting powder with appropriate composition, particle size, organic content and the amount of the pore formers.

6.1.2.1. Screen printing. Screen printing paste generally consists of ceramic powder, a binder (e.g. ethyl cellulose or methyl cellulose) and a solvent (e.g. terpineol). Typical powder loading is in the range of 60%. Viscosities of the paste are generally in the range of few Pa s and the rheological behaviour of the slip possesses special time dependence [153,154]. The paste is pressed through a screen by a squeegee. On being pressed through the mesh, the paste must flow, and after removing the screen from the substrate to be coated, the paste must fill the remaining channels formed by the chaining and weft thread of the screen. After filling the cavities, the paste must stop flowing to ensure the dimensional accuracy of the layer. After sintering, screen-printed layers have thicknesses ranging from 5 to 100 μm.

6.1.2.2. Wet powder spraying. In wet powder spraying (WPS), a stable suspension of NiO/YSZ is sprayed on to the NiO/YSZ substrate, dried and subsequently fired at 1400 °C. The slurry is placed into an air-spray gun with a continual supply of compressed air to aid in the mixing of the cermet while spraying. Depending on the spraying equipment, viscosity of the spraying mixture needs to be fixed in the range suitable for spraying. Stable and homogeneous suspension of the powder is generally obtained by high energy milling assisted by ultrasonication of the powder in a suitable solvent along with appropriate dispersant, binders and additives. Suspension is considered to be stable if no powder settlement is observed even hours after milling. Contrary to screen printing, WPS can be employed to spray on non-uniform or non-planar geometries. The quality of the spray stream, which decides uniformity, homogeneity and thickness of the coating, depends on the suspension rheology, spray velocity, the distance and angle between the air-brush nozzle and the substrate, and the number of passes. Ethylene glycol or ethanol is generally used as a solvent. Binders used are generally ethyl cellulose or polyvinyl butyral. WPS is specially suited for tubular geometry [155,156].

6.1.2.3. Dip coating. In dip-coating process, the substrate to be deposited is dipped into a liquid solution containing the powder and withdrawn from the solution at a controlled speed. The thickness of the coating is primarily affected by fluid viscosity, fluid density, and surface tension and the withdrawal speed. Thickness of the layer can be increased by repeating the dip coating by curing the previous layer. Coating may be cured by

variety of means including conventional thermal, UV, or IR techniques depending on the coating solution formulation. Once the desired thickness is achieved, the coating can be dried and fired at desired temperature. In addition to being a simple fabrication process, dip coating process can be applied to both planar and tubular geometry. The major parameters during dip-coating are the suspension viscosity the time of coating, the powder loading of the suspension, the coating temperature and the speed with which the part is moved through the suspension. Normally, it is easier to coat porous substrates (such as SOFC anode) because of the capillary forces which support the adhesion of the coating than to coat dense structures. Suspension for dip coating of NiO/YSZ contains the following constituents: NiO/YSZ powder, organic vehicle, and a solvent. Constituents of organic vehicles are generally plasticizer, dispersant and binder [96,157]. Generally used chemicals for each constituent are given below.

Solvent: Ethanol, azeotropic mixture of butanone and ethyl alcohol, azeotropic mixture of toluene and ethanol, isopropanol, azeotropic mixture of toluene and ethanol
Plasticizer: Terpinol, polyethylene glycol, phthalates
Dispersant: Triethanolamine, fish oil
Binder: Ethylcellulose, polyvinyl butyral

Ball milling followed by ultrasonic assistance is generally applied to obtain a stable suspension. Viscosity in the range of 5 mPa s is generally used for dip coating.

6.1.2.4. Plasma spraying. Plasma spray (PS) processing is a promising method for the deposition of the anode coatings because of its high deposition rate, cost effectiveness, and flexibility for automatic production [158–160]. In metal supported SOFC, PS is used to deposit anode functional layer on the top of the metallic anode. In plasma spraying, coatings are fabricated by injecting the stock powders into energetic plasma flow. Coatings are developed by the successive stacking of thin lamellae formed by the impact of molten or softened droplets on a substrate followed by flattening, rapid cooling and solidification processes. Typically a powder with an agglomerate size in the range of some tens of micrometers (~50 μm) is used. In addition to the spray operating conditions and the mode of feedstock injection into the energetic plasma flow, structure and properties of plasma sprayed coatings are known to be critically dependent on the feed stock powders characteristics. The most commonly used powder processing methods for the production of stock powders is spray drying (SD). Normally, thickness of plasma sprayed coating is generally between ~40 and 300 μm. Porosity in the plasma sprayed coating can be generated either by optimizing the spraying conditions or by including the pore former such as graphite in the stock powder. NiO/YSZ powders ball milled along with the graphite powders are agglomerated by the processes such as spray drying or coat mix to produce plasma sprayable powders. Instead of using graphite powders independently, graphite coated nickel can be used to produce fine porosity in the plasma sprayed coatings [161–164].

Table 6 summarizes the ceramic coating technologies, typical layer thicknesses and their industrialization status.

Table 6
Typical ceramic coating technologies used in the fabrication of anode functional layers in anode supported configuration and anode coating in the cathode/electrolyte supported configuration.

Technique	Film thickness (after sintering)	Industrialization status
Screen printing	5–100 μm	Established
Wet powder spraying	5–100 μm	Established
Dip-, spin coating	2–10 μm for powder-based and 10 nm–2 μm for sol–gel-based	Lab scale
Atmospheric plasma spraying	50–500 μm	Under development

7. Degradation in Ni/YSZ

Structural and long-term performance stability of Ni/YSZ cermet is a critical issue in the development of SOFC anode. Degradation problems in long term operation of SOFCs are characterized by a gradual decrease in performance of the fuel cell systems, measured by the percentage of increased over potential or decreased cell potential, over a certain period of operation. On using H_2 as a fuel, degradation in Ni/YSZ might occur through phenomenon such as redox cycling and nickel coarsening. Degradation in anode could be in its electrochemical, electrical and mechanical properties or a combination of them. Apart from the above mentioned phenomenon, while using hydrocarbon as the fuel, Ni/YSZ anodes undergo degradation through carburization and sulfidation also. Phenomenon of carburization and sulfidation are discussed in the next section.

7.1. Redox instability

Redox instability refers to the chemo-mechanical instability of the SOFC anode under oxygen partial pressure variation of more than 20 orders of magnitude during reduction and oxidation (redox cycle). On a long term operation, SOFCs are expected to

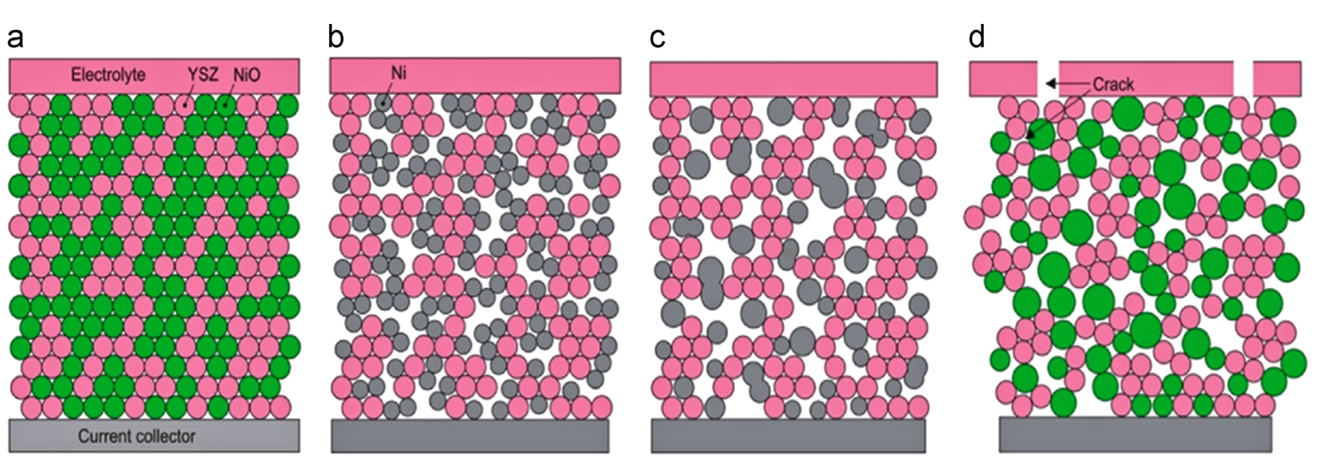


Fig. 23. Microstructural changes during a redox process in cermet anodes [166]. (a) As-sintered state, (b) Short-term reduced state, (c) Long-term reduced state and (d) First re-oxidized state.

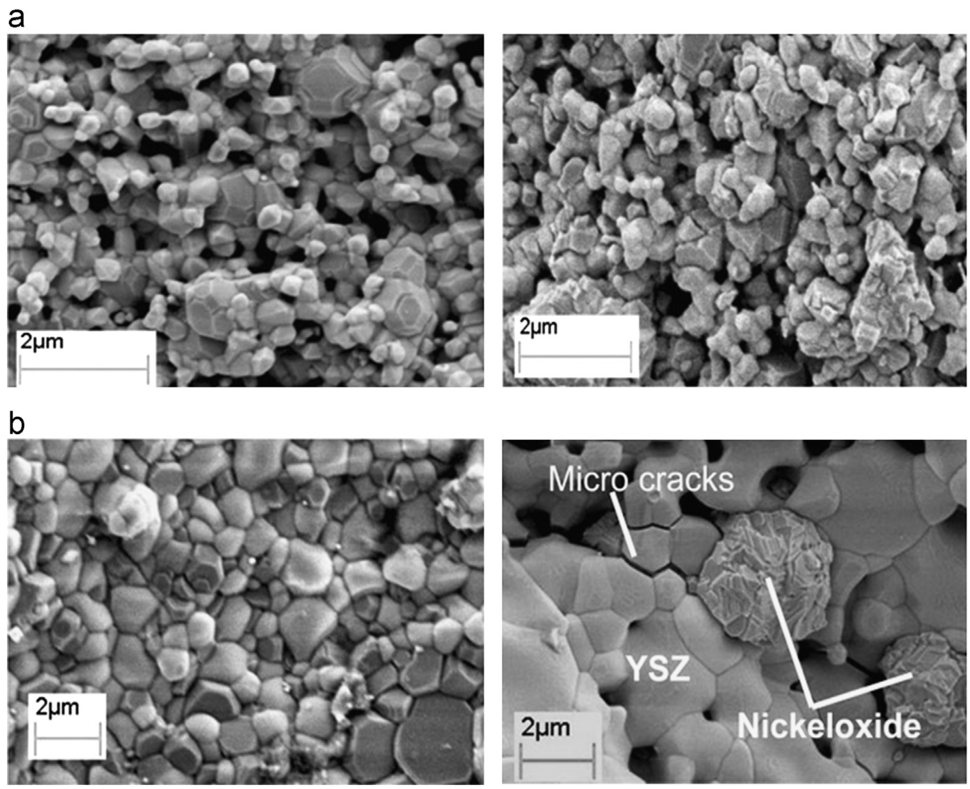


Fig. 24. NiO (0.5 μm)/YSZ (0.2 μm) anode sample (58.7 wt% NiO) sintered at (a) 1200 °C and (b) 1400 °C (oxidized). Left: before redox cycle, right: after passing through 4 redox cycles [175].

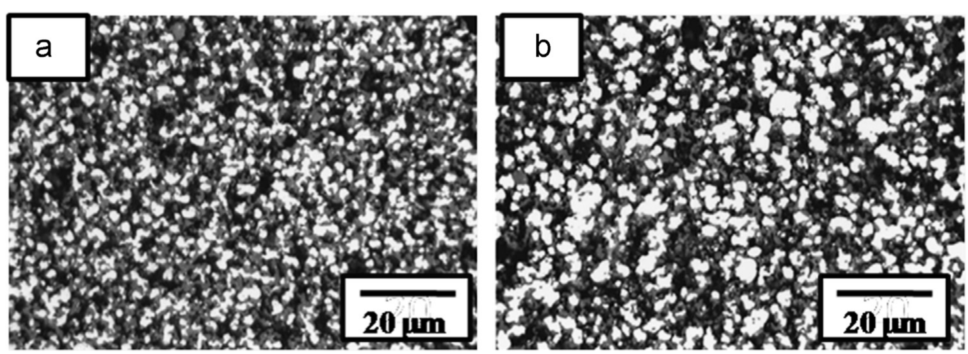


Fig. 25. Microstructure of anode cermet after reduction (a) and after an exposure for 4000 h in Ar/4% H_2/3% H_2O at 1000 °C (b) [205].

go through several such redox cycles. On uninterrupted supply of fuel, Ni would continue to remain in metallic form and anode would be maintained in a reduced state. However, if the fuel supply gets interrupted due to some reasons, oxygen will continue to pass through the electrolyte, or through the imperfect seals, and oxidize Ni to NiO. Oxidation of the anode can also occur if H_2O content in fuel and fuel utilization are high. Based on their molar volumes, the oxidation of Ni to NiO is accompanied by an increase of solid volume by 69.9%. Subsequent restoration of the fuel will convert NiO back to Ni, but the original state of anode is not generally recovered. The volume changes thus developed during successive redox cycles is detrimental for the anode unity and cell integrity. This expansion has three origins: (1) the reorganization of the metallic nickel during operation, (2) the fast oxidation kinetics of the nickel at the operating temperature and (3) formation of intra particles pores in NiO during the oxidation process. Redox strain thus developed are reported to be sensitive to many factors like Ni content, ratio of NiO and YSZ particle sizes, porosity, sintering temperature, oxidation temperature, and oxidation environment. Expectedly, when compared to electrolyte supported cells, redox cycle degradation effects are more severe in anode supported SOFC due to the larger dimensions of anode.

General observations with regard to the redox cycling are provided in the beginning of this section. Its influence on the microstructure, electrical, electrochemical and mechanical properties are provided in the subsequent section in detail. Approaches adopted to minimize the redox instability are provided at the end of the section.

7.1.1. General observations on redox cycle

Single redox cycle experiments on NiO/YSZ anodes (56 wt% NiO, 44 wt% of YSZ) at 1000 °C have shown a significant volume increase (3–9%) on re-oxidation [165]. It was suggested that simultaneous to the reduction, coalescing and sintering of Ni takes place, leading to a network of coarser particles in anode, which otherwise had a very fine distribution of NiO in YSZ. In such cases, local volume changes upon re-oxidation would be too great to be

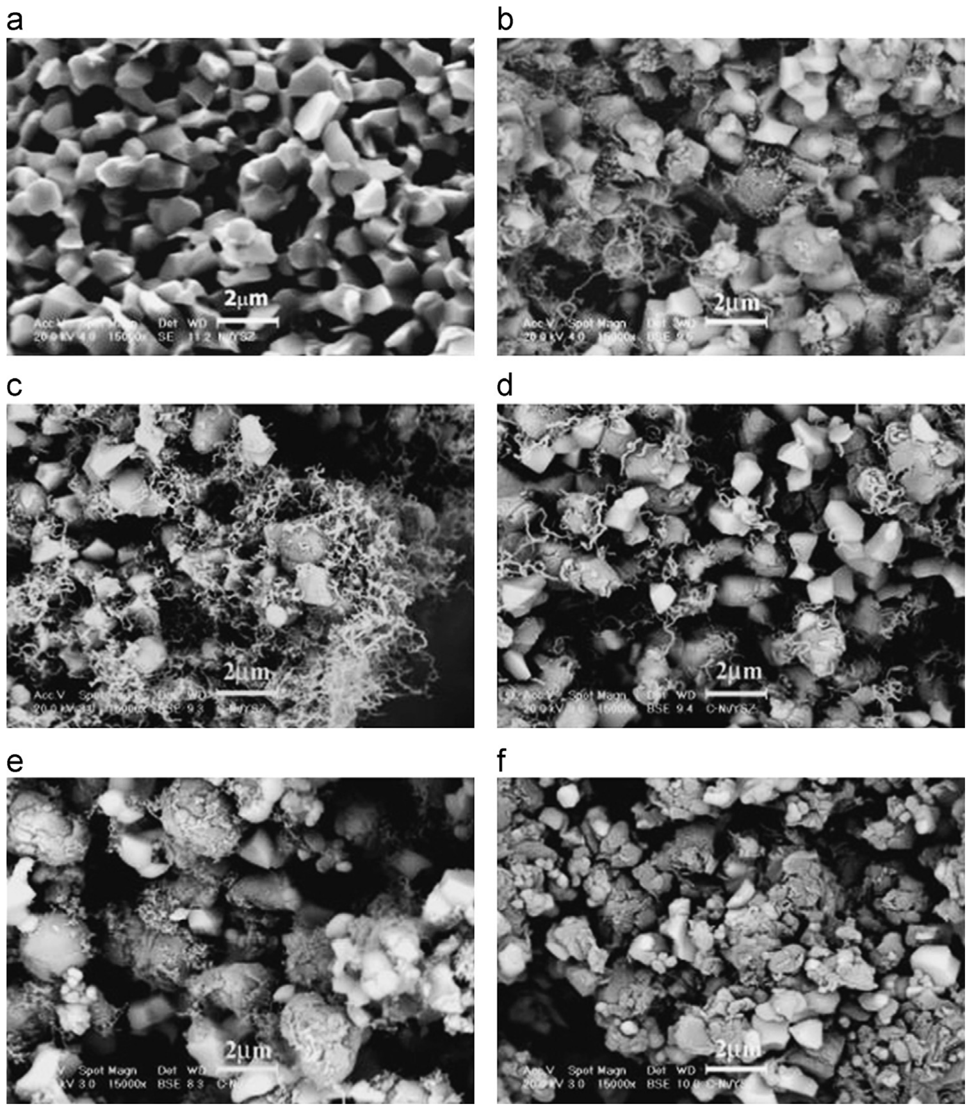


Fig. 26. SEM images of Ni/YSZ (a) as-prepared, and after carbon deposition in humidified methane for 4 h at (b) 773 K, (c) 873 K, surface, (d) 873 K, (e) 973 K, and (f) 1073 K [233].

accommodated in the local porosity which results in a mechanical degradation. Mechanisms underlying the anode expansion during a redox process through reorganization of metallic Ni are often schematically depicted as shown Fig. 23 [166,167]. Higher expansion for a sample reduced at 1100 °C compared to a sample reduced at 800 °C [168] reinforces the model depicted for redox process [165,167].

Increase in oxidation temperature results in the increased oxidation rate and macroscopic strain leading to spontaneous mechanical failure at higher temperatures [167–169]. The difference in expansion reported in different articles under similar experimental conditions could be related to the difference in microstructure [170,171]. Nearly linear behaviour between the oxidation strain and the degree of oxidation has been reported [172]. Redox safe temperature zone for re-oxidation has been reported to be as low as 550 °C.

Oxidation rate was also found to be strongly dependent on the vapour pressure of water in the input gas. At 850 °C, expansion increased from 0.68% to 0.96% on adding 6% H_2O to the dry air [168].

Extensive redox studies on the effect of the substrate composition suggested that even if high NiO amount gives rise to high oxidation strain, amount of irreversible strain is negligible. On the other hand, high YSZ ratios showed very high values of irreversible strain. Optimization of composition and microstructure is essential in order to minimize redox strain and mechanical degradation [173,174].

It was found that samples with smaller sized initial NiO particles and the ones sintered below 1300 °C exhibited better redox dimensional stability. Figs. 24–26. shows the microstructural effects of 4 redox cycles on samples sintered at 1200 and 1400 °C. The cracks developed in the latter samples were attributed to the presence of less porosity and its inability to accommodate the volume change on oxidation [175]. Due to same porosity factor, samples with fine microstructure (like functional layer) cracked after re-oxidation while the anodes with coarse microstructure (anode substrate) remained nearly unchanged [171]. Redox cycling alters the microstructure of the anode and thereby degrades the performance of the anode through its effect on the electrical, electrochemical and mechanical properties. Sub-sections below describe each aspect of these in detail.

7.1.1.1. Microstructural modifications and stress development. It has been shown that redox cycle leads to sponge like NiO structure with entrapped pores. Re-oxidised NiO thus occupies more

volume than original oxidized state causing microcracks in the YSZ skeleton. Re-reduction of such a NiO/YSZ leads to coarse Ni particles. FIB–SEM studies have been carried out on pure Ni to understand the evolution of sponge like structures with trapped pores during oxidation. FIB–SEM studies on the Ni/YSZ composites re-oxidized at different temperature have revealed the presence of bigger pores in the samples re-oxidized at elevated temperatures and small well dispersed pores in the samples re-oxidized at lower temperatures. Due to the expansion of NiO during redox cycle, anode component of the cell expands, whereas electrolyte and cathode layers cannot keep up with this expansion, due to which tensile stresses arise in the cell. If the tensile residual stresses in the electrolyte exceed its tensile strength, cracks develop in the electrolyte resulting in catastrophic failure of the cell. The major factors affecting re-oxidation stability appear to be: (a) the degree of re-oxidation, (b) the homogeneity of re-oxidation, and (c) the temperature at which re-oxidation occurs [170,172,176–181].

7.1.1.2. Effect on the electrical conductivity. Redox cycle has a strong influence on the electrical conductivity of the Ni/YSZ cermet through the phenomenon of coalescence and breaking of Ni–Ni bond, leading to significant increase in the electrode ohmic resistance. Though in few cases increase in conductivity was observed after a first redox cycle, the conductivity degraded at faster rate after multiple redox cycles. Increase in Ni contact after a redox cycle due to breaking of the YSZ skeleton and the creation of porosity during the subsequent redox cycle is believed to be the reason for such behaviour. Overall, substantial conductivity reduction was observed and in some cases conductivity values decreased by more than 50% [27,181–183].

7.1.1.3. Effect on electrochemical performance. Apart from conductivity reduction, redox cycling affects the performance of the cell through its influence on OCV and activation polarization resistance of the anode. Reduction in the OCV is due to the weakening of the anode–electrolyte interfaces and resultant gas leakage. A decrease of OCV from 0.85 to 0.4 V was observed in the anode supported half cell on redox cycle due to the cracking of the electrolyte [165]. Single Redox tests on sulzer cells resulted in the decrease of OCV from 990 to 800 mV as a result of leakage. They also observed a rapid drop in OCV at 800 °C for the cells fabricated by die cold pressing of the substrate and spray pyrolysis of the electrolyte [182,184]. Waldbillig et al. [171,177] observed that the loss in performance increased with the extent of oxidation and the number of redox cycles and performance degradation was attributed to the tensile cracking of the electrolyte.

In few cases, decrease in the polarization resistance was observed after a redox cycle, which has been attributed to the evolution of finer microstructure [185]. However, reports of decreased electrochemical performance far exceed the reports of improved performance [170,186–188]. Electrochemical impedance studies on the redox cycled anode showed a decrease in the frequency of the peak corresponding to charge transfer resistance, suggesting an increase in the polarization resistance due to decrease in the TPB sites [188]. Impedance studies have even suggested that apart from increase in the polarization resistance due to decrease in TPB, decrease in the performance could also be due to the increase in the gas diffusion impedance after redox cycling [187]. A correlative investigation based on the FIB–SEM and polarization studies showed that anode polarization loss increased from 0.06 to 0.09 $\Omega\,cm^2$ due to decrease in TPB length from 2.49 to 2.11 μm^{-2} after 4 redox cycles [189,190].

7.1.1.4. Effect on mechanical properties. Effects of redox cycling on the mechanical properties of NiO/YSZ anode are through its effect on the level of bonding between Ni–Ni and Ni–YSZ and porosity [191–193]. For instance, improvement in the bending strength of the specimens oxidized in air below 650 °C has been attributed to the porosity reduction. A decrease of Young's modulus by 5 GPa on single redox cycle was attributed to an increase of porosity from 26.4% to 27.6% [172,191]. Correlation established between redox strain and Young's modulus suggests that redox cycles linearly degrade the elastic properties with elastic strain leading to the subsequent failure [192]. Strength evolution studies of fine microstructured tubular anode with redox cycles resulted in a decrease of the strength on redox cycling after an initial increase. For coarse microstructured anodes strength decreased continuously with redox cycling. Similar results were observed even for planar anodes [172,191].

7.1.2. Improving the redox instability

This section explains the means of improving the redox stability of the Ni/YSZ anode via the microstructural and compositional modifications.

7.1.2.1. Microstructural modification. Study pertaining to the effect of particle size on the anode expansion suggested that the NiO particle size and the ratio between NiO and YSZ particle sizes are the main deciding factors influencing the anode expansion. The NiO/YSZ expansion varied with particle size ratio as follows: The lower expansion is for 0.5 μm/0.2 μm followed by 0.5 μm/0.8 μm and by 1.4 μm/0.2 μm [170]. It was showed that YSZ with bimodal distribution (fine and course) led to a more stable anode [23]. On varying the proportion of fine to coarse YSZ particle it was noticed that expansion is higher in the case of anodes with higher content of fine YSZ [194]. Observed expansion was respectively 2.5% and 0.23% for fine and coarse microstructure during a redox cycle at 750 °C [171].

7.1.2.2. Sintering temperature. Anodes sintered at lower temperature exhibited lower expansion and better stability. However, this approach cannot be adopted for anodes supported SOFC, as it would lead to poorly sintered electrolyte [170,194].

7.1.2.3. Porosity. Increased porosity would be useful in accommodating the expansion during redox cycles [185]. It was concluded that porosity higher than 45% in the as-sintered state should give redox stable supports with an expansion limit lower than 0.2% [195]. Robert et al. proposed that microstructure containing macro and micro-pores is optimum to limit the expansion during redox cycles [196].

7.1.2.4. Composition. Anode instability decreased with decrease in the NiO content in the anode. However, NiO content cannot be decreased below the percolation threshold as it would lead to the increased ohmic and activation polarization. Thus attempts should be focused to decrease the percolation threshold. Strategies for the same can be: (1) using smaller metal particles with larger aspect ratio, (2) usage of Ni coated pore former instead of independent usage the pore former, (3) use of Ni foam impregnated with a mixture of Ni, YSZ and pore former [18,20,197,198] and (4) adopting wet impregnation method [199].

7.1.2.5. Graded anode. Waldbillig et al. [200] improved the redox stability by using an AFL with a graded Ni content and porosity. The redox sensitivity of the cell after a full cycle for the graded AFL was only half that of the standard one.

7.2. Nickel coarsening

The predominant microstructural change in the porous anode cermet on operating the SOFC at high temperature is the Ni particle coarsening and densification. Since Ni particles produced during the reduction of NiO/YSZ are high surface area solids, there will always be a thermodynamical driving force to decrease the free energy through coalescence [45,201,202]. Low melting point of Ni is another reason for their high tendency to sinter at SOFC operation temperatures. Non-wettability between metallic Ni and ceramic YSZ (even molten Ni shows no wettability towards YSZ ceramic phase ($\theta = 117\,^{\circ}$)) further facilitates the coarsening of Ni [203,204].

Experimentally, Ni coarsening studies have been conducted through analysis of the images obtained through optical microscope [205], SEM [45,202,206] and very recently through FIB–SEM [207]. Theoretical studies on Ni coarsening have been based on the percolation model with Monte Carlo simulation, effective medium theory and phase-field approach [52]. There are also the reports of the extraction of the nickel diffusion values from nickel coarsening. Through the combination of experimental and modelling results, it has been shown that anode degradation through coarsening contributes substantially to the total degradation of cell or the stack.

Ni coarsening is believed to occur through the phenomenon of Ostwald ripening with possible underlying mechanism of transport of volatile nickel species via the gas phase or vacancy diffusion [208]. Ni coarsening by mechanism of vacancy diffusion has been explained by two particle models, in which, the driving force for Ni grain growth has been attributed to curvature difference between neighboring particles [10]. Experimental techniques like X-ray nanotomography along with differential absorption have been used to prove above mechanisms [209]. Ni particle size evolution with time has been analyzed with 'charging capacitor model' with growth curves asymptotically approaching maximum nickel grain size.

Phenomenon of Ni growth is strongly influenced by composition, microstructure and experimental conditions [210]. As can be expected, agglomeration increases with increase in the Ni content of the cermet [205]. With regard to the microstructure, coarse grained microstructure exhibit relatively stable structure, whereas fine grained anode show much higher growth [211]. Effectively, small average grain sizes, wide distribution of particle size and high contents of Ni lead to higher coarsening and degradation rates [212].

Among experimental conditions, reduction temperature has a strong influence on the coarsening with level of agglomeration increasing with increase in the reduction temperature [213]. Ni particle size increased on thermal cycling of the anode [45]. Presence of water in the gas phase is reported to accelerate the kinetics of growth significantly. Experimentally and through density functional theory (DFT) calculations, Sehested et al. [214,215] have shown that humidity boosts Ni growth through increased surface diffusivity of the Ni_2–OH complex. Simwonis et al. [205] observed that nickel coarsening is relatively slow during the entire experimental period of 4000 h (at 1000 °C, 3% H_2O) with a clear tendency of decreasing growth rates with increasing time. In contrast, Jiang [202] observed higher growth rates during the early periods of operation (200–800 h) and decreasing rates at longer times. Holzer et al. [212] reported that in humid atmosphere (60 vol% H_2O, 40% N_2/H_2) the growth rates of nickel are very high (up to 140%/100 h) during the initial period (<100 h). At longer exposure time (>1000 h) the growth rates decrease significantly to nearly 0%/100 h. In contrast, under dry conditions (97 vol% N_2, 3 vol% H_2) the growth rates during the initial period are much lower (1%/100 h) but did not decrease over a period of 2000 h.

Table 7
Volume fraction, percolation connectivity, surface area of three phases, inter-phases contacting surface area and TPB density for the Ni/YSZ anode after different discharge time [216].

Parameter	Phase	After reduction	100 h discharge	250 h discharge
Volume fraction (%)	Ni	22.23	23.95	20.75
	YSZ	35.41	33.55	33.31
	Pore	42.36	42.5	45.94
Volume fraction (%)	Ni	87.75	79.5	52.41
	YSZ	99.08	98.34	98.75
	Pore	99.72	99.82	99.82
Unknown-status phase fraction (%)	Ni	6.75	15.72	34.37
Isolated phase fraction (%)	Ni	5.5	4.78	13.22
Specific surface area ($\mu m^2/\mu m^3$)	Ni	0.52	0.44	0.42
	YSZ	1.01	0.96	0.96
	Pore	0.95	0.89	0.92
Specific inter-phases surface area ($\mu m^2/\mu m^3$)	Ni–YSZ	0.29	0.25	0.23
	Ni–Pore	0.23	0.18	0.19
	YSZ–Pore	0.73	0.71	0.72
TPB density ($\mu m/\mu m^3$)	Total	1.29	1.02	0.98

Ni agglomeration degrades the performance of anode through its influence on ohmic and the activation polarizations. Due to Ni coarsening, electrical conductivity of the anode substrates decreases substantially through the interruption of Ni–Ni connectivity [205]. Simwonis et al. [205] have correlated Ni agglomeration, microstructural modification and electrical conductivity of Ni/YSZ anode. In their study, a large decrease in electrical conductivity was observed in 4000 h exposure in humidified hydrogen. Decrease was substantial during initial hours of exposure with gradual saturation. In another conductivity Vs Ni coalescence study, increase in the ohmic resistance from 0.75 to 0.98 Ω, of which, increase from 0.75 to 0.97 Ω was observed in initial 100 h, while in the last 150 h increase was only 0.01 Ω.

While stable conductivity was observed in the cermets reduced at lower temperatures ($\sim$600 °C), conductivity reduction increased with increase in reducing temperature and at 1000 °C it was more than 50%. Presence of water further amplified the conductivity reduction [213]. Thermal cycling of Ni/YSZ anode also resulted in decreased conductivity [45]. Thus, influence of experimental conditions on the conductivity variations were in concordance with its effect on the kinetics of Ni growth.

Apart from the Ni connectivity, Ni coarsening also decreases Ni/YSZ and Ni–pore inter phase area and effectively active TPB length, leading to activation polarization losses. Nearly unchanged surface area of YSZ with time and thermal cycle indicates that inter-phase area reduction originates mainly due to Ni coarsening. In recent times, quantitative correlation between Ni coarsening, inter-phase area reductions, TPB variation and performance degradation have become increasingly possible by FIB–SEM reconstruction techniques. Like Ni connectivity, surface area reduction is prominent during initial hours of operation and initial thermal cycles. Concomitantly, major portion of TPB reduction occurs in the early period of operation, which has been proved both by simulation and experimental evidences.

Table 7 summarizes results of one of such study in which variation of volume fraction, percolation fraction, and surface area, inter phases surface area and the TPB networks are studied with discharge time by using FIB-SEM. As can be noted, the specific TPB density reduced by about 20% and 22% after 100 and 250 h respectively. However, due to the interruption of Ni network percolation connectivity, the active TPB density decreases more substantially (by about 31% and 57% after 100 and 250 h discharge, respectively). Thermal cycling too had similar kind of effect on the TPB density. For the non-cycled anode, 65% of the total TPBs were

interconnected, measuring $\sim 2.19 \times 10^{12}\ m^{-2}$. The connected TPB of the anode after eight thermal cycles was only $\sim 0.67 \times 10^{12}\ m^{-2}$. Based on TPB quantification, models have shown that stack degradation corresponding to anode performance decreases mainly due to particle sintering, which might amount upto 50% of initial stack degradation. In terms of polarization loss, degradation rate in anode due to coarsening could be as high as 14 mV over 1000 h.

Prevention or minimisation of agglomeration and sintering of metallic Ni phase in the Ni/YSZ cermet electrodes rely heavily on the phase distribution between Ni and YSZ. Achieving uniform distribution and homogenization between NiO and YSZ phases during the preparation of NiO/YSZ cermets through milling and de-agglomeration is effective in preventing the coarsening of Ni and improving the stability of the anodes. Anodes synthesized by solution based methods might be more effective in yielding the required microstructure. By proper combination of coarse and fine YSZ particles in the cermets, improvement in the performance stability of the Ni/YSZ cermet anodes can be achieved [23]. Upon sintering, the coarse YSZ particles can be expected to get connected by a network of fine YSZ particles forming a framework, which prevent the agglomeration and coarsening of Ni particles.

8. Usage of direct hydrocarbon in SOFC – Issues of carburization and sulfidation in Ni/YSZ

One of the main limitations of present day fuel cell technology is the requirement of H_2 as fuel. Although H_2 is often referred to as being the ideal fuel of the future, there are a number of problems related to H_2 generation and storage that must be overcome before it can be implemented on a wide scale. At present, one of the biggest problems is that an estimated 96% of H_2 is produced by reforming hydrocarbons and between 20% and 30% of the fuel value of the hydrocarbons is lost during this process. A second major problem for portable applications is fuel storage since it is difficult and expensive to store H_2 in a form that has an energy density comparable to that of hydrocarbon liquids. In this perspective, SOFCs operating at high temperature, in principle gives rise to an excellent fuel flexibility which allows for the internal reformation of the hydrocarbon fuels on the anode or even direct oxidation of carbon-based fuels and hence gives an opportunity to move away from expensive H_2. Such simplified internal reforming operation of SOFC system results in low costs owing to the elimination of pre-reformer. For instance, natural gas, whose main hydrocarbon component is methane, can be an excellent fuel for SOFC. Inside a Ni/YSZ cermet, following reforming reactions takes place at anode while using natural gas directly as a fuel.

$$CH_4 + H_2O = 3H_2 + CO$$

$$CO + H_2O = CO_2 + H_2$$

8.1. Carburization

Unfortunately, with Ni/YSZ cermet, internal reforming of hydrocarbon fuels is often accompanied by carbon deposition, phenomenon often termed as carburization [217–221]. Carbon deposition takes place through the catalytic dissociative adsorption of hydrocarbons on the Ni surface. For example, with alkane based fuels (e.g., methane, propane, and butane), carbon formation occurs through the following reactions:

$$C_nH_{2n+2} = nC + (n+1)H_2$$

$$2CO = C + CO_2$$

$$CO + H_2 = C + H_2O$$

For methane containing natural gas, the formation of carbon proceeds either via methane dissociation or according to the Boudouard reaction:

$$CH_4 \leftrightarrow C + 2H_2$$

$$2CO \leftrightarrow C + CO_2$$

Carbon deposition covers the active sites of the anodes, resulting in the loss of cell performance. Carbon can form diverse structures including adsorbed, polymeric, vermicular filaments, carbide, and graphitic, which affects carbon reactivity, and the extent of catalyst deactivation [222,223]. By having strict control over the operating conditions, it might however be possible to utilize hydrocarbons directly in SOFC with Ni-based anodes. At low operating temperatures, due to kinetic limitations on the methane cracking reaction, carbon-free SOFC operation can be achieved. Stable operations without coking have been reported over a wide range of current densities at lower temperatures ($\sim$700 °C) [224,225]. However, at higher temperatures, large currents are required to avoid coking and cell failure. Even when carbon does form on Ni-based anodes, it may be possible to remove this carbon as fast as it forms if the O^{2-} flux from the electrolyte is sufficient to remove carbon faster than it is formed [225]. Possibilities of stable operation of SOFC in methane have also been reported. Though there are reports about the possibility of operating a fuel cell with hydrocarbon fuels under the controlled conditions, the problem of carbon formation is catastrophic if system control is lost. Hence carbon deposition has become an extensive area of research in SOFC fuelled by hydrocarbons [226–235]. Many groups have focused on kinetics of internal reforming of hydrocarbons in Ni/YSZ cermets [236–238].

It has been found that the quantity of deposited carbon during methane reforming is strongly affected by the operating temperature. Though thermodynamic calculations predict the absence of carbon formation at 800 °C and 1 atm with a steam to carbon (S/C) ratio greater than one, experimentally carbon formation was observed not only at this temperature, but also at other conditions in which carbon formation was not thermodynamically predicted [239,240]. The formation of carbon results in the disintegration of Ni metal into powder and hence the process is sometimes known as “metal dusting”. The Ni becomes dust due to the presence of graphite inside the metal structure, which forms as the carbon diffuses through the Ni. Corrosion process is strongly dependent on the temperature and the gas composition and in general Ni corrosion rate increases with temperature. Filamentous carbon was formed at temperatures up to 600 °C. The amount of carbon deposited significantly increased at temperatures above 650 °C, and the carbon got dissolved in the bulk of the Ni particles. Both the formation of carbon fibers and dissolved carbon significantly expanded the dimensions of the Ni/YSZ pellets and resulted in cell fracture [233].

The amount and stability of the carbon deposits formed on Ni/YSZ exposed to methane at higher temperatures are affected by current density, exposure time, water content in the gas, and anode thickness [231]. Amount of carbon deposited decreased with increase in the current density [228,241]. The deposits formed under the load remain on the surface of the Ni, with a minor effect on the structure of the anode compared to the carbon deposits formed at open circuit conditions in which the carbon appears to have dissolved into the bulk of the Ni structure.

On using methane, methanol, and ethanol with steam as a direct feed to Ni/YSZ anode, it was found that methane with appropriate steam content can be directly fed to Ni/YSZ anode without the problem of carbon formation, while methanol can also be introduced at a temperature as high as 1000 °C [242]. High

power density operation of anode-supported cells with methanol as a fuel have been indeed demonstrated [243]. In contrast, ethanol cannot be used as the direct fuel for SOFC operation even at high steam content and high operating temperature due to the easy degradation of Ni/YSZ by carbon deposition. Incomplete reformation of ethanol leaves significant amounts of ethane and ethylene in the product gas and they act as very strong promoters for carbon formation. The deposition problems will become even more pronounced if biogas is used as a fuel in the future due to the presence of tars.

There are different strategies to prevent carbon formation in SOFC. Typically high steam/carbon (S/C) (e.g., up to 3) ratios are used in conventional steam reformers to suppress the carbon formation. The problem of carbon formation is even more severe for hydrocarbons larger than methane and still higher amount of S/C should be used to avoid carbon formation [244].Carbon deposited with humidified methane is reversible when it is oxidized at a current load of thermodynamically carbon-free condition [241,245]. However, high S/C ratio is unattractive for fuel cells as it lowers the electrical efficiency of the fuel cell by steam dilution of the fuel. In addition, endothermic nature of steam reforming reaction can cause local cooling and steep thermal gradients generated are potentially capable of mechanically damaging the cell stack. Nevertheless, the impact of the endothermicity of methane steam reforming process on the cell stability can be reduced by the combination of both external and internal reforming activity or by using the so called gradual internal reforming (GIR) of methane. Other strategies include microstructural modifications [85,246,247], addition of some dopants and additives [241,244,248–251], changing the geometry of the anode with barriers or with bi-layers [252], use of materials or alloys that reduce the tendency of nickel to produce carbon [253–257].

Factors such as anode formulation, pre-treatment and operating conditions have strong influence on the internal reforming over Ni/YSZ anodes in SOFCS operating on methane. It was observed that the cermet containing higher amount of Ni exhibited higher steady-state activity at higher reforming temperatures. It has been reported that CeO_2 addition or coating can increase the methane oxidation rates and can be effective in minimizing carbon deposition in Ni/YSZ [258–260]. Use of an additional catalyst layer consisting of a ceria supported precious metal (Ru–CeO_2) is effective for internally reforming the hydrocarbons. Ceria may also enhance anode performance by promoting charge-transfer reactions at the TPB due to its mixed, ionic–electronic conductivity [261,262]. The amount of carbon deposited can also be minimized by placing zirconia-doped ceria pellets on each side of the Ni/YSZ pellet [245]. The addition of a ceria layer did not completely eliminate the carbon formation but the carbon that was formed was weakly attached to the Ni/YSZ such that the structure was not irreversibly changed.

8.2. Sulfidation

Owing to the high operating temperature, SOFCs have great potential for direct utilization of hydrocarbon fuels, including hydrogen-rich synthesis fuels derived from coal or natural gas. Such an option would eliminate the need for a separate fuel processing subsystem and hence reduce the cost and complexities in the fuel cell stack. Unfortunately, all fossil fuels contain some amounts of contaminants with H_2S dominating among them. Sulfur compounds might as well present as additives in many commercially available fuel sources, and their concentration can reach high level in some fuels such as coal syngas. These Sulfur compounds are known to interact with Ni in Ni/YSZ cermet and passivate the active sites and hence resulting in a performance loss and degradation of the anode [263–277]. Sulfur tolerance capability of SOFC anode has become a critical standard for the advance of SOFC towards commercialization.

Several research groups have experimentally studied the effect of sulfur containing fuels on the performance and durability of SOFC's by varying several factors, such as temperature, current/voltage load, time and H_2S concentration [267–269,278,279]. To study the poisoning effect of sulfur and mechanism of degradation, many experimental tools such as polarization studies, complex impedance analysis, Raman spectroscopy, X-ray diffraction studies have been extensively used.

Following observations can be made about the effect of sulfidation on the Ni/YSZ cermet:

- Even a small amount of H_2S in ppm level causes a sharp drop in cell performance within the first few minutes of exposure, followed by a gradual but persistent deterioration in performance for several days [265,280,281].
- Extent of degradation caused by the sulfur poisoning is strongly dependent on the sulfur concentration. If the H_2S content is low (0.02–15 ppm), the performance loss caused by the sulphur poisoning could be recovered after switching to sulfur-free hydrogen fuel [280]. At higher levels of H_2S concentration ($\sim$105 ppm H_2S at 1000 °C), poisoning effect is irreversible [281].
- With decrease in the operation temperature, the critical H_2S concentration for Ni/YSZ degradation decreases suggesting that sulfur poisoning of SOFC systems operating at intermediate temperatures (IT) (typically 700–850 °C) which are known as IT-SOFC systems can be irreversible, whereas the performance degradation in high temperature (HT)-SOFC ($>$900 °C) can be reversible [264,267,268].
- Internal resistance caused by sulphur poisoning is smaller at higher current densities [269] and sulfur poisoning increases with increase in cell voltage.

As there was no significant change in the microstructure of the anode or the formation of any insulating phase in the presence of sulfur, poisoning effect has been primarily attributed to blockage of the active Ni sites for hydrogen adsorption by the process of chemisorptions. Due to the complexity of sulfur poisoning phenomenon, providing an unambiguous explanation for the reactions of sulfur-compounds in the anode and its effects on performance has been very difficult, mostly due to its dependence on the variety of experimental conditions. The reported results of experimental and theoretical research on specific degradation mechanisms of Ni cermet anode throughout different operation conditions tend to vary with each other and do not yield a thorough understanding of this issue. However, it seems to be generally accepted now that, depending on the H_2S concentrations, reaction of Ni with H_2S might be a physical adsorption (adsorption of molecular H_2S on Ni surface), chemisorption (dissociative adsorption of sulfur atom from H_2S) or a sulfidation [276,282,283].

9. Conclusions

Traditional material systems continue to dominate the SOFC technology due to the issues/challenges associated with the newly discovered material systems. It is particularly true with regard to Ni/YSZ: anode material envisaged four decades ago, as it continues to be used in SOFC, despite of the development of new systems suitable for anode applications. Though poor carburization and sulfidation abilities are serious drawbacks with Ni/YSZ, its good catalytic activity for H_2 oxidation and methane reforming, high

electronic conductivity, when compared to new materials system, make it most appealing anode system. Assisted by modern microstructural and electrochemical characterization techniques, complex inter-relations between the powder characteristics, microstructure, electrochemical process and the fabrication process parameters of Ni/YSZ have been better understood now and substantial improvements in its performance from its inception have been achieved. Factors influencing ohmic, activation and concentration polarizations of Ni/YSZ are complexly intertwined and optimization of each factor must be done through knowledge of its influence on all the three polarizations. Inability to simultaneously fulfill all the criteria for the minimization of all the three polarizations in homogeneous anodes have led to the development of gradient anodes possessing the necessary features in accordance with the local requirements. Realization of importance of initial powder characteristics in dictating the final anode microstructure has resulted in the acceptance of solution based synthesis method for the preparation of homogeneous NiO/YSZ powders and by altering the synthesis conditions, powders with desired characteristics have been prepared. While extrusion and tape casting methods have emerged as commercially successful fabrication methods for tubular and planar anode substrates, options available for the fabrication of anode functional layers are many. Degradations such as redox cycling and Ni agglomeration associated with Ni/YSZ have been minimized through the fine tuning of the microstructure and operating conditions. Carburization and sulfidation disabilities of Ni/YSZ on using hydrocarbons have been improved through manoeuvring of operation condition.

Acknowledgements

The authors acknowledge the financial assistance received from the supra institutional project (SIP-SED-06) and CSIR network project on advanced ceramic materials and components for energy and structural applications (CERMESA-ESC-01-04). The authors thank the Director, NAL for the encouragement.

References

[1] Mobius HH. On the history of solid electrolyte fuel cells. J Solid State Electrochem 1997;1:2–16.
[2] Jiang SP, Badwal SPS. Hydrogen oxidation at the nickel and platinum electrodes on yttria-tetragonal zirconia electrolyte. J Electrochem Soc 1997;144:3777–84.
[3] Uchida H, Yoshida M, Watanabe M. Effects of ionic conductivities of zirconia electrolytes on polarization properties of platinum anodes in solid oxide fuel cells. J Phys Chem 1995;99:3282–7.
[4] Suzuki M, Sasaki H, Otoshi S, Kajimura A, Ippommatsu M. High power density solid oxide electrolyte fuel cells using Ru/Y_2O_3 stabilized zirconia cermet anodes. Solid State Ionics 1993;62:125–30.
[5] Setoguchi T, Okamoto K, Eguchi K, Arai H. Effects of anode material and fuel on anodic reaction of solid oxide fuel cells. J Electrochem Soc 1992;139:2875–80.
[6] Tsipis EV, Kharton VV. Electrode materials and reaction mechanisms in solid oxide fuel cells: a brief review: I Electrochemical behavior vs. materials science aspects. J Solid State Electrochem 2008;12:1367–91.
[7] Ruiz-Morales JC, Canales-Vázquez J, Marrero-López D, Irvine JTS, Núñez P. Improvement of the electrochemical properties of novel solid oxide fuel cell anodes, $La_{0.75}Sr_{0.25}Cr_{0.5}Mn_{0.5}O_{3-\delta}$ and $La_4Sr_8Ti_{11}Mn_{0.5}Ga_{0.5}O_{37.5-\delta}$, using Cu–YSZ-based cermets. Electrochim Acta 2007;52:7217–25.
[8] Goodenough JB, Huang YH. Alternative anode materials for solid oxide fuel cells. J Power Sources 2007;173:1–10.
[9] Huang YH, Dass RI, King ZL, Goodenough JB. Double perovskites as anode materials for solid-oxide fuel cells. Science 2006;312:254–7.
[10] Huang YH, Liang G, Croft M, Lehtimäki M, Karppinen M, Goodenough JB. Double-perovskite anode materials Sr_2MMoO_6 (M=Co, Ni) for solid oxide fuel cells. Chem Mater 2009;21:2319–26.
[11] Huang YH, Dass RI, Denyszyn JC, Goodenough JB. Synthesis and characterization of $Sr_2MgMoO_{6-\delta}$. J Electrochem Soc 2006;153:A1266–72.
[12] Spacil HS. Electrical device including nickel-containing stabilized zirconia electrode. US Patent 3,558,360; 1970.
[13] Jiang SP. Resistance measurement in solid oxide fuel cells. J Electrochem Soc 2001;148:A887–97.
[14] Mori M, Yamamoto T, Itoh H, Inaba H, Tagawa H. Thermal expansion of nickel–zirconia anodes in solid oxide fuel cells during fabrication and operation. J Electrochem Soc 1998;145:1374–81.
[15] Dees DW, Claar TD, Easler TE, Fee DC, Mrazek FC. Conductivity of porous Ni/ZrO_2–Y_2O_3. J Electrochem Soc 1987;l34:2141–6.
[16] Li Y, Xie Y, Gong J, Chen Y, Zhang Z. Preparation of Ni/YSZ materials for SOFC anodes by buffer-solution method. Mater Sci Eng B 2001;86:119–22.
[17] Pratihar SK, Dassharma A, Maiti HS. Processing microstructure property correlation of porous Ni–YSZ cermets anode for SOFC application. Mater Res Bull 2005;40:1936–44.
[18] Clemmer RMC, Corbin SF. Influence of porous composite microstructure on the processing and properties of solid oxide fuel cell anodes. Solid State Ionics 2004;166:251–9.
[19] Corbin SF, Clemmer RMC, Yang Q. Development and characterization of porous composites for solid oxide fuel cell anode conduction layers using ceramic-filled highly porous ni foam. J Am Ceram Soc 2009;92:331–7.
[20] Corbin SF, Qiao X. Development of solid oxide fuel cell anodes using metal-coated pore-forming agents. J Am Ceram Soc 2003;86:401–6.
[21] Tietz F, Dias FJ, Simwonis D, Stöver D. Evaluation of commercial nickel oxide powders for components in solid oxide fuel cells. J Eur Ceram Soc 2000;20:1023–34.
[22] Yu JH, Park GW, Lee S, Woo SK. Microstructural effects on the electrical and mechanical properties of Ni–YSZ cermet for SOFC anode. J Power Sourcess 2007;163:926–32.
[23] Itoh H, Yamamoto T, Mori M, Horita T, Sakai N, Yokokawa H, et al. Configurational and electrical behavior of Ni–YSZ cermet with novel microstructure for solid oxide fuel cell anodes. J Electrochem Soc 1997;144:641–6.
[24] Matsushima T, Ohrui H, Hirai T. Effects of sinterability of YSZ powder and NiO content on characteristics of Ni–YSZ cermets. Solid State Ionics 1998;111:315–21.
[25] Jia L, Lu Z, Miao J, Liu Z, Li G, Su W. Effects of pre-calcined YSZ powders at different temperatures on Ni–YSZ anodes for SOFC. J Alloys Compd 2006;414:152–7.
[26] Fukui T, Ohara S, Naito M, Nogi K. Performance and stability of SOFC anode fabricated from NiO–YSZ composite particles. J Power Sources 2002;110:91–95.
[27] Grahl-Madsen L, Larsen PH, Bonanos N, Engell J, Linderoth S. Mechanical strength and electrical conductivity of Ni–YSZ cermets fabricated by viscous processing. J Mater Sci 2006;41:1097–107.
[28] Vivet N, Chupin S, Estrade E, Piquero T, Pommier PL, Rochais D, et al. 3D Microstructural characterization of a solid oxide fuel cell anode reconstructed by focused ion beam tomography. J Power Sources 2011;196:7541–7549.
[29] Guan Y, Li W, Gong Y, Liu G, Zhang X, Chen J, et al. Analysis of the three-dimensional microstructure of a solid-oxide fuel cell anode using nano X-ray tomography. J Power Sources 2011;196:1915–9.
[30] Vivet N, Chupin S, Estrade E, Richard A, Bonnamy S, Rochais D, et al. Effect of Ni content in SOFC Ni–YSZ cermets: a three-dimensional study by FIB–SEM tomography. J Power Sources 2011;196:9989–97.
[31] Bieberle A, Meier LP, Gauckler LJ. The electrochemistry of Ni pattern anodes used as solid oxide fuel cell model electrodes. J Electrochem Soc 2001;148:A646–A656.
[32] Goodwin DG, Zhu H, Colclasure AM, Kee RJ. Modeling electrochemical oxidation of hydrogen on Ni–YSZ pattern anodes. J Electrochem Soc 2009;156:B1004–21.
[33] Lynch ME, Mebane DS, Liu Y, Liu M. Triple-phase boundary and surface transport in mixed conducting patterned electrodes. J Electrochem Soc 2008;155:B635–43.
[34] Wilson JR, Kobsiriphat W, Mendoza R, Chen HY, Hiller JM, Miller DJ, et al. Three-dimensional reconstruction of a solid-oxide fuel-cell anode. Nat Mater 2006;5:541–4.
[35] Ali A, Wen X, Nandakumar K, Luo J, Chuang KT. Geometrical modeling of microstructure of solid oxide fuel cell composite electrodes. J Power Sources 2008;185:961–6.
[36] Deseure J, Bultel Y, Schneider LCR, Dessemond L, Martin C. Micromodeling of functionally graded SOFC cathodes. J Electrochem Soc 2007;154:B1012–6.
[37] Kenney B, Karan K. Engineering of microstructure and design of a planar porous composite SOFC cathode: a numerical analysis. Solid State Ionics 2007;178:297–306.
[38] Li DS, Saheli G, Khaleel M, Garmestani H. Quantitative prediction of effective conductivity in anisotropic heterogeneous media using two-point correlation functions. Comput Mater Sci 2006;38:45–50.
[39] Golbert J, Adjiman CS, Brandon NP. Microstructural modeling of solid oxide fuel cell anodes. Ind Eng Chem Res 2008;47:7693–9.
[40] Kenney B, Valdmanis M, Baker C, Pharoah JG, Karan K. Computation of TPB length, surface area and pore size from numerical reconstruction of composite solid oxide fuel cell electrodes. J Power Sources 2009;189:1051–9.
[41] Metcalfe C, Kesler O, Rivard T, Gitzhofer F, Abatzoglou N. Connected three-phase boundary length evaluation in modeled sintered composite solid oxide fuel cell electrodes. J Electrochem Soc 2010;157:B1326–35.
[42] Sanyal J, Goldin GM, Zhu H, Kee RJ. A particle-based model for predicting the effective conductivities of composite electrodes. J Power Sources 2010;195:6671–6679.

[43] Schneider LCR, Martin CL, Bultel Y, Bouvard D, Siebert E. Discrete modelling of the electrochemical performance of SOFC electrodes. Electrochim Acta 2006;52:314–24.
[44] Abel J, Kornyshev AA, Lehnert W. Correlated resistor network study of porous solid oxide fuel cell anodes. J Electrochem Soc 1997;144:4253–9.
[45] Lee JH, Moon H, Lee HW, Kim J, Kim JD, Yoon KH. Quantitative analysis of microstructure and its related electrical property of SOFC anode, Ni–YSZ cermet. Solid State Ionics 2002;148:15–26.
[46] Grew KN, Chu YS, Yi J, Peracchio AA, Izzo Jr JR, Hwu Y, et al. Nondestructive nanoscale 3D elemental mapping and analysis of a solid oxide fuel cell anode. J Electrochem Soc 2010;157:B783–92.
[47] Iwai H, Shikazono N, Matsui T, Teshima H, Kishimoto M, Kishida R, et al. Quantification of SOFC anode microstructure based on dual beam FIB–SEM technique. J Power Sources 2010;195:955–61.
[48] Shearing PR, Golbert J, Chater RJ, Brandon NP. 3D reconstruction of SOFC anodes using a focused ion beam lift-out technique. Chem Eng Sci 2009;64:3928–33.
[49] Wilson JR, Gameiro M, Mischaikow K, Kalies W, Voorhees PW, Barnett SA. Three-dimensional analysis of solid oxide fuel cell Ni–YSZ anode interconnectivity. Microsc Microanal 2009;15:71–7.
[50] Kishimoto M, Miyawaki K, Iwai H, Saito M, Yoshida H. Effect of composition ratio of Ni–YSZ anode on distribution of effective three-phase boundary and power generation performance. Fuel Cells 2013;13:476–86.
[51] Yakal-Kremski K, Cronin JS, Chen-Wiegart YCK, Wang J, Barnett SA. Studies of solid oxide fuel cell electrode evolution using 3D tomography. Fuel Cells 2013;13:449–54.
[52] Ioselevich A, Kornyshev AA, Lehnert W. Statistical geometry of reaction space in porous cermet anodes based on ion-conducting electrolytes patterns of degradation. Solid State Ionics 1999;124:221–37.
[53] Abbaspour A, Luo JL, Nandakumar K. Three-dimensional random resistor-network model for solid oxide fuel cell composite electrodes. Electrochim Acta 2010;55:3944–50.
[54] Abbaspour A, Wen X, Nandakumar K, Luo J, Chuang KT. Geometrical modeling of microstructure of solid oxide fuel cell composite electrodes. J Power Sources 2008;185:961–6.
[55] Martinez AS, Brouwer J. Percolation modeling investigation of TPB formation in a solid oxide fuel cell electrode–electrolyte interface. Electrochim Acta 2008;53:3597–609.
[56] Wilson JR, Cronin JS, Barnett SA. Linking the microstructure, performance and durability of Ni-yttria-stabilized zirconia solid oxide fuel cell anodes using three-dimensional focused ion beam-scanning electron microscopy imaging. Scr Mater 2011;65:67–72.
[57] Cai Q, Adjiman CS, Brandon NP. Investigation of the active thickness of solid oxide fuel cell electrodes using a 3D microstructure model. Electrochim Acta 2011;56:10809–11.
[58] Shearing PR, Cai Q, Golbert JI, Yufit V, Adjiman CS, Brandon NP. Microstructural analysis of a solid oxide fuel cell anode using focused ion beam techniques coupled with electrochemical simulation. J Power Sources 2010;195:4804–10.
[59] Shearing PR, Gelb J, Brandon NP. X-ray nano computerised tomography of SOFC electrodes using a focused ion beam sample-preparation technique. J Eur Ceram Soc 2010;30:1809–14.
[60] Cai Q, Adjiman CS, Brandon NP. Modelling the 3D microstructure and performance of solid oxide fuel cell electrodes: computational parameters. Electrochim Acta 2011;56:5804–14.
[61] Poon M, Kesler O. The influence of pore formers on the microstructure of plasma-sprayed NiO–YSZ anodes. J Power Sources 2012;210:204–17.
[62] Simwonis D, Naoumidis A, Dias FJ, Linke J, Moropoulou A. Material characterization in support of the development of an anode substrate for solid oxide fuel cells. J Mater Res 1997;12:1508–18.
[63] Kong J, Sun K, Zhou D, Zhang N, Mu J, Qiao J. Ni–YSZ gradient anodes for anode-supported SOFCs. J Power Sources 2007;166:337–42.
[64] Chen K, Lü Z, Ai N, Huang X, Zhang Y, Xin X, et al. Development of yttria-stabilized zirconia thin films via slurry spin coating for intermediate-to-low temperature solid oxide fuel cells. J Power Sources 2006;160:436–8.
[65] Liu J, Barnett SA. Thin yttrium-stabilized zirconia electrolyte solid oxide fuel cells by centrifugal casting. J Am Ceram Soc 2002;85:3096–8.
[66] Haslam JJ, Pham AQ, Chung BW, DiCarlo JF, Glass RS. Effects of the use of pore formers on performance of an anode supported solid oxide fuel cell. J Am Ceram Soc 2005;88:513–8.
[67] Prabhakaran K, Melkeri A, Beigh MO, Gokhale NM, Sharma SC. Preparation of a porous cermet SOFC anode substrate by gelcasting of NiO–YSZ powders. J Am Ceram Soc 2007;90:622–5.
[68] Srivastava PK, Quach T, Duan YY, Donelson R, Jiang SP, Ciacchi FT, et al. Electrode supported solid oxide fuel cells: electrolyte films prepared by DC magnetron sputtering. Solid State Ionics 1997;99:311–9.
[69] Huebener W., Anderson H.U., Harlan U., Reed D.M., Sehlin S.R.,Deng X. Microstructure–property relationships of Ni:ZrO_2 anodes. In: Proceedings of the fourth international symposium on Solid Oxide Fuel Cells (SOFC-IV); 1995. p. 696–705.
[70] Choi YG, Park JY, Song H, Kim HR, Son JW, Lee JH, et al. Microstructure–polarization relations in nickel/gadolinia-doped ceria anode for intermediate-temperature solid oxide fuel cells. Ceram Int 2013;39:4713–8.
[71] Chen K, Lü Z, Chen X, Ai N, Huang X, Wei B, et al. Characteristics of NiO–YSZ anode based on NiO particles synthesized by the precipitation method. J Alloys Compd 2008;454:447–53.
[72] Horri BA, Selomulya C, Wang H. Characteristics of Ni/YSZ ceramic anode prepared using carbon microspheres as a pore former. Int J Hydrogen Energy 2012;37:15311–9.
[73] Kim M, Lee J, Han JH. Fabrication of anode support for solid oxide fuel cell using zirconium hydroxide as a pore former. J Power Sources 2011;196: 2475–2482.
[74] Pan WP, Lü Z, Chen KF, Zhu XB, Huang XQ, Zhang YH, et al. Paper-fibres used as a pore-former for anode substrate of solid oxide fuel cell. Fuel Cells 2011;11:172–7.
[75] Vural Y, Ma L, Ingham DB, Pourkashanian M. Comparison of the multi-component mass transfer models for the prediction of the concentration overpotential for solid oxide fuel cell anodes. J Power Sources 2010;195: 4893–4904.
[76] Lee JH, Heo JW, Lee DS, Kim J, Kim GH, Lee HW, et al. The impact of anode microstructure on the power generating characteristics of SOFC. Solid State Ionics 2003;158:225–32.
[77] Jiang SP, Badwal SPS. An electrode kinetics study of H_2 oxidation on Ni/Y_2O_3–ZrO_2 cermet electrode of the solid oxide fuel cell. Solid State Ionics 1999;123:209–24.
[78] Mogensen M, Skaarup S. Kinetic and geometric aspects of solid oxide fuel cell electrodes. Solid State Ionics 1996;86-88:1151–60.
[79] Holtappels P, Vinke IC, De Haart LGJ, Stimming U. Reaction of hydrogen/water mixtures on nickel–zirconia cermet electrodes. II. AC polarization characteristics. J Electrochem Soc 1999;146:2976–82.
[80] Mizusaki J, Tagawa H, Saito T, Kamitani K, Yamamura T, Hirano K, et al. Preparation of nickel pattern electrodes on YSZ and their electrochemical properties in H_2–H_2O atmospheres. J Electrochem Soc 1994;141:2129–34.
[81] Brown M, Primdahl S, Mogensen M. Structure/performance relations for Ni/yttria-stabilized zirconia anodes for solid oxide fuel cells. J Electrochem Soc 2000;147:475–85.
[82] Kek D, Bonanos N, Mogensen M, Pejovnik S. Effect of electrode material on the oxidation of H_2 at the metal–$Sr_{0.99}5Ce_{0.95}Y_{0.05}O_{2.970}$ interface. Solid State Ionics 2000;131:249–59.
[83] De Boer B, Gonzalez M, Bouwmeester HJM, Verweij H. Effect of the presence of fine YSZ particles on the performance of porous nickel electrodes. Solid State Ionics 2000;127:269–76.
[84] Holtappels P, De Haart LGJ, Stimming U. Reaction of hydrogen/water mixtures on nickel–zirconia cermet electrodes. I. DC polarization characteristics. J Electrochem Soc 1999;146:1620–5.
[85] Vels Jensen K, Primdahl S, Chorkendorff I, Mogensen M. Microstructural and chemical changes at the Ni/YSZ interface. Solid State Ionics 2001;144: 197–209.
[86] Horita T, Kishimoto H, Yamaji K, Xiong Y, Sakai N, Brito ME, et al. Materials and reaction mechanisms at anode/electrolyte interfaces for SOFCs. Solid State Ionics 2006;177:1941–8.
[87] Ihara M, Kusano T, Yokoyama C. Competitive adsorption reaction mechanism of Ni/Yttria-stabilized zirconia cermet anodes in H_2–H_2O solid oxide fuel cells. J Electrochem Soc 2001;148:A209–19.
[88] Brown M, Primdahl S, Mogensen M. Structure/performance relations for Ni/yttria-stabilized zirconia anodes for solid oxide fuel cells. J Electrochem Soc 2000;147:475–85.
[89] Primdahl S, Mogensen M. Oxidation of hydrogen on Ni/yttria-stabilized zirconia cermet anodes. J Electrochem Soc 1997;144:3409–19.
[90] Moon H, Kim SD, Park EW, Hyun SH, Kim HS. Characteristics of SOFC single cells with anode active layer via tape casting and co-firing. Int J Hydrogen Energy 2008;33:2826–33.
[91] Chan SH, Xia ZT. Anode micro model of solid oxide fuel cell. J Electrochem Soc 2001;148:A388–94.
[92] Sunde S. Monte Carlo simulations of polarization resistance of composite electrodes for solid oxide fuel cells. J Electrochem Soc 1996;143:1930–9.
[93] Shikazono N, Kanno D, Matsuzaki K, Teshima H, Sumino S, Kasagi N. Numerical assessment of SOFC anode polarization based on three-dimensional model microstructure reconstructed from FIB–SEM images. J Electrochem Soc 2010;157:B665–72.
[94] Suzue Y, Shikazono N, Kasagi N. Micro modeling of solid oxide fuel cell anode based on stochastic reconstruction. J Power Sources 2008;184:52–9.
[95] Virkar AV, Chen J, Tanner CW, Kim JW. Role of electrode microstructure on activation and concentration polarizations in solid oxide fuel cells. Solid State Ionics 2000;131:189–98.
[96] Yoon D, Lee JJ, Park HG, Hyun SH. NiO/YSZ–YSZ nanocomposite functional layer for high performance solid oxide fuel cell anodes. J Electrochem Soc 2010;157:B455–62.
[97] Basu RN, Blass G, Buchkremer HP, Stover D, Tietz F, Wessel E, et al. Simplified processing of anode-supported thin film planar solid oxide fuel cells. J Eur Ceram Soc 2005;25:463–71.
[98] Mukhopadhyay M, Mukhopadhyay J, Das Sharma A, Basu RN. Engineered anode structure for enhanced electrochemical performance of anode-supported planar solid oxide fuel cell. Int J Hydrogen Energy 2012;37: 2524–2534.
[99] Mukhopadhyay M, Mukhopadhyay J, Basu RN. Functional anode materials for solid oxide fuel cell – a review. Trans Indian Ceram Soc 2013;72:145–68.
[100] Lee KT, Vito NJ, Wachsman ED. Comprehensive quantification of Ni–$Gd_{0.1}Ce_{0.9}O_{1.95}$ anode functional layer microstructures by three-dimensional reconstruction using a FIB/SEM dual beam system. J Power Sources 2013;228:220–8.

[101] Müller AC, Herbstritt D, Ivers-Tiffée E. Development of a multilayer anode for solid oxide fuel cells. Solid State Ionics 2002;152-153:537–42.
[102] Wang ZR, Qian JQ, Wang SR, Cao JD, Wen TL. Improvement of anode-supported solid oxide fuel cells. Solid State Ionics 2008;179:1593–6.
[103] Holtappels P, Sorof C, Verbraeken MC, Rambert S, Vogt U. Preparation of porosity-graded SOFC anode substrates. Fuel Cells 2006;6:113–6.
[104] Jono K, Suda S, Hattori M. Effect of graded porous structure on Ni–YSZ anode performance. ECS Trans 2007;7:1541–6.
[105] Shao Z, Zhou W, Zhu Z. Advanced synthesis of materials for intermediate-temperature solid oxide fuel cells. Prog Mater Sci 2012;57:804–74.
[106] Torknik FS, Keyanpour-Rad M, Maghsoudipour A, Choi GM. Effect of microstructure refinement on performance of $Ni/Ce_{0.8}Gd_{0.2}O_{1.9}$ anodes for low temperature solid oxide fuel cell. Ceram Int 2014;40:1341–50.
[107] Cho HJ, Choi GM. Effect of milling methods on performance of $Ni–Y_2O_3$-stabilized ZrO_2 anode for solid oxide fuel cell. J Power Sources 2008;176: 96–101.
[108] Sato K, Abe H, Misono T, Murata K, Fukui T, Naito M. Enhanced electrochemical activity and long-term stability of Ni–YSZ anode derived from NiO–YSZ interdispersed composite particles. J Eur Ceram Soc 2009;29:1119–24.
[109] Fukui T, Murata K, Ohara S, Abe H, Naito M, Nogi K. Morphology control of Ni–YSZ cermet anode for lower temperature operation of SOFCs. J Power Sources 2004;125:17–21.
[110] Aruna ST, Mukasyan AS. Combustion synthesis and nanomaterials. Curr Opin Solid State Mater Sci 2008;12:44–50.
[111] Merzhanov AG. The chemistry of self-propagating high-temperature synthesis. J Mater Chem 2004;14:1779–86.
[112] Munir ZA, Anselmi-Tamburini U. Self-propagating exothermic reactions: the synthesis of high-temperature materials by combustion. Mater Sci Rep 1989;3:277–365.
[113] Patil KC, Aruna ST, Ekambaram S. Combustion synthesis. Curr Opin Solid State Mater Sci 1997;2:158–65.
[114] Patil KC, Aruna ST, Mimani T. Combustion synthesis: an update. Curr Opin Solid State Mater Sci 2002;6:507–12.
[115] Yi HC, Moore JJ. Self-propagating high-temperature (combustion) synthesis (SHS) of powder-compacted materials. J Mater Sci 1990;25:1159–68.
[116] Aruna ST, Muthuraman M, Patil KC. Synthesis and properties of Ni–YSZ cermet: anode material for solid oxide fuel cells. Solid State Ionics 1998;111: 45–51.
[117] Kim SJ, Lee W, Lee WJ, Park SD, Song JS, Lee EG. Preparation of nanocrystalline nickel oxide–yttria-stabilized zirconia composite powder by solution combustion with ignition of glycine fuel. J Mater Res 2001;16:3621–7.
[118] Ringuedé A, Frade JR, Labrincha JA. Combustion synthesis of zirconia-based cermet powders. Ionics 2000;6:273–8.
[119] Shri Prakash B, William Grips VK, Aruna ST. A single step solution combustion approach for preparing gadolinia doped ceria solid oxide fuel cell electrolyte material suitable for wet powder and plasma spraying processes. J Power Sources 2012;214:358–64.
[120] Marinšek M, Zupan K, Maèek J. Ni–YSZ cermet anodes prepared by citrate/nitrate combustion synthesis. J Power Sources 2002;106:178–88.
[121] Marinšek M, Zupan K. Microstructure evaluation of sintered combustion-derived fine powder NiO–YSZ. Ceram Int 2010;36:1075–82.
[122] Xi X, Abe H, Kuruma K, Harada R, Shui A, Naito M. Novel Co-precipitation method to synthesize NiO–YSZ nanocomposite powder for solid oxide fuel cell. Adv Powder Technol 2013.
[123] Grgicak CM, Green RG, Du WF, Giorgi JB. Synthesis and characterization of NiO–YSZ anode materials: precipitation, calcination, and the effects on sintering. J Am Ceram Soc 2005;88:3081–7.
[124] Hashigami S, Yoshida H, Ueno D, Kawano M, Inagaki T. Improvement of the redox durability of Ni–gadolinia doped ceria anodes due to the use of the composite particles prepared by spray pyrolysis method. J Power Sources 2014;248:190–5.
[125] Messing GL, Zhang S-C, Jayanthi GV. Ceramic powder synthesis by spray pyrolysis. J Am Ceram Soc 1993;76:2707–26.
[126] Fukui T, Ohara S, Naito M, Nogi K. Synthesis of NiO–YSZ composite particles for an electrode of solid oxide fuel cells by spray pyrolysis. Powder Technol 2003;132:52–6.
[127] Fukui T, Ohara S, Naito M, Nogi K. Performance and stability of SOFC anode fabricated from NiO/YSZ composite particles. J Eur Ceram Soc 2003;23: 2963–2967.
[128] Razpotnik T, Maček J. Synthesis of nickel oxide/zirconia powders via a modified Pechini method. J Eur Ceram Soc 2007;27:1405–10.
[129] Kim SD, Moon H, Hyun SH, Moon J, Kim J, Lee HW. Ni–YSZ cermet anode fabricated from NiO–YSZ composite powder for high-performance and durability of solid oxide fuel cells. Solid State Ionics 2007;178:1304–9.
[130] Razpotnik T, Maček J. Synthesis of nickel oxide/zirconia powders via a modified Pechini method. J. Eur. Ceram. Soc. 2007;27:1405–10.
[131] Durán P, Tartaj J, Capel F, Moure C. Processing and characterisation of a fine nickel oxide/zirconia/composite prepared by polymeric complex solution synthesis. J Eur Ceram Soc 2003;23:2125–33.
[132] Kim SD, Moon H, Hyun SH, Moon J, Kim J, Lee HW. Nano-composite materials for high-performance and durability of solid oxide fuel cells. J Power Sources 2006;163:392–7.
[133] Mukhopadhyay M, Mukhopadhyay J, Sharma AD, Basu RN. Ball mill assisted synthesis of Ni–YSZ cermet anode by electroless technique and their characterization. Mater Sci Eng B 2009;163:120–7.
[134] Mukhopadhyay M, Mukhopadhyay J, Das Sharma A, Basu RN. High performance planar solid oxide fuel cell fabricated with Ni–yttria stabilized zirconia anode prepared by electroless technique. Int J Appl Ceram Technol 2012;9:999–1010.
[135] Mukhopadhyay J, Banerjee M, Basu RN. Influence of sorption kinetics for zirconia sensitization in solid oxide fuel cell functional anode prepared by electroless technique. J Power Sources 2008;175:749–59.
[136] Pratihar SK, Sharma AD, Basu RN, Maiti HS. Preparation of nickel coated YSZ powder for application as an anode for solid oxide fuel cells. J Power Sources 2004;129:138–42.
[137] Menzler NH, Tietz F, Uhlenbruck S, Buchkremer HP, Stover D. Materials and manufacturing technologies for solid oxide fuel cells. J Mater Sci 2010;45: 3109–3135.
[138] Liu QL, Chan SH, Fu CJ, Pasciak G. Fabrication and characterization of large-size electrolyte/anode bilayer structures for low-temperature solid oxide fuel cell stack based on gadolinia-doped ceria electrolyte. Electrochem Commun 2009;11:871–4.
[139] Basu RN, Sharma AD, Dutta A, Mukhopadhyay J. Processing of high-performance anode-supported planar solid oxide fuel cell. Int J Hydrogen Energy 2008;33:5748–54.
[140] Le S, Sun KN, Zhang N, Zhu X, Sun H, Yuan YX, et al. Fabrication and evaluation of anode and thin Y_2O_3-stabilized ZrO_2 film by co-tape casting and co-firing technique. J Power Sources 2010;195:2644–8.
[141] Christiansen N, Hansen JB, Holm-Larsen H, Linderoth S, Larsen PH, Hendriksen PV, et al. Solid oxide fuel cell development at topsoe fuel cell A/S and Risø National Laboratory. ECS Trans 2007;7:31–8.
[142] Ramousse S, Menon M, Brodersen K, Knudsen J, Rahbek U, Larsen PH. Manufacturing of anode-supported SOFC's: processing parameters and their influence. ECS Trans 2007;7:317–27.
[143] Schafbauer W, Menzler NH, Buchkremer HP. Influence of thermal treatment during cell manufacturing on the performance of tape cast solid oxide fuel cells. ECS Trans 2009;25:649–54.
[144] Takahashi M, Unuma H. Gelcasting. Ceram Jpn 1997;32:102–5.
[145] Omatete OO, Janney MA, Strehlow RA. Gelcasting – a new ceramic forming process. Am Ceram Soc Bull 1991;70:1641–9.
[146] Young AC, Omatete OO, Janney MA, Menchofer PA. Gelcasting of alumina. J Am Ceram Soc 1998;81:581–91.
[147] Huang WL, Zhu Q, Xie Z. Gel-cast anode substrates for solid oxide fuel cells. J Power Sources 2006;162:464–8.
[148] Sammes NM, Du Y, Bove R. Design and fabrication of a 100 W anode supported micro-tubular SOFC stack. J Power Sources 2005;145:428–34.
[149] Du Y, Sammes NM. Fabrication and properties of anode-supported tubular solid oxide fuel cells. J Power Sources 2004;136:66–71.
[150] Lawlor V. Review of the micro-tubular solid oxide fuel cell (Part II: Cell design issues and research activities). J Power Sources 2013;240:421–41.
[151] Ding J, Liu J, Yuan W, Zhang Y. Slip casting combined with colloidal spray coating in fabrication of tubular anode-supported solid oxide fuel cells. J Eur Ceram Soc 2008;28:3113–7.
[152] Ding J, Liu J. A novel design and performance of cone-shaped tubular anode-supported segmented-in-series solid oxide fuel cell stack. J Power Sources 2009;193:769–73.
[153] Somalu MR, Brandon NP. Rheological studies of nickel/scandia-stabilized-zirconia screen printing inks for solid oxide fuel cell anode fabrication. J Am Ceram Soc 2012;95:1220–8.
[154] Somalu MR, Yufit V, Brandon NP. The effect of solids loading on the screen-printing and properties of nickel/scandia-stabilized-zirconia anodes for solid oxide fuel cells. Int J Hydrogen Energy 2013;38:9500–10.
[155] Oishi N, Yoo Y, Davidson I. Fabrication of gas electrodes by wet powder spraying of binder-free particle suspensions using a pulse injection process. J Am Cera. So. 2007;90:1365–9.
[156] Sammes NM, Brown MS, Ratnaraj R. Wet powder spraying of a cermet anode for a planar solid oxide fuel cell system. J Mater Sci Lett 1994;13:1124–6.
[157] Torabi A, Etsell TH, Sarkar P. Dip coating fabrication process for micro-tubular SOFCs. Solid State Ionics 2011;192:372–5.
[158] Fauchais P, Montavon G, Lima RS, Marple BR. Engineering a new class of thermal spray nano-based microstructures from agglomerated nanostructured particles, suspensions and solutions: an invited review. J Phys D: Appl Phys 2011:44.
[159] Henne R. Solid oxide fuel cells: a challenge for plasma deposition processes. J Therm Spray Technol 2007;16:381–403.
[160] Hui R, Wang Z, Kesler O, Rose L, Jankovic J, Yick S, et al. Thermal plasma spraying for SOFCs: applications, potential advantages, and challenges. J Power Sources 2007;170:308–23.
[161] Li C-X, Li C-J, Guo L-J. Effect of composition of NiO/YSZ anode on the polarization characteristics of SOFC fabricated by atmospheric plasma spraying. Int J Hydrogen Energy 2010;35:2964–9.
[162] Hwang C, Yu C-H. Formation of nanostructured YSZ/Ni anode with pore channels by plasma spraying. Surf Coat Technol 2007;201:5954–9.
[163] Vaßen R, Hathiramani D, Mertens J, Haanappel VAC, Vinke IC. Manufacturing of high performance solid oxide fuel cells (SOFCs) with atmospheric plasma spraying (APS). Surf Coat Technol 2007;202:499–508.
[164] Stover D, Hathiramani D, Vaßen R, Damani RJ. Plasma_sprayed components for SOFC applications. Surf Coat Technol 2006;201:2002–5.
[165] Cassidy M, Lindsay G, Kendall K. The reduction of nickel–zirconia cermet anodes and the effects on supported thin electrolytes. J Power Sources 1996;61:189–92.

[166] Klemensoe T. Relationships between structure and performance of SOFC anodes. Topsoe fuel cell. Risø, Denmark: Technical University of Danemark, Risoe National Laboratory; 2005 (Ph.D. thesis).
[167] Klemensø T, Chung C, Larsen PH, Mogensen M. The mechanism behind redox instability of anodes in high-temperature SOFCs. J Electrochem Soc 2005;152:A2186–92.
[168] Pihlatie M, Kaiser A, Larsen PH, Mogensen M. Dimensional behavior of Ni–YSZ composites during redox cycling. J Electrochem Soc 2009;156:B322–9.
[169] Stathis G, Simwonis D, Tietz F, Moropoulou A, Naoumides A. Oxidation and resulting mechanical properties of Ni/8Y_2O_3-stabilized zirconia anode substrate for solid-oxide fuel cells. J Mater Res 2002;17:951–8.
[170] Fouquet D, Müller AC, Weber A, Ivers-Tiffée E. Kinetics of oxidation and reduction of Ni/YSZ cermets. Ionics 2003;9:103–8.
[171] Waldbillig D, Wood A, Ivey DG. Thermal analysis of the cyclic reduction and oxidation behaviour of SOFC anodes. Solid State Ionics 2005;176:847–59.
[172] Sarantaridis D, Chater RJ, Atkinson A. Changes in physical and mechanical properties of SOFC Ni–YSZ composites caused by redox cycling. J Electrochem Soc 2008;155:B467–72.
[173] Robert G, Kaiser A,Batawi E. Anode substrate design for redox-stable ASE cells. In: Proceedings of the sixth European solid oxide fuel cell forum proceedings; 2004. p. 193–200.
[174] Robert G, Kaiser A, Honegger K,Batawi E. Anode supported solid oxide fuel cells with a thick anode substrate. In: Proceedings of 5th European SOFC forum; 2002. p. 116–22.
[175] Fouquet D, Müller AC, Weber A,Ivers-Tiffee E. In: Proceedings of the 5th European SOFC Forum; 2002. p. 467–74.
[176] Iwanschitz B, Mai A, Holzer L, Hocker T,Schütze M. Degradation of Ni–cermet anodes in solid oxide fuel cells. In: Proceedings of the 9th European solid oxide fuel cell forum; 2010. p. 7–61.
[177] Waldbillig D, Wood A, Ivey DG. Electrochemical and microstructural characterization of the redox tolerance of solid oxide fuel cell anodes. J Power Sources 2005;145:206–15.
[178] Faes A, Jeangros Q, Wagner JB, Hansen TW, Van Herle J, Brisse A, et al. in situ reduction and oxidation of nickel from solid oxide fuel cells in a transmission electron microscope. ECS Trans 2009;25:1985–92.
[179] Zhang Y, Liu B, Tu B, Dong Y, Cheng M. Redox cycling of Ni–YSZ anode investigated by TPR technique. Solid State Ionics 2005;176:2193–9.
[180] Faes A, Nakajo A, Hessler-Wyser A, Dubois D, Brisse A, Modena S, et al. RedOx study of anode-supported solid oxide fuel cell. J Power Sources 2009;193:55–64.
[181] Malzbender J, Wessel E, Steinbrech RW. Reduction and re-oxidation of anodes for solid oxide fuel cells. Solid State Ionics 2005;176:2201–3.
[182] Robert G, Kaiser A, Honegger K,Batawi E. Anode supported solid oxide fuel cells with a thick anode substrate. In: Proceedings of the 5th European SOFC Forum; 2002. p. 193.
[183] Klemensø T, Mogensen M. Ni–YSZ solid oxide fuel cell anode behavior upon redox cycling based on electrical characterization. J Am Ceram Soc 2007;90:3582–8.
[184] Holtappels P, Graule T, Gut B, Vogt U, Gauckler L, Jorger M, Perednis D, Honegger K, Robert G, Rambert S, McEvoy AJ. Fabrication and performance of the anode-supported solid oxide fuel cells, Solid Oxide Fuel Cells VIII: (SOFC VIII): Proceedings of the international symposium, Vol. 8, 2003, p. 1003–1010.
[185] Pihlatie M, Ramos T, Kaiser A. Testing and improving the redox stability of Ni-based solid oxide fuel cells. J Power Sources 2009;193:322–30.
[186] Glauche A, Betz T, Mosch S, Trofimenko N, Kusnezoff M. Long-term, redox and thermal cycling stability of electrolyte supported cells. ECS Trans 2009;25:411–9.
[187] Laurencin J, Delette G, Sicardy O, Rosini S, Lefebvre-Joud F. Impact of 'redox' cycles on performances of solid oxide fuel cells: case of the electrolyte supported cells. J Power Sources 2010;195:2747–53.
[188] Iwanschitz B, Sfeir J, Mai A, Schütze M. Degradation of SOFC anodes upon redox cycling: a comparison between Ni/YSZ and Ni/CGO. J Electrochem Soc 2010;157:B269–78.
[189] Sumi H, Kishida R, Kim JY, Muroyama H, Matsui T, Eguchi K. Correlation between microstructural and electrochemical characteristics during redox cycles for Ni–YSZ anode of SOFCs. J Electrochem Soc 2010;157:B1747–52.
[190] Muroyama H, Sumi H, Kishida R, Kim JY, Matsui T, Eguchi K. Correlation between microstructure and electrochemical characteristics of Ni–YSZ anode subjected to redox cycles. ECS Trans 2011;35:1379–87.
[191] Atkinson A, Selçuk A. Mechanical behaviour of ceramic oxygen ion-conducting membranes. Solid State Ionics 2000;134:59–66.
[192] Pihlatie M, Kaiser A, Mogensen M. Mechanical properties of NiO/Ni–YSZ composites depending on temperature, porosity and redox cycling. J Eur Ceram Soc 2009;29:1657–64.
[193] Radovic M, Lara-Curzio E. Mechanical properties of tape cast nickel-based anode materials for solid oxide fuel cells before and after reduction in hydrogen. Acta Mater 2004;52:5747–56.
[194] Robert G, Kaiser A,Batawi E. Anode substrate design for redox-stable ASE cells. In: Proceedings of the 6th European SOFC forum; 2004. p. 193.
[195] Faes A, Fuerbringer JM, Mohamedi D, Hessler-Wyser A, Caboche G, Van Herle J. Design of experiment approach applied to reducing and oxidizing tolerance of anode supported solid oxide fuel cell. Part I: Microstructure optimization. J Power Sources 2011;196:7058–69.
[196] Robert G, Kaiser AFJ,Batawi E. Structured body for an anode used in fuel cells. U.S. Patent 20030165726 A1 2003; 4 September 2003.
[197] Clemmer RMC,Corbin SF. Co-sintering behaviour of porous Ni–YSZ composite sofc anodes. In: Ceramic engineering and science proceedings, vol. 26; 2005. p. 331–40.
[198] Clemmer RMC, Corbin SF. The influence of pore and Ni morphology on the electrical conductivity of porous Ni/YSZ composite anodes for use in solid oxide fuel cell applications. Solid State Ionics 2009;180:721–30.
[199] Jiang SP. A review of wet impregnation – an alternative method for the fabrication of high performance and nano-structured electrodes of solid oxide fuel cells. Mater Sci Eng A 2006;418:199–210.
[200] Waldbillig D, Wood A, Ivey DG. Enhancing the redox tolerance of anode-supported SOFC by microstructural modification. J Electrochem Soc 2007;154:B133–8.
[201] Ioselevich A, Kornyshev AA, Lehnert W. Degradation of solid oxide fuel cell anodes due to sintering of metal particles: correlated percolation model. J Electrochem Soc 1997;144:3010–9.
[202] Jiang SP. Sintering behavior of Ni/Y_2O_3–ZrO_2 cermet electrodes of solid oxide fuel cells. J Mater Sci 2003;38:3775–82.
[203] Nikolopoulos P, Sotiropoulou D. Wettability between zirconia ceramics and the liquid metals copper, nickel and cobalt. J Mater Sci Lett 1987;6:1429–30.
[204] Tsoga A, Naoumidis A, Nikolopoulos P. Wettability and interfacial reactions in the systems Ni/YSZ and Ni/Ti–TiO_2/YSZ. Acta Mater 1996;44:3679–92.
[205] Simwonis D, Tietz F, Stöver D. Nickel coarsening in annealed Ni/8YSZ anode substrates for solid oxide fuel cells. Solid State Ionics 2000;132:241–51.
[206] Hagen A, Barfod R, Hendriksen PV, Liu YL, Ramousse S. Degradation of anode supported SOFCs as a function of temperature and current load. J Electrochem Soc 2006;153:A1165–71.
[207] Cronin JS, Wilson JR, Barnett SA. Impact of pore microstructure evolution on polarization resistance of Ni–Yttria-stabilized zirconia fuel cell anodes. J Power Sources 2011;196:2640–3.
[208] Vaßen R, Simwonis D, Stover D. Modelling of the agglomeration of Ni-particles in anodes of solid oxide fuel cells. J Mater Sci 2001;36:147–51.
[209] Nelson GJ, Grew KN, Izzo Jr JR, Lombardo JJ, Harris WM, Faes A, et al. Three-dimensional microstructural changes in the Ni–YSZ solid oxide fuel cell anode during operation. Acta Mater. 2012;60:3491–500.
[210] Iwata T. Characterization of Ni–YSZ anode degradation for substrate-type solid oxide fuel cells. J Electrochem Soc 1996;143:1521–5.
[211] Faes A, Hessler-Wyser A, Presvytes D, Vayenas CG, Vanherle J. Nickel–zirconia anode degradation and triple phase boundary quantification from microstructural analysis. Fuel Cells 2009;9:841–51.
[212] Holzer L, Iwanschitz B, Hocker T, Münch B, Prestat M, Wiedenmann D, et al. Microstructure degradation of cermet anodes for solid oxide fuel cells: quantification of nickel grain growth in dry and in humid atmospheres. J Power Sources 2011;196:1279–94.
[213] Pihlatie MH, Kaiser A, Mogensen M, Chen M. Electrical conductivity of Ni–YSZ composites: degradation due to Ni particle growth. Solid State Ionics 2011;189:82–90.
[214] Sehested J, Gelten JAP, Helveg S. Sintering of nickel catalysts: effects of time, atmosphere, temperature, nickel-carrier interactions, and dopants. Appl Catal A 2006;309:237–46.
[215] Sehested J, Gelten JAP, Remediakis IN, Bengaard H, Nørskov JK. Sintering of nickel steam-reforming catalysts: effects of temperature and steam and hydrogen pressures. J Catal 2004;223:432–43.
[216] Jiao Z, Shikazono N, Kasagi N. Quantitative characterization of SOFC nickel–YSZ anode microstructure degradation based on focused-ion-beam 3d-reconstruction technique. J Electrochem Soc 2012;159:B285–91.
[217] Wang Z, Weng W, Cheng K, Du P, Shen G, Han G. Catalytic modification of Ni–Sm-doped ceria anodes with copper for direct utilization of dry methane in low-temperature solid oxide fuel cells. J Power Sources 2008;179:541–6.
[218] Tang Y, Liu J. Effect of anode and Boudouard reaction catalysts on the performance of direct carbon solid oxide fuel cells. Int J Hydrogen Energy 2010;35:11188–93.
[219] Zhou X, Zhen J, Liu L, Li X, Zhang N, Sun K. Enhanced sulfur and carbon coking tolerance of novel co-doped ceria based anode for solid oxide fuel cells. J Power Sources 2012;201:128–35.
[220] Mermelstein J, Millan M, Brandon N. The impact of steam and current density on carbon formation from biomass gasification tar on Ni/YSZ, and Ni/CGO solid oxide fuel cell anodes. J Power Sources 2010;195:1657–66.
[221] Offer GJ, Mermelstein J, Brightman E, Brandon NP. Thermodynamics and kinetics of the interaction of carbon and sulfur with solid oxide fuel cell anodes. J Am Ceram Soc. 2009;92:763–80.
[222] Bartholomew CH. Carbon deposition in steam reforming and methanation. Catal Rev 1982;24:67–112.
[223] Menon PG. Coke on catalysts—harmful, harmless, invisible and beneficial types. J Mol Catal 1990;59:207–20.
[224] Lin Y, Zhan Z, Liu J, Barnett SA. Direct operation of solid oxide fuel cells with methane fuel. Solid State Ionics 2005;176:1827–35.
[225] Cheng JG, Zha SW, Huang J, Liu XQ, Meng GY. Sintering behavior and electrical conductivity of $Ce_{0.9}Gd_{0.1}O_{1.95}$ powder prepared by the gel-casting process. Mater Chem Phys 2003;78:791–5.
[226] Kim T, Liu G, Boaro M, Lee SI, Vohs JM, Gorte RJ, et al. A study of carbon formation and prevention in hydrocarbon-fueled SOFC. J Power Sources 2006;155:231–8.
[227] Maček J, Novosel B, Marinšek M. Ni–YSZ SOFC anodes—minimization of carbon deposition. J Eur Ceram Soc 2007;27:487–91.

[228] Horita T, Yamaji K, Kato T, Kishimoto H, Xiong Y, Sakai N, et al. Imaging of CH_4 decomposition around the Ni/YSZ interfaces under anodic polarization. J Power Sources 2005;145:133–8.
[229] McIntosh S, He H, Lee SI, Costa-Nunes O, Krishnan VV, Vohs JM, et al. An examination of carbonaceous deposits in direct-utilization SOFC anodes. J Electrochem Soc 2004;151:A604–8.
[230] Nikooyeh K, Clemmer R, Alzate-Restrepo V, Hill JM. Effect of hydrogen on carbon formation on Ni/YSZ composites exposed to methane. Appl Catal A 2008;347:106–11.
[231] Alzate-Restrepo V, Hill JM. Effect of anodic polarization on carbon deposition on Ni/YSZ anodes exposed to methane. Appl Catal A 2008;342:49–55.
[232] Chun CM, Mumford JD, Ramanarayanan TA. Carbon-induced corrosion of nickel anode. J Electrochem Soc 2000;147:3680–6.
[233] He H, Hill JM. Carbon deposition on Ni/YSZ composites exposed to humidified methane. Appl Catal A 2007;317:284–92.
[234] Singh D, Hernández-Pacheco E, Hutton PN, Patel N, Mann MD. Carbon deposition in an SOFC fueled by tar-laden biomass gas: a thermodynamic analysis. J Power Sources 2005;142:194–9.
[235] Alzate-Restrepo V, Hill JM. Carbon deposition on Ni/YSZ anodes exposed to CO/H_2 feeds. J Power Sources 2010;195:1344–51.
[236] Bebelis S, Zeritis A, Tiropani C, Neophytides SG. Intrinsic kinetics of internal steam reforming of CH_4 over a Ni–YSZ–cermet catalyst-electrode. Ind Eng Chem Res 2000;39:4920–7.
[237] Dicks AL, Pointon KD, Siddle A. Intrinsic reaction kinetics of methane steam reforming on a nickel/zirconia anode. J Power Sources 2000;86:523–30.
[238] Ahmed K, Foger K. Kinetics of internal steam reforming of methane on Ni/YSZ-based anodes for solid oxide fuel cells. Catal Today 2000;63:479–87.
[239] Alstrup I, Clausen BS, Olsen C, Smits RHH, Rostrup-Nielsen JR. Promotion of steam reforming catalysts. Stud Surf Sci Catal 1998;119:5–14.
[240] Sasaki K, Teraoka Y. Equilibria in fuel cell gases. I. Equilibrium compositions and reforming conditions. J Electrochem Soc 2003;150:A878–84.
[241] Finnerty CM, Coe NJ, Cunningham RH, Ormerod RM. Carbon formation on and deactivation of nickel-based/zirconia anodes in solid oxide fuel cells running on methane. Catal Today 1998;46:137–45.
[242] Laosiripojana N, Assabumrungrat S. Catalytic steam reforming of methane, methanol, and ethanol over Ni/YSZ: the possible use of these fuels in internal reforming SOFC. J Power Sources 2007;163:943–51.
[243] Jiang Y, Virkar AV. A high performance, anode-supported solid oxide fuel cell operating on direct alcohol. J Electrochem Soc 2001;148:A706–9.
[244] Takeguchi T, Kani Y, Yano T, Kikuchi R, Eguchi K, Tsujimoto K, et al. Study on steam reforming of CH_4 and C_2 hydrocarbons and carbon deposition on Ni–YSZ cermets. J Power Sources 2002;112:588–95.
[245] Koh JH, Yoo YS, Park JW, Lim HC. Carbon deposition and cell performance of Ni–YSZ anode support SOFC with methane fuel. Solid State Ionics 2002;149:157–66.
[246] Finnerty CM, Ormerod RM. Internal reforming over nickel/zirconia anodes in SOFCs operating on methane: influence of anode formulation, pre-treatment and operating conditions. J Power Sources 2000;86:390–4.
[247] Koide H, Someya Y, Yoshida T, Maruyama T. Properties of Ni/YSZ cermet as anode for SOFC. Solid State Ionics 2000;132:253–60.
[248] Quincoces CE, Dicundo S, Alvarez AM, González MG. Effect of addition of CaO on Ni/Al_2O_3 catalysts over CO_2 reforming of methane. Mater Lett 2001;50:21–7.
[249] Choudhary VR, Uphade BS, Mamman AS. Oxidative conversion of methane to syngas over nickel supported on commercial low surface area porous catalyst carriers precoated with alkaline and rare earth oxides. J Catal 1997;172:281–293.
[250] Frusteri F, Arena F, Calogero G, Torre T, Parmaliana A. Potassium-enhanced stability of Ni/MgO catalysts in the dry-reforming of methane. Catal Commun 2001;2:49–56.
[251] Takeguchi T, Kikuchi R, Yano T, Eguchi K, Murata K. Effect of precious metal addition to Ni–YSZ cermet on reforming of CH_4 and electrochemical activity as SOFC anode. Catal Today 2003;84:217–22.
[252] Zhu H, Colclasure AM, Kee RJ, Lin Y, Barnett SA. Anode barrier layers for tubular solid-oxide fuel cells with methane fuel streams. J Power Sources 2006;161:413–9.
[253] Boder M, Dittmeyer R. Catalytic modification of conventional SOFC anodes with a view to reducing their activity for direct internal reforming of natural gas. J Power Sources 2006;155:13–22.
[254] Shabaker JW, Huber GW, Dumesic JA. Aqueous-phase reforming of oxygenated hydrocarbons over Sn-modified Ni catalysts. J. Catal. 2004;222:180–91.
[255] Nikolla E, Holewinski A, Schwank J, Linic S. Controlling carbon surface chemistry by alloying: carbon tolerant reforming catalyst. J Am Chem Soc 2006;128:11354–5.
[256] Besenbacher F, Chorkendorff I, Clausen BS, Hammer B, Molenbroek AM, Nørskov JK, et al. Design of a surface alloy catalyst for steam reforming. Science 1998;279:1913–5.
[257] Shabaker JW, Simonetti DA, Cortright RD, Dumesic JA. Sn-modified Ni catalysts for aqueous-phase reforming: characterization and deactivation studies. J Catal 2005;231:67–76.
[258] Nakagawa N, Sagara H, Kato K. Catalytic activity of Ni–YSZ–CeO_2 anode for the steam reforming of methane in a direct internal-reforming solid oxide fuel cell. J Power Sources 2001;92:88–94.
[259] Perry Murray E, Tsai T, Barnett SA. A direct-methane fuel cell with a ceria-based anode. Nature 1999;400:649–51.
[260] Yoon SP, Han J, Nam SW, Lim TH, Hong SA. Improvement of anode performance by surface modification for solid oxide fuel cell running on hydrocarbon fuel. J Power Sources 2004;136:30–6.
[261] Zhan Z, Barnett SA. An octane-fueled solid oxide fuel cell. Science 2005;308:844–7.
[262] Ahn K, He H, Vohs JM, Gorte RJ. Enhanced thermal stability of SOFC anodes made with CeO_2–ZrO_2 solutions. Electrochem Solid-State Lett 2005;8:A414–A417.
[263] Bartholomew CH. Mechanisms of catalyst deactivation. Appl Catal A 2001;212:17–60.
[264] Matsuzaki Y, Yasuda I. Poisoning effect of sulfur-containing impurity gas on a SOFC anode: Part I. Dependence on temperature, time, and impurity concentration. Solid State Ionics 2000;132:261–9.
[265] Bartholomew CH, Agrawal PK, Katzer JR. Sulfur poisoning of metals. Adv Catal 1982;31:135–242.
[266] Rasmussen JFB, Hagen A. The effect of H_2S on the performance of Ni–YSZ anodes in solid oxide fuel cells. J Power Sources 2009;191:534–41.
[267] Sasaki K, Susuki K, Iyoshi A, Uchimura M, Imamura N, Kusaba H, et al. H_2S poisoning of solid oxide fuel cells. J Electrochem Soc 2006;153:A2023–9.
[268] Zha S, Cheng Z, Liu M. Sulfur poisoning and regeneration of Ni-based anodes in solid oxide fuel cells. J Electrochem Soc 2007;154:B201–6.
[269] Cheng Z, Zha S, Liu M. Influence of cell voltage and current on sulfur poisoning behavior of solid oxide fuel cells. J Power Sources 2007;172:688–693.
[270] Kurokawa H, Sholklapper TZ, Jacobson CP, De Jonghe LC, Visco SJ. Ceria nanocoating for sulfur tolerant Ni-based anodes of solid oxide fuel cells. Electrochem Solid-State Lett 2007;10:135–8.
[271] Zhang L, Jiang SP, He HQ, Chen X, Ma J, Song XC. A comparative study of H_2S poisoning on electrode behavior of Ni/YSZ and Ni/GDC anodes of solid oxide fuel cells. Int J Hydrogen Energy 2010;35:12359–68.
[272] Hagen A, Rasmussen JFB, Thydén K. Durability of solid oxide fuel cells using sulfur containing fuels. J Power Sources 2011;196:7271–6.
[273] Cheng Z, Wang JH, Choi Y, Yang L, Lin MC, Liu M. From Ni–YSZ to sulfur-tolerant anode materials for SOFCs: electrochemical behavior, in situ characterization, modeling, and future perspectives. Energy Environ Sci 2011;4:4380–409.
[274] Kishimoto H, Horita T, Yamaji K, Brito ME, Xiong YP, Yokokawa H. Sulfur poisoning on SOFC Ni anodes: thermodynamic analyses within local equilibrium anode reaction model. J Electrochem Soc 2010;157:B802–13.
[275] Peng C, Luo J, Sanger AR, Chuang KT. Sulfur-tolerant anode catalyst for solid oxide fuel cells operating on H H_2S-containing syngas. Chem Mater 2010;22:1032–7.
[276] Gong M, Liu X, Trembly J, Johnson C. Sulfur-tolerant anode materials for solid oxide fuel cell application. J Power Sources 2007;168:289–98.
[277] Choi S, Wang J, Cheng Z, Liu M. Surface modification of Ni–YSZ using niobium oxide for sulfur-tolerant anodes in solid oxide fuel cells. J Electrochem Soc 2008;155:B449–54.
[278] Marquez AI, Ohrn TR, Trembly JP, Ingram DC, Bayless DJ. Effects of coal syngas and H_2S on the performance of solid oxide fuel cells. Part 2. Stack tests. J Power Sources 2007;164:659–67.
[279] Trembly JP, Marquez AI, Ohrn TR, Bayless DJ. Effects of coal syngas and H_2S on the performance of solid oxide fuel cells: single-cell tests. J Power Sources 2006;158:263–73.
[280] Geyer J, Kohlmuller H, Landes H, Stubner R. Investigation into kinetics of the Ni–YSZ cermet-anode of a solid oxide fuel cell. Solid Oxide Fuel Cells 1997;V:585–94.
[281] Dees DW, Balachandran U, Dorris SE, Heiberger JJ, McPheeters CC,Picciolo JJ. Sofc-I. The Electrochemical Society Proceedings Series 1989. p. 317–21.
[282] Wang JH, Liu M. Computational study of sulfur-nickel interactions: a new S-Ni phase diagram. Electrochem Commun 2007;9:2212–7.
[283] Choi YM, Compson C, Lin MC, Liu M. A mechanistic study of H_2S decomposition on Ni- and Cu-based anode surfaces in a solid oxide fuel cell. Chem Phys Lett 2006;421:179–83.